INSIGHT INTO THE LIGHT DRIVEN ASSEMBLY OF THE OXYGEN EVOLVING COMPLEX OF PHOTOSYSTEM II

By

ANTON AVRAMOV

Bachelor of Science in Biological Science
Siberian Federal University
Krasnoyarsk, Russia
2009

Master of Science in Biological Science
Siberian Federal University
Krasnoyarsk, Russia
2011

Submitted to the Faculty of the
Graduate College of the
Oklahoma State University
in partial fulfillment of
the requirements for
the Degree of
DOCTOR OF PHILOSOPHY
May, 2021

INSIGHT INTO THE LIGHT DRIVEN ASSEMBLY

OF THE OXYGEN EVOLVING COMPLEX

OF PHOTOSYSTEM II

Dissertation Approved:

Robert L. Burnap

Dissertation Adviser

Marianna A. Patrauchan

Tyrrell Conway

Wouter D. Hoff

William J. Henley

ACKNOWLEDGEMENTS

First and foremost, I want to thank my advisor and mentor Dr. Robert Burnap who kindly accepted me into his lab as a PhD student. I am grateful for the support, scientific advice, motivation, and inspiration that I have received from him during my PhD program in Oklahoma State University. I would like to thank my dissertation committee Dr. Mariana Patrauchan, Dr. Tyrrell Conway, Dr. Wouter Hoff and Dr. William Henley for their crucial support and advice throughout my PhD program. I am grateful to Dr. Charles Yocum for fruitful discussions and important suggestions regarding my experimental results and conclusions. Special gratitude is directed at Dr. Johannes Messinger and Dr. Casper de Lichtenberg for the collaboration resulted in the additional publication. I also want to thank Dr. Dave Britt and Dr. David Marchiori for exciting collaboration and training in UC Davis. I am especially grateful to Dr. Rich Debus for creating and kindly sharing the site-directed mutants that I have studied over the course of my PhD program. My dissertation was only possible due the financial support of National Science Foundation (NSF) grant no. MCB-1716408.

I want to thank the faculty and staff of the Department of Microbiology and Molecular Genetics for creating an atmosphere of professional growth. I appreciate the efforts of faculty in organizing Monday's scientific seminars, which have broadened my scientific scope and expanded my professional network. Special gratitude is addressed towards the office staff, Alice Bules, Marty Coldiron, Becky Hergenreder and Sallie Robinson for their impeccable ability to help with any question I ever had. I want personally thank the Oklahoma State University instrument shop and particularly Larry Vaughn and Wes Cash for their great help in maintaining and designing new tools which improved my ability to run smooth experiments.

I owe my gratitude to Steven Holland, Juliana Artier and Neil Miller for teaching me a majority of the lab techniques that I currently know, and for helping me troubleshoot and understanding my experiments and result. I want especially thank Juliana Artier and Neil Miller for their great support during the hardest times of my professional and personal life. I would especially like to thank Ms. Kathy Burnap for her care and moral support. I want to thank my current lab mates Ross Walker and Clark Jett for their friendship and for creating enjoyable environment in Burnap's lab. I specifically want to thank Dr. Minquan Zhang for all the unique knowledge and experience that he has passed to me during these years, I am thankful for his tremendous help with biochemical preparations, technical advice, and friendship. I am extremely thankful to my friends that I met here in Oklahoma State University, thank you to Victor Andreev, Jonny Riggs, Shahrouz Mohagheghian, Egor and Tanya Antipov for your endless support and your friendship.

Lastly, I cannot describe how grateful I am to my family for their support. I cannot describe in words the endless love that they gave me for all these years during my stay in Oklahoma State University. I want to thank my father Dr. Pavel Avramov and my mother Elena Avramova for the inspiration, moral support and for being always ready to help. I am grateful to my brother, Roman Avramov, who was always here for me despite being almost 10000 km away. This journey would not be possible without my family, friends, and colleagues; I am thankful to everyone who was in my life during this time.

Name: ANTON AVRAMOV

Date of Degree: MAY, 2021

Title of Study: INSIGHT INTO THE LIGHT DRIVEN ASSEMBLY OF THE OXYGEN EVOLVING COMPLEX OF PHOTOSYSTEM II

Major Field: MICROBIOLOGY, CELL AND MOLECULAR BIOLOGY

Abstract: Photosystem II (PSII) of plants, algae, and cyanobacteria utilize solar energy to catalyze one of the most important and most thermodynamically demanding reactions in nature: the oxidation of water into protons and molecular oxygen. Oxygen produced by PSII is toxic byproduct, however it is essential for respiration, the ozone layer and the extracted electrons drive the fixation of atmospheric CO_2 to create biomass. The mechanism of water splitting driven by the light-induced charge separation is relatively well studied and high-resolution crystal structures are available to reveal the molecular aspects of PSII complex, however considerably less is known about how the inorganic Mn_4O_5Ca cluster is assembled *de novo*.

The photosynthetic apparatus continuously experiences damage due to high light intensity and this results in the loss of photosynthetic activity. The primary photodamage occurs within main functional PSII unit, the D1 protein. To perform a highly efficient and sustained photosynthetic activity, damaged D1 protein should be replaced, with consequent reassembly of PSII. The key step in obtaining functional PSII *de novo* is the assembly of Mn_4CaO_5 core, driven by series of photo-oxidative reactions with incorporation of Mn and Ca ions into the coordination environment of PSII. The initial rate-limiting steps of the assembly of the PSII Mn_4CaO_5 core requires at least two quanta of light with the rate-limiting dark rearrangement step between them. A sensitive polarographic technique was used to track the assembly process under flash illumination as a function of the constituent Mn^{2+} and Ca^{2+} ions in genetically engineered membranes of the cyanobacterium *Synechocystis* sp. PCC6803 to elucidate the action of Ca^{2+} and peripheral proteins. We show that the protein scaffolding that organizes this process is allosterically modulated by the assembly protein Psb27, which together with Ca^{2+}, stabilizes photoactivation intermediates.

Photoactivation experiments with site-directed mutants D1-E189K and D1-E189R identified the role of D1-E189 in the formation the high affinity site of PSII. We have concluded that D1-E189 ligand is crucial during initial steps of photoactivation since it supports photoactivation intermediates by coordinating Ca^{2+} at its effectors site, which prevents the formation of inappropriately bound high-valency Mn at the oxygen evolving complex site.

TABLE OF CONTENTS

Chapter Page

Chapter Page

LIST OF TABLES

Table Page

LIST OF FIGURES

Figure Page

Figure Page

CHAPTER I

INTRODUCTION

The location and size of the planet Earth within the circumstellar habitable zone supports sufficient atmospheric pressure and allows water to be in liquid phase to support the existence of life. Incorporation of the inorganic carbon to organic molecules is a distinct and critical feature of carbon-based life, organisms capable of inorganic carbon fixation are called autotrophs. Autotrophs have been fueling primary biomass production on Earth for almost 4 billion years (Tashiro *et al.* 2017). Earth's first organisms were chemotrophs, microorganisms utilizing H_2 from the hydrothermal vents as a sole energy source and using obtained energy for atmospheric CO_2 fixation and biomass production (Fuchs 2011, Poehlein *et al.* 2012, Takami *et al.* 2012). Although chemotrophic communities were able to live using the energy provided by Earth's geological activity, energetically CO_2 fixation was not efficient and required complex flavin-based electron bifurcation to reduce ferredoxin for CO_2 conversion to the complex organic molecules (Herrmann *et al.* 2008, Li *et al.* 2008, Lubner *et al.* 2017). Among all the electron donors available on the ecological niches, only H_2 has a sufficiently low midpoint potential to drive CO_2 fixation and fuel primary production by microorganisms (Thauer *et al.* 1977, Brune 1989, Griffin *et al.* 2007, Sharma *et al.* 2012). The emergence of photosynthesis was the key evolutionary step to increase the primary production and not be limited by the hydrothermal vents constraints associated with Wood-Ljungdahl acetyl-CoA metabolic pathway (Martin *et al.* 2018). Photosynthesis evolved into two distinct groups, anoxygenic and oxygenic photosynthesis. It is considered that the evolution of photosynthesis started from anoxygenic form that was not capable of extracting electrons from water, rather used less abundant substrates such as sulfide, organic substrates and metals [reviewed

in (Olson *et al.* 2004, Björn *et al.* 2009, Hohmann-Marriott *et al.* 2011)]. Probably the most significant evolutionary step in photosynthesis for phototrophs was the emergence of the oxygenic photosynthesis, which uses widespread water molecules as sole electron source and the energy of light to drive water oxidation. Oxygenic photosynthesis allowed cyanobacteria to overcome substrate limitations, diversify and spread widely throughout the diverse habitats of the earth including in nutrition-poor and extreme temperature environments. The oxidation of water allowed cyanobacteria to synthesize complex organic molecules and release oxygen as a byproduct. Virtually all the oxygen in Earth's atmosphere has been produced during photosynthesis (Hohmann-Marriott *et al.* 2011). Over the course of 2.7 billion years (Gy), cyanobacteria have been utilizing the energy of light for water oxidation, which resulted in enrichment of Earth's atmosphere with oxygen and evolution of vast diversity of aerobic organisms. The production of the complex organic molecules by autotrophic organisms supported the emergence of the heterotrophic organisms, which utilize the biomass produced by autotrophs. Ancient cyanobacteria evolved into contemporary photosynthetic organisms, which include algae (via endosymbiosis), plants and the diversity of extant modern cyanobacteria. These organisms drive water oxidation and primary biomass production utilizing the same fundamental principles developed nearly 3 billion years ago. All photoautotrophs, including sulfur bacteria, purple bacteria, and all other photosynthetic organisms have evolved special reaction centers (RCs) that are all derived from a common ancestor and share remarkable compositional and 3D similarities of co-factors and protein structure, despite considerable loss of amino acid sequence similarities. All RCs capture photons from sunlight and use them to create highly reactive state of (bacterio)chlorophyll, which serves as the photochemical electron donor and transfers its energized electron to a bioenergetically coupled electron transport chain. The photooxidized primary electron donor (bacterio)chlorophyll later extracts the electron from the primary substrate to restore its capacity for further electron transfer. RCs are membrane-bound multiprotein centers that organize a significant number (~50-150) of organic (e.g., carotenoids and chlorophyll) and

inorganic (e.g. metal ions) cofactors which partake in electron transport from the primary electron donor, which drives energy conversion and biomass production. The RCs donate electrons either to mobile quinones (Type II RC) or bound iron sulfur (FeS) cluster (Type I RC). Oxygenic phototrophs such as cyanobacteria, algae and plants utilize both type of RCs, the Type II RC, photosystem II (PSII) and the Type I RC, photosystem I (PSI). The highly endergonic extraction of electrons from water is accomplished by PSII, which donates them to PSI via the photosynthetic electron transport (PSET) chain. PSI further boosts the energy level of the electron such that it can be transferred to the low potential electron acceptors ferredoxin and NADPH, and ultimately, to reductive anabolic metabolism with the fixation of CO_2 and concomitant production of sugars through the utilization of NADPH and ATP via the Calvin-Benson Cycle (CBC). Protons extracted from water contribute to the proton gradient across the membrane to drive ATP production, while O_2 is released as a byproduct (Hohmann-Marriott *et al.* 2011, Martin *et al.* 2018).

CHAPTER II

REVIEW OF LITERATURE

2.1 Photosynthetic electron transport chain

The light-driven reactions of oxygenic photosynthesis, and PCET in particular, take place in the thylakoid membranes (TM) of cyanobacteria and chloroplasts. For light to be efficiently utilized as an energy source, sunlight first must be absorbed by light harvesting antennae and trapped by the RC before it is converted to the chemical energy equivalents. The photosynthetic RC PSII is connected to the Chl-protein complexes CP43 and CP47, which constitute the 'proximal antenna,' forming a minimally functional PSII core complex. For the purpose of efficient light harvesting, PSII core complexes in cyanobacteria are further connected to the special multiprotein light harvesting antenna complex, called the phycobilisomes (PBS). The PBS complexes, working as a distal antenna, contain several soluble pigment proteins, while CP43 and CP47 contain only Chl *a* (Renger *et al.* 2008). Among the diverse PBS, two pigment proteins, phycocyanin and allophycocyanin are blue, while phycoerythrin is red. The combination of Chl *a* and PBS in cyanobacteria allow these organisms to effectively harvest a wide spectrum of light, funneling the absorbed energy to the RC. The light-harvesting PBS complexes are linked to the PSII core complexes containing reaction centers that are located in the thylakoid membranes (TMs). The reaction centers, photosystem I and photosystem II are deeply embedded within the thylakoid membrane and associated with all chlorophyll molecules in the photosynthetic machinery. Captured light energy, by either the PBS or by chlorophyll molecules in membrane-bound light harvesting protein complexes, is funneled to the so-called "special" pair of Chl *a* P_{680} (Döring *et al.* 1967, Döring *et al.* 1969) in PS II (**Fig. 1**). Photoexcitation of the multimeric chlorophyll

designated P_{680}, which functions as the primary photochemical electron donor, results in the primary charge separation on a picosecond timescale, during which the electron is promoted from the highest occupied molecular orbital to the lowest or second lowest unoccupied molecular orbital forming a strong reductant followed by electron transfer to a pheophytin yielding the highly oxidizing radical cation $P_{680}^{+\bullet}$ and radical anion $Pheo^{-\bullet}$. The electron deficient $P_{680}^{+\bullet}$ state of P_{680} represents the highest redox state of the entire process (E_m=1260 mV), which is a strong enough oxidant to drive water oxidation (Rappaport *et al.* 2002, Cardona *et al.* 2012). The $Pheo^{-\bullet}$ radical rapidly transfers the energized electron to a special noncovalently- and permanently-bound plastoquinone-9 acceptor, Q_A, leading to the formation of relatively stable $P_{680}^{+\bullet}$ $PheoQ_A^-$ in the picosecond time domain. To minimize the backreaction or oxidation of nearby chlorophylls and/or neighboring proteins, the highly reactive $P_{680}^{+\bullet}$ is re-reduced (20-250 ns scale) by the redox active tyrosine, D1-Tyr161 (Y_Z) of the D1 protein. Y_Z, located on the donor side proximal to P_{680} (Umena *et al.* 2011) extracts electrons from the Mn-containing water oxidizing complex (WOC) of PSII (**Fig. 1**), which is capable of storing the oxidizing equivalents. The fast re-reduction of $P_{680}^{+\bullet}$ by Y_Z ensures that the $P_{680}^{+\bullet}$ $PheoQ_A^-$ does not accumulate, except under conditions where the WOC is disrupted (e.g. removal of the Mn), in which case, the oxidant becomes relatively long-lived and shared in an equilibrium ($P_{680}^{+\bullet}$ $Y_Z \rightleftharpoons Y_Z^{+\bullet}$ P_{680}). This and other kinetic features strongly affect the fluorescence yield of PSII, which can be exploited experimentally. Specifically, the $P_{680}^{+\bullet}$ $PheoQ_A^-$ state is a strong quencher of fluorescence, whereas the $P_{680}PheoQ_A^-$ state has a high fluorescence yield. I use fluorescence measurements later in the thesis to monitor the redox states of the PSII complex during assembly.

During the course of four consecutive charge separation events, the WOC passes through a series of oxidation states (S-states) with the catalytic cycle balanced by removing four electrons from two bound water molecules, the release of O_2 and four protons into the lumen (Bao *et al.* 2013) and contribute to ATP production. $P_{680}^{+\bullet}$ $PheoQ_A^{-\bullet}$ subsequently transfers the electron to a mobile

plastoquinone Q_B. The lipid-soluble plastoquinone Q_B pool acts as mobile electron carrier between PSII and multiprotein complex Cyt *b*$_6$*f* within the lipid bilayer of the thylakoid membrane. The Q_B binding site in the D1 protein facilitates binding and subsequent exchange of a mobile Q_B molecule, which involves the transfer of two electrons from Q_A to Q_B, and coordinated protonation to form PQH_2 (Golbeck 2003). Since each Q_A molecule can be reduced only one electron at a time, the formation of PQH_2 represents two one-electron transfer events from the nearby $Q_A^{-\bullet}$ anion radical (Renger *et al.* 2008). This PQH_2 molecule has lower binding affinity to the Q_B site, thus is easily replaced by the Q_B molecule and consequently transferred to the PQ pool in the membrane bilayer. PQH_2 is later oxidized by Cyt *b*$_6$*f* with the release of protons into the thylakoid lumen, hence contributing to the formation of the proton gradient for ATP production (Aoki *et al.* 1982, Wenk *et al.* 2005, Cramer *et al.* 2011). Electron transport via Cyt *b*$_6$*f* complex is described by the Q-cycle scheme, with two quinone binding sites: one on the n-side (Q_N site) of the membrane and the other on the p-side (Q_p site). There is also a plastocyanin/cytochrome c oxidoreductase on the positive (p) side and plastoquinone reductase (essentially, the Q_N site) on the negative (n) side. The Q cycle occurs in two stages and involves the sequential binding and complete oxidation of two PQH_2 molecules, one PQH_2 per stage, at the Q_p site. Oxidation of each PQH_2 at the Q_p binding involves an electron transfer to the high potential [2Fe-2S] cluster of the iron-sulfur protein (ISP), then to plastocyanin, which transfers the electron to Photosystem I (PSI). The first electron donation at the at the Q_p site on the p-side leads to the formation of the plasto-semiquinone anion, $PQ^{-\bullet}$ (E_m~-160mV), while transfers the relatively reducing electron from the semiquinone anion to the cyt b_n heme and then to the PQ (first stage of the cycle) or $PQ^{-\bullet}$ (second stage of the cycle) at the Q_N binding site on n-side of the complex, thus regenerating one PQH_2 for every two PQH_2 consumed (Baniulis *et al.* 2008).

Unlike in PSII where four photons of light are required for the catalytic cycle, PSI's photochemical cycle is univalent and requires a single photon harvested by the light harvesting

complex and funneled to the "special" chlorophyll pair P_{700} to promote a single charge separation that then leads to univalently oxidized plastocyanin and univalently reduced ferredoxin. When the light energy arrives to at the primary electron donor P_{700} (a special electron pair of Chl *a* and Chl *a'* molecules (Jordan *et al.* 2001)), the excited state is converted to a charge separated state, similar to PSII. Charge separation results in oxidized P_{700}^{+} and reduced primary electron acceptor Chl A_0^{+}, which is stabilized by rapid electron transfer across the membrane to the mobile single electron carrier ferredoxin (Fd) through several intermediate electron carriers including bound, phylloquinone (PhQ) molecule (also known as vitamin K1), Chl A_1, and F_X and F_A/F_B iron sulfur centers. Once charge separation produces an electron hole, P_{700}^{+} is re-reduced by the mobile electron carrier plastocyanin (Jensen *et al.* 2007). The electron transferred to Fd by PSI could be transferred (i) back to Cyt b_6f complex to increase proton transport across the membrane, thus inducing ATP synthesis (cyclic electron flow), or (ii) to NADP reductase to produce NADPH (linear electron flow), for utilization in CO_2 fixation and anabolic metabolism.

As well as electrons, the redox reactions of PSET establish an electrochemical potential (proton gradient) across the thylakoid membrane. The free energy of proton movement (pmf) is used by the ATPase complex embedded in the thylakoid membrane to drive synthesis of ATP from ADP and inorganic phosphate. Protons are transferred through the ATP synthase complex, which uses a ratchet-like mechanism to drive phosphorylation of ADP and release of ATP on the stromal side of thylakoid membrane (Martin *et al.* 2018). Thus, PSET drives the production of both essential energy molecules required for CO_2 fixation and sugar production by photosynthetic organisms.

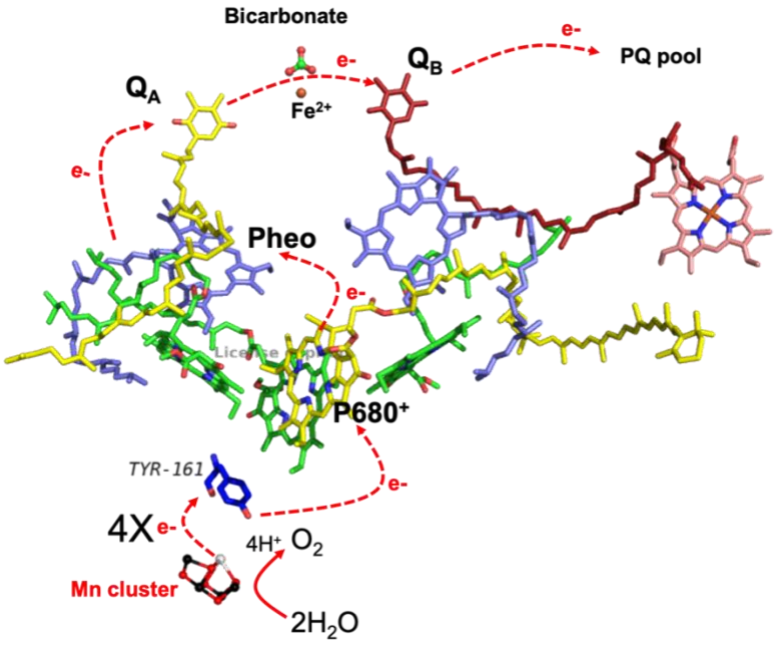

Figure 1. Schematic representation of the electron transport chain and redox cofactors in PSII. Electron excited by light leave P_{680}^+ towards mobile plastoquinone QB, the electron transport mediated by pheophytin and stationary plastoquinone (Q_A). The electron hole in P_{680}+ is rapidly filled by extracting the electron from redox active D1-Tyr161 (Y_Z), which is reduced by the electron pulled from the Mn cluster.

2.2 Photosystem II – structure and function

Photosystem II is a transmembrane protein complex located in the thylakoid membranes (**Fig. 2A**) of oxygenic photosynthesizing organisms and performs a series of light-induced charge separations, splitting water into protons and molecular oxygen and providing electrons for NADPH production. According with the most precise crystal structure (Protein Data Bank entry 3ARC) (Umena *et al.* 2011) each PSII monomer has a molecular weight of 350 kDa and composed of 17 transmembrane subunits, three peripheral proteins and several cofactors.

In the assembled state, PSII is a dimer where each monomer contains 20 proteins, 35 chlorophylls, two pheophytins, 11 ß-carotenes, more than 20 lipids, two plastoquinone molecules, two heme irons and one non-heme iron, four manganese atoms, four calcium atoms, three Cl^- ions

and a bicarbonate ion (see **Fig. 2B**). Four manganese ions and one calcium ion compose the catalytic center of photosystem II, a Mn_4O_5Ca cluster. The PSII core is composed of a D1 and D2 heterodimer structure (RC core) that provides all redox active residues interacting with the PSII electron transport chain. Two closely related proximal protein antenna proteins, CP43 and CP47, surround the RC core and contain the majority of PSII chlorophylls, which funnel the light energy into the primary electron donor chlorophyll, P_{680}. Within the RC core, the exciton is converted to electrochemical potential energy by charge separation as discussed above (see **Fig. 1**). Several other intrinsic proteins associated with PSII are required for photoautotrophic growth and oxygen evolution, including PsbF (cyt b_{559}), PsbE and PsbI. These short polypeptides span the membrane once; PsbE and F, which coordinate a heme, form the poorly understood cyt b_{559}. Other small, single copy intrinsic proteins associated with PSII, such as PsbJ, PsbK, PsbL, PsbTc, PsbY and PsbZ, are rather featureless or less studied than PSII core subunits. Three extrinsic polypeptides, PsbO, PsbV, and PsbU, enclose and stabilize the cyanobacterial WOC; plants and certain eukaryotic algae instead possess PsbO, PsbQ, and PsbP (Roose *et al.* 2016). The extrinsic polypeptides prevent the reduction of the Mn cluster by exogenous reductants (Tamura *et al.* 1985, Mei *et al.* 1991, Mei *et al.* 1992) and help retain the Ca^{2+} cofactor, which is otherwise prone to loss during the catalytic cycle (Boussac *et al.* 1988, Miqyass *et al.* 2008). PsbO forms a structural bridge between the E-loop of CP43, and the D1 C-terminal domain, which is involved in the coordination of the metals of the water oxidation catalyst. The structural bridges formed by PsbO appear to prevent structural fluctuations in E-loop of CP43 and the D1 C-terminal domain of apo-PSII (Tokano *et al.* 2020, Huang *et al.* 2021), which will be discussed in Chapter 3.

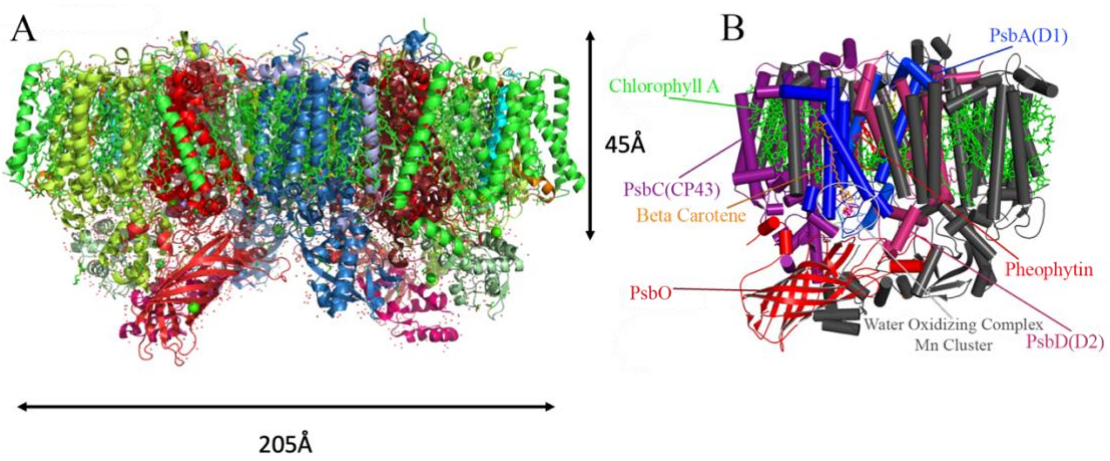

Figure 2. **Schematic representation of A) PSII dimer and B) PSII monomer derived from 1.9Å resolution crystal structure** (Umena *et al.* 2011). Key protein and organic subunits assigned on the panel B: protein subunits PsbA (D1), PsbD (D2), PsbC (CP43), PsbO, and organic cofactors Chl *a*, pheophytin and beta carotene. Water oxidizing complex is embedded in the protein environment of each PSII monomer and covered by extrinsic protein cap formed by PsbO, PsbU and PsbV proteins. For more information review (Umena *et al*., 2011)

2.2.1 Function of photosystem II

Photosystem II (PSII) utilizes solar energy to catalyze one of the most important and most thermodynamically demanding reactions in nature: the oxidation of water into protons and molecular oxygen. The electrons extracted from the substrate water molecules are transferred through the redox-active cofactors of the photosynthetic electron transport chain eventually to reduce the electron acceptor $NADP^+$, thereby forming the primary reductant for the synthesis of biomass from CO_2 and other inorganic nutrients. Thus, the H_2O-oxidation reaction is the basis of oxygenic photosynthetic metabolism and the primary driver of biomass accumulation on the planet (Vinyard *et al.* 2017, Lubitz *et al.* 2019). PSII drives water oxidation through the complex and thermodynamically expensive process utilizing a powerful oxidant (P_{680}^+) formed via light-induced charge separation as noted above. Two water molecules undergoing oxidation by PSII are bound to the Mn_4O_5Ca cluster buried in the PSII protein environment (Umena *et al.* 2011). Mn_4O_5Ca cluster catalytic mechanism is best characterized by the Kok-cycle (Kok *et al.* 1970) describing the

oxidation event occurring at the Mn cluster after each charge separation created at the primary electron donor, P_{680} (Holzwarth *et al.* 2006). As with all known RCs, P_{680} consists of a 'special pair' of interacting Chls that are excitonically coupled, which means the excitation energy is distributed between them so that they tend to act as a single entity. This excitonic coupling tunes the redox potential for the photochemical oxidation of special pair and, in the case of P_{680}, contributes to the strong oxidizing ability of the P_{680}^{+} necessary to extract the tightly bound electrons of substrate water. An absorbed photon of light creates a charge separated state $P_{680}^{+\square}Q_A^{-}$ comprising oxidized $P_{680}^{+\square}$ on the donor side and reduced plastoquinone Q_A^{-} on the acceptor side. The complete oxidation of two substrate water molecules results in the net release of molecular oxygen, four protons, and four electrons aimed to reduce the Mn cluster its ground state. The Mn cluster comprises four Mn and one Ca ions linked via μ-oxo bridges (Mn_4CaO_5); it undergoes four oxidation events and accumulates the oxidation "power" termed as storage states (S-states) (Joliot *et al.* 1969, Kok *et al.* 1970, Forbush *et al.* 1971). After four consecutive oxidations, the Mn cluster splits two water molecules, using the extracted electrons for self-reduction.

2.2.2 Kok model of S state-cycle

The ability of the WOC to store oxidative equivalents was first discovered in 1969 by Joliot and coworkers (Joliot *et al.* 1969). The illumination of the chloroplasts extracted from alga with single-turnover saturating flashes illustrated that the oxygen release occurs with a characteristic periodicity of four. Later Kok et al. (Kok *et al.* 1970) proposed a model, where WOC cycles during the water oxidation through 5 oxidative S_i-states, where i = 0, 1, ..4 is the number of oxidizing equivalents stored by the Mn cluster.

2.2.3 Mn cluster structure

The 1.9Å structure of photosystem II indicates that Mn_4O_5Ca cluster is coordinated by one nitrogen ligand of D1-His332, and six carboxylate ligands from D1-Asp170, D1-Glu189, D1-Glu333, D1-Asp342, D-Ala344, CP43-Glu354 (**Fig. 3**). Ligands provided by D1-Glu333, D1-

Asp342, and CP43-Glu354 form μ-carboxylate bridges between Mn atoms, Asp342 with Mn(1)-Mn(2), CP43-Glu354 with Mn(2)-Mn(3) and Glu333 with Mn(3)-Mn(4). Ca is ligated with Mn(2) and Mn(4) through Asp170 and the C-terminal carboxylate group of Ala344 (Umena *et al.* 2011). The Mn atoms of the Mn_4O_5Ca are designated Mn(1)-Mn(4), with Mn(4) identified earlier using EPR spectroscopy (Peloquin *et al.* 2000) as the "dangler manganese" because it was deduced to be relatively remote from other four metals (Mn1-3, 1Ca) of the cluster that are now known to form a semi-cubane structure (Umena *et al.* 2011). The Mn(4) atom (**Fig. 3**, atom rendered in purple) is of particular significance, because it appears to be, or at least occupy, the position of the so-called high affinity site (HAS) of Mn^{2+} binding, as discussed in more depth below. The D1-Asp170 carboxyl group forms a high affinity Mn^{2+} binding site and serves as a main player of the initial photooxidation of the first Mn ion during light-driving assembly of WOC (Nixon *et al.* 1992), and is thus critical for my studies of the assembly of the Mn_4CaO_5. As we will additionally see, D1-Glu189 and D1-His332, which form a monodentate ligands with Mn(1) in the fully assembled structure (Umena *et al.* 2011), also appear to play critical roles in the HAS.

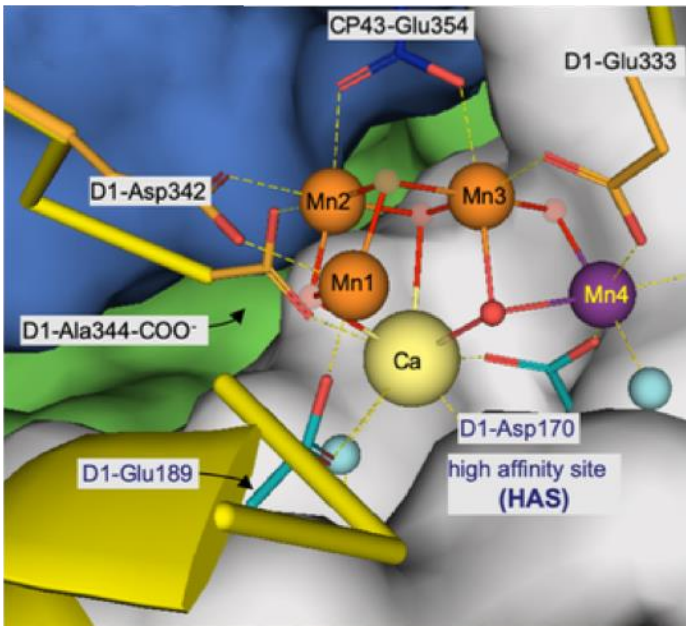

Figure 3. Schematic representation of the catalytic Mn_4CaO_5 cluster at the interface between the D1 (PsbA) and CP43 (PsbC) subunits. Most of the ligands coordinating the Mn_4O_5Ca cluster are provided by the C terminus of the D1 protein: D1-His332 D1-Asp170, D1-Glu189, D1-Glu333, D1-Asp342, Ala344; one ligand is provided by CP43 protein: CP43-Glu354.

2.3 PSII photodamage

The PSII complex is subject to incessant damage and a remarkable feature is its ability to undergo self-repair. Strong light results in a serious stress on photosynthetic machinery causing both reversible and irreversible damage termed photodamage or photoinhibition (Aro *et al.* 1993, Adir *et al.* 2003, Vass *et al.* 2009). Although the entire photosynthetic mechanism is prone to damage due to the high light intensity, photodamage primarily occurs within PSII and much of the damage is localized in the D1 (PsbA) protein, which binds the main redox cofactors involved in photochemical charge separation. Known mechanisms of photodamage may be differentiated by the location of damage within PSII, and is usually discussed as either acceptor-side or donor-side inhibition (Adir *et al.* 2003). The precise molecular bases for these forms of photodamage remain poorly understood, but both types share inefficient electron transport through the redox active cofactors of PSII. High rates of P_{680} oxidation can result in donor side photodamage due to inability of the Mn_4O_5Ca cluster to provide electrons at a sufficient rate, thereby allowing the potentially damaging oxidized $P_{680}^{+\bullet}$ species to accumulate and causing oxidative destruction of the Mn_4O_5Ca cluster (Murata *et al.* 2007). Acceptor side photoinhibition is induced by the formation of the highly reactive singlet oxygen radical via interaction with the triplet state of P_{680} reaction center. The formation of $^3(P_{680})$ state occurs due to the charge recombination of the charge-separated state $P_{680}^{+\bullet}$ and the electron acceptor ($^3[P_{680}Pheo]$), which tends to occur when acceptors side electron transfer is limited, such as when CO_2 limitation restricts downstream utilization of electrons limitation (Vass *et al.* 2009).

2.4 PSII repair and biogenesis

Since the main photodamage during photoinhibition occurs in the D1 protein, and to a lesser extent in the other reaction center proteins, efficient mechanisms have evolved to remove and replace damaged reaction center proteins and assemble them with their requisite cofactors (Adir *et al.* 2003). PSII biogenesis and repair pathways are tightly regulated by a set of cofactor proteins, such as Psb28, Psb34, Psb27, and others that transiently associate with the main PSII proteins during biogenesis (Roose *et al.* 2004, Chen *et al.* 2006, Nowaczyk *et al.* 2006, Dobáková *et al.* 2009, Nowaczyk 2012, Zabret *et al.* 2020). More than 20 of these auxiliary polypeptides have been identified. Until recently, the molecular mechanisms by which they facilitate the assembly of the holo-PSII complex have remained obscure. Each of these assembly proteins are associated with purified partial PSII subcomplexes. These subcomplexes, containing combinations of main PSII proteins and assembly proteins, may represent intermediates in a stepwise assembly process, which are then joined together to form monomeric apo-PSII lacking the WOC and several extrinsic proteins (Nixon *et al.* 2010, Nickelsen *et al.* 2013, Heinz *et al.* 2016). Subsequently, the metals of the Mn_4CaO_5 cluster are assembled and the remaining extrinsic proteins bind to form the holo-complex, although the timing of these events remain poorly understood.

2.4.1 Assembly of the apo-PSII

Current evidence suggests that the process of assembly of new apo-PSII complex starts from the assembly of the D1/D2 heterodimer core subunit to form a reaction center (RC) intermediate from the unprocessed D1 precursor pD1 protein and D2 protein [reviewed in (Nixon *et al.* 2010, Nickelsen *et al.* 2013, Heinz *et al.* 2016)]. Then Psb28 protein facilitates binding of CP47 antenna protein to RC complex to form RC47 complex, where pD1 protein is being processed to a mature form by CtpA protease (Anbudurai *et al.* 1994, Dobáková *et al.* 2009, Boehm *et al.* 2012). CryoEM structure of apo-PSII with attached Psb28 identified significant molecular perturbation at the PSII acceptor side mainly formed by D1 D-E loops. Binding of Psb28 with the support of Psb34 disrupts

the Q_B binding site, which involves the replacement of bicarbonate with glutamate as a ligand of non-heme iron. These structural changes are suggested to be a part of a protective mechanism that reduces $^1O_2$ formation during the indirect charge recombination via $P^{\bullet+}/Pheo^{\bullet-}$ in the apo-PSII (Zabret *et al.* 2020). The next assembly step is association of a second antenna protein CP43 with RC47 complex, that triggers the disassembly of auxiliary Psb28 protein. Psb27 binds to CP43 protein, which is suggested to facilitate light-driven assembly of the WOC (Nowaczyk *et al.* 2006, Roose *et al.* 2008, Liu *et al.* 2011). Psb27 is of particular significance to my thesis work since I will be showing that the protein plays an intimate role in facilitating the assembly of the Mn_4CaO_5. Once the WOC has been assembled Psb27 dissociates from apo-PSII and three extrinsic luminal proteins PsbO, PsbU and PsbV bind to the PSII monomer and cover PSII catalytic site (Burnap *et al.* 1991, Burnap *et al.* 1996, Bricker *et al.* 2012). The final step in PSII maturation is the dimerization of two fully assembled and catalytically active PSII monomers and the attachment of the phycobilisome light harvesting antenna complex.

2.4.2 Light-induced assembly of the Mn_4O_5Ca cluster

A final step in both *de novo* and repair synthesis of PSII is assembly of the Mn_4CaO_5 core into the ligation environment of the PSII protein matrix. Light driven assembly of Mn_4CaO_5 occurs through a series of photochemical reactions that involve the oxidation of Mn^{2+} ions using the same electron extraction pathway of the fully mature PSII. Understanding the mechanism of this process is the central topic of my thesis.

2.4.3 Two-quantum mechanism of photoactivation

Assembly of Mn_4CaO_5 occurs via a series of primary photooxidation reactions that involve the oxidation of Mn^{2+} ions using the same electron extraction pathway of the fully mature PSII. The kinetics of photoactivation as described by the "two-quantum series model" (**Fig. 4**) (Radmer *et al.* 1971) was derived by Cheniae and coworkers from a series of photoactivation experiments involving either variable light intensity or flash interval experiments using Xe light flashes

(Cheniae *et al.* 1971, Radmer *et al.* 1971, Cheniae *et al.* 1972). These experiments showed a strong correlation between quantum efficiency of photoactivation and the light intensity where at low intensity the quantum efficiency is low, at intermediate intensities it reaches maximal values and at high light intensities the efficiency declined. Similar observations were made with sequences of saturating flashes of light given at different flash intervals ranging from milliseconds to seconds apart. The quantum efficiency of photoactivation increased from low flash interval to the maximum efficiency at ~1 s, and declined rapidly with increasing t flash intervals > 1 s. From these results Cheniae inferred the presence of at least one unstable intermediate during photoactivation and derived a minimal model describing the light induced Mn^{2+} incorporation into the PSII. The multistep process begins with the binding of a single Mn^{2+} ion (Ono *et al.* 1999), as its hydroxide (Ananyev *et al.* 1999) to HAS. Site-directed mutagenesis experiments showed that D1-Asp170 is critical for photooxidation of Mn^{2+} at the HAS (Nixon *et al.* 1992). This consistent with the observation that D1-Asp170 provides a monodentate ligand to Mn(4) occupying the 'dangler' position of Mn4 in the fully assembled Mn_4CaO_5 cluster (Boerner *et al.* 1992, Nixon *et al.* 1992, Umena *et al.* 2011). Interestingly, mutations at D1-Glu333, which provides the only other ligand to Mn4 in the assembled Mn_4CaO_5 structure, did not produce a similar perturbation of the HAS (Cohen *et al.* 2007). As discussed later, this is likely due to the fact that D1-Glu333 far away from its final position in the apo-PSII complex and must move into position during the assembly process.

The first photoevent removes electron from a $[Mn^{2+}\text{-}(OH^{-})]$ species ((**Fig. 4**, **intermediate "A"**) at the HAS, resulting in $[Mn^{3+}\text{-}(OH^{-})]$ (Ananyev *et al.* 1999, Ono *et al.* 1999) and allowing the formation of oxo-bridges between the metal ions via oxygen atoms links. The newly formed Mn^{3+} ion potentially leads to an intermediate with a Ca^{2+} ion (**Intermediate "B"**) forming a $[Mn^{3+}\text{-}(OH^{1-})\text{-}Ca^{2+}] \rightleftharpoons [Mn^{3+}\text{-}(O^{2-})\text{-}Ca^{2+}]$ oxide complex (Tyryshkin *et al.* 2006). Resulting species "**B**" can spontaneously convert to species "**C**" (**Intermediate "C"**) in the dark (**Dark rearrangement**) with 100-200 ms half-time (**Constant k_R**). The **B→C** conversion potentially allows binding of the

second Mn^{2+} ion to the HAS or another site, which allows the binding and/or photooxidation of the second Mn^{2+} on the path toward the WOC assembly. This photooxidation of a second Mn^{2+} corresponds to the **C→D** transition, which is the first stable photoactivation intermediate (**Intermediate "D"**). Additional Mn^{2+} ions are photooxidatively incorporated into the growing metal cluster via the oxo-bridges that are presumably derived from water ligands of the incoming metal ions. The remarkable feature is that photoactivation is very inefficient with an overall quantum efficiency typically below 1%, despite the fact that photooxidative assembly uses the same charge separation cofactors, notably the oxidized forms of the primary and secondary electron donors, P_{680} and Y_Z, respectively. Whereas the quantum efficiency of photosynthetic H_2O-oxidation in the fully functional PSII is greater than 90% (Radmer *et al.* 1971). Thus, despite efficient charge separation in the photochemical reaction center, one or more of the photoactivation intermediates forms much less efficiently indicating photochemical charge separation only occasionally succeeds in photooxidizing the incoming Mn^{2+} ions used as building blocks for assembly the Mn_4CaO_5. Flash spacing (frequency of charge separations) at intervals of ~1 s is optimal since it provides enough time for the dark rearrangement (***k_R***) to happen but short enough so the labile photoactivation intermediates do not decay during the assembly. Flashes given with longer flash spacing leads to the decay of unstable photoactivation "C" and blocks the further assembly of the WOC. Interestingly the formation of the intermediate "C" seems to be a bottleneck in quantum efficiency of photoactivation and limits the rate of the assembly, suggesting that the oxidation of the second Mn^{2+} cannot be utilized towards the assembly unless the intermediate "C" is formed. Kinetic analysis of the photoactivation of a mutant lacking the extrinsic PsbO protein indicated that the low overall quantum efficiency is due to the low efficiency events after the initial photooxidation (**A→B)**, but could be increased with increasing accessibility of Mn and/or Ca to the WOC (Burnap *et al.* 1996).

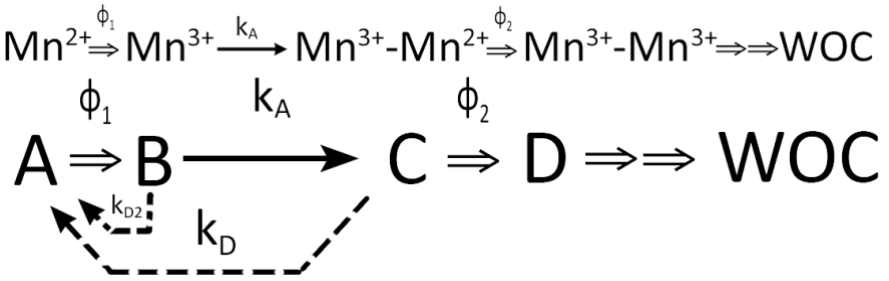

Figure 4. Kinetic scheme of basic two-quantum mechanism of PSII photoactivation. Double arrows indicate light-activated processes with the quantum efficiencies $\boldsymbol{\phi}_1$ and $\boldsymbol{\phi}_2$ representing the first and second photooxidative events in the assembly sequence, k_A representing the "dark" rearrangement, and k_D, representing the decay of intermediates. After the initial two Mn are photoligated, subsequent Mn appear to be added with high quantum yield.

2.4.4 Dark rearrangement

The rate of the dark rearrangement has a ~100-200 ms halftime estimated from flash interval experiments. This is a very long time for events occurring at the molecular scale, such as diffusion of ions and amino acid side chain rotations, which should occur in the sub-microsecond time domain (**Fig. 4**). However, more complex protein conformational rearrangements can occur in times scales of milliseconds or longer, especially in cases involving hinge motions involving high transition barriers between what may be otherwise similar energy wells (Bucher *et al.* 2011). It was suggested that a slow protein conformational change allows the coordination of the second Mn^{2+} (**C**) and its subsequent oxidation (**C→D)** (Chen *et al.* 1995, Ananyev *et al.* 1996, Burnap *et al.* 1996, Qian *et al.* 1999, Burnap 2004). However, the nature of the conformational change was not clear at the time. Chen showed that Ca^{2+} stabilizes the light-induced intermediates against reductive loss and facilitates proper assembly of the Mn_4CaO_5 and avoiding the formation of malformed, catalytically inactive Mn deposits (Chen *et al.* 1995), which they suggested might be due to the ability of Ca^{2+} to induce a conformational change at the intrinsic polypeptides of PSII. Debus speculated that the protein conformational change protects Mn^{3+} species from the reduction and

that protection does not occur in the absence of Ca^{2+} (Debus 1992). Based upon an analysis of the then newly available PSII crystal structure, it was suggested that the conformational change occurring during the photoactivation involves the movement of CP43 E-loop region via a hinge located between CP43-Pro304 and CP43-Pro400 amino acid (Burnap 2004). Recent work by Noguchi and coworkers demonstrated this predicted movement using time-resolved atomic force microscopy (Tokano *et al.* 2020) raising the possibility of its involvement of CP43 E-loop movement in the photoactivation. In those experiments it was shown that upon the removal of the Mn cluster causes the luminal domain of CP43 protein to start to stochastically fluctuate between "high" and "low" states with the lifetimes of 0.23 and 0.13 s, respectively corresponding to an opening and closing of the access to the WOC from the soluble phase. That fluctuation was observed in both Mn-depleted and intact PSII without extrinsic proteins bound to the luminal side of PSII. However, the fluctuation in intact PSII did not occur until after the dissociation of PsbO, which was interpreted to mean that the intact Mn_4CaO_5 readily disassembles in the absence of PsbO, thereby allowing the mobilization of the E-loop. Interestingly, this fluctuation was not observed with extrinsic proteins bound to the PSII, supporting the idea that binding of PsbO to CP43 (Liu *et al.* 2011) forms a structural bridge between E-loop and D1 protein including C-terminal domain. Considering the participation of C-terminus of D1 protein in the coordination of the WOC (Umena *et al.* 2011) and the fact that upon removal of the extrinsic proteins the Mn cluster loses 2 Mn ions (Miyao *et al.* 1985) the closed conformation of PSII will be favorable to keep the Mn cluster intact. The relaxed open configuration (Tokano *et al.* 2020) could potentially be more favorable for PSII *de novo* assembly allowing the of C-terminus of D1 protein to also adopt an alternative, more open configuration, with increase of ion diffusion rate to the apo-PSII. Moreover, keeping the apo-PSII open could potentially be beneficial during the repair cycle and insertion of the newly synthesized pD1 protein, open configuration could facilitate the proteolytic maturation of D1 protein by CtpA (Diner *et al.* 1988, Seibert *et al.* 1989, Nixon *et al.* 1992, Trost

et al. 1997). Observed "low" state of Cp43 E-loop corresponds with the open configuration of apo-PSII and strikingly has a similar lifetime with the dark rearrangement halftime (k_A).

The nature of the dark rearrangement is still a matter of debate and alternatives to the protein conformational change hypothesis can be considered. One possibility that the dark rearrangement is the slow formation of the oxo bridge between the Mn^{3+} and second Mn^{2+} located at the HAS. As mentioned above, the Mn^{2+} bound at the HAS binds as the metal hydroxide (Ananyev *et al.* 1999) and Mn^{3+} formed by photooxidation is linked to a Ca^{2+} ion through the oxo bridge forming [Mn^{3+}-(OH^{1-})-Ca^{2+}] ⇌ [Mn^{3+}-(O^{2-})-Ca^{2+}] oxide complex (Tyryshkin *et al.* 2006). The dark rearrangement may therefore correspond to the time required to form a second oxo linkage between Mn^{3+} and Mn^{2+}, which would be the precursor to the di-μ-oxo bridges that link the Mn ions in the assembled cluster. For this hypothesis to be true, the subsequent photooxidations should occur not at the HAS but rather at the Mn specific binding site. In this regard, it is still not clear whether efficient oxidation of Mn^{2+} is possible at another site besides the HAS. Other sites are similar distances from the oxidant, Y_Z, and current models for the water oxidation reaction propose oxidation at Mn1. One weakness with the hypothesis is that bridge formation chemistry is expected to be faster than the 100-200 ms time range of the dark rearrangement (Sorokin 2019) so I consider this hypothesis less likely.

Another potentially interesting hypothesis involves the ion translocation mechanism from the HAS (Bao *et al.* 2016, Zhang *et al.* 2017). The Mn^{3+} ion produced as the first unstable intermediate (**B**) in a form of [Mn^{3+}-(OH^-)-Ca^{2+}] ⇌ [Mn^{3+}-(O^{2-})-Ca^{2+}] oxide ion (Tyryshkin *et al.* 2006) is proposed to diffuse from the HAS and migrate to a second binding site of higher affinity than at the HAS, but that this unbinding-rebinding is relatively slow and accounts for the rearrangement time. Thus, the slow rate of **B→C** is hypothesized to be due to slow unbinding of the first photooxidized Mn from the HAS and, its rebinding to a second site. By vacating the HAS, a second

Mn^{2+} can be oxidized **C→D** promoting the formation of a second bridge to produce the expected di-μ-oxo bridge of the intermediate **D**, perhaps with another translocation(s) out of the HAS to allow further photoassembly progress.

With the recent cryoEM structures of apo-PSII, it seems highly likely that the slow or infrequent movements of the CP-43 E-loop and D1-c-terminus are the main basis for the dark rearrangement, but such protein conformational changes may also involve one or more of the other proposed mechanisms to account for the slowness of the dark rearrangement, since these are not mutually exclusive. In Chapter 3, I suggest that the allosteric interaction between Psb27 and CP-43 E-loop is involved in the dark rearrangement during the photoactivation. Thus, movements of the E-loop are likely coupled to movements of the C-terminal domain, and *vice versa*. The E-loop is connected to the membrane intrinsic portion of the protein via a narrow neck that potentially gives the domain mobility to accommodate the assembly/disassembly of the WOC by rocking in and out of contact with the Mn assembly site (Burnap 2004) and these postulated structural fluctuations may be part of the dark rearrangement.

2.4.5 High affinity site

The location of the high affinity site (HAS) is still a matter of debate. As discussed earlier, the initial Mn^{2+} oxidation occur at the specific oxidation site or the HAS. Most of the experiments analyzing the Mn-binding characteristics at the HAS utilize the unique feature of Mn^{2+}, which is the ability to provide an electron to Y_z^+. The PSII crystal structure have shown that D1-Asp170 provides coordination for Mn(4) in intact WOC (**Fig. 3**) (Umena *et al.* 2011). Mutagenesis experiments carried out by several research groups revealed that D1-Asp170 supports the assembly of the WOC with the strongest affinity for Mn^{2+} in apo-PSII and can deliver an electron to Y_z^+ with high efficiency (Boerner *et al.* 1992, Nixon *et al.* 1992, Nixon *et al.* 1992, Chu *et al.* 1994, Cohen *et al.* 2007). Although, most of the mutants at D1-Asp170 perturb the electron donation from Mn^{2+} to Y_z^+, mutants are still capable of photooxidizing Mn^{2+}, however with lower efficiency (Diner *et*

al. 1992, Nixon *et al.* 1992, Chu *et al.* 1994). Several mutational substitutions (His, Glu, and Val) can even assemble functional WOC (Diner *et al.* 1992, Nixon *et al.* 1992, Chu *et al.* 1994), but again, with lower efficiency (Hwang *et al.* 2007). Biochemical experiments that tested the binding affinity for Mn^{2+} revealed a range of K_D values from 0.1 μM to 40 μM in non-equilibrium and equilibrium assays (Hsu *et al.* 1987, Diner 2001). Mn^{2+} K_D has strong pH dependence (pK_a 6-7) suggesting that an amino acid residue(s) with near neutral pK_a value is implicated in the binding of Mn^{2+} (Ono *et al.* 1999). The initial ligation and photooxidation of Mn^{2+} at the HAS is independent from Ca^{2+}, however, Ca^{2+} seems to be important for the formation of the first Mn^{3+} photoactivation intermediate (Tyryshkin *et al.* 2006). This observation is especially interesting considering the carboxyl group of D1-Asp170 provides one monodentate ligand, D1-Asp170, and one Ca^{2+} cation, and thus bridges both metals in the intact Mn_4CaO_5 of PSII (Umena *et al.* 2011).

According to the crystal structure (Umena *et al.* 2011), Mn(4) is coordinated by D1-Asp170 and D1-Glu333. However, the role of Glu333 as the ligand for the high affinity site is not evident in experiments assaying the binding Mn^{2+} by apo-PSII (Cohen *et al.* 2007). The mutations of Glu333 do not show any significant effect on initial binding and photooxidation of Mn^{2+} with subsequent electron donation to Y_z^+ (Nixon *et al.* 1994, Cohen *et al.* 2007). Progressive fluorescence quenching in the corresponding mutants indicate a low fraction of photooxidized Mn ions in the PSII centers, suggesting that mutations at D1-Glu333 position perturb the assembly of the WOC (Chu *et al.* 1995). The results suggest that D1-Glu333 potentially could provide a weak coordination for Mn^{2+} initially bound to the HAS, however this ligation is not crucial for the photooxidation of the Mn^{2+} and could be substituted by other amino acid residues. Pulsed electron-electron double resonance (PELDOR) experiments support the hypothesis regarding the location of the HAS at Mn(4) position where the first photooxidized Mn^{2+} found to be coordinated with axial ligands from Asp170 and Glu333 (Asada *et al.* 2015). However, that same study concluded that the alternative coordination could be Asp170 and Glu189. Recent cryoEM structures of apo-

PSII lacking the Mn cluster indeed show that Glu333 far from its final position in the assembled WOC. Although the authors favored coordination by Asp170 and Glu333, they noted that their data also supported a "…site between Glu189 and Ala344. Although the position between Glu189 and Ala344 is not the position for any Mn or Ca atoms in the native crystal structure and the distance between the amino acids is slightly long, Mn^{2+} might bind to these amino acids if there is a structural modification" (Asada *et al.* 2015). Taken together, these results suggest that although the ability photooxidize Mn^{2+} is retained in mutants of D1-Glu333, the subsequent assembly of the full Mn_4CaO_5 is not possible. As I will show later, these observations are also consistent with the recent cryoEM structures of the apo-PSII lacking the Mn_4CaO_5, where considerable structural rearrangements occur upon the loss of the Mn_4CaO_5 (Gisriel *et al.* 2020, Huang *et al.* 2021).

Structural modeling work utilizing a QM/MM computational approach suggested the location of the HAS to be either at Mn1 or Mn2 binding sites (Nakamura *et al.* 2019). The computational experiments agree with the later experimental ESEEM data, showing that the initial Mn^{2+} binding and photooxidation occur at the N-donor ligand, assuming D1-His332 or D1-His337 (Dasgupta *et al.* 2007). One should carefully evaluate these results. In the experimental procedures a relatively high concentration of Mn^{2+} (120 μM) was used, which might be sufficient to occupy the secondary Mn bindings site. New cryoEM results on the structure of the WOC in apo-PSII structures show considerable deviations in the 3D arrangement of Mn cluster ligands, compared to the assembled WOC (Gisriel *et al.* 2020, Huang *et al.* 2021). Importantly, D1-Glu333 is shifted away from its final position as a monodentate ligand of Mn(4) in the assembled WOC. Given these structural results, it is possible that the HAS is located between D1-Asp170 and D1-Glu189, which is closer to D1-His332 even in the apo-PSII structure. Therefore, the HAS potentially involves D1-His332 as suggested by the modeling and ESEEM results. Therefore, the HAS potentially involves D1-His332, as suggested by the modeling and ESEEM results. Computational modeling also revealed that the strongest ligation of Mn^{2+} could be achieved when both Asp170 and Glu333 are ionized

and the K_D for Mn^{2+} ligation increase when Glu333 is protonated (Vinyard *et al.* 2019). The calculations suggest that D1-Asp170 will always be fully ionized, while ionization of D1-Glu333 is pH dependent, consistent with the strongly pH dependent affinity for Mn^{2+} (Ono *et al.* 1999). Summing up, the HAS minimally involves coordination by D1-Asp170 as originally shown (Diner *et al.* 1992, Nixon *et al.* 1992, Chu *et al.* 1994), yet there is still debate about the other residues involved. To help resolve this question I address the question in Chapter 5, by testing the involvement of D1-Glu189 in the assembly of the Mn_4CaO_5 as suggested by the most recent structural results on apo-PSII (Gisriel *et al.* 2020, Huang *et al.* 2021).

2.5 Photoactivation cofactors

2.5.1 Proteins affecting the assembly of the Mn_4CaO_5

Three extrinsic polypeptides, PsbO, PsbV, and PsbU, serve to enclose and stabilize the cyanobacterial WOC, whereas plants and certain eukaryotic algae possess PsbO, PsbQ, and PsbP. Access to the Mn_4CaO_5 is provided by channels allowing permeation of substrate H_2O and release of the product O_2 and protons [for review see (Roose *et al.* 2016)]. The extrinsic polypeptides prevent the reduction of the Mn cluster by exogenous reductants (Tamura *et al.* 1985, Mei *et al.* 1991, Mei *et al.* 1992) and help retain the Ca^{2+} cofactor, which is otherwise prone to loss during the catalytic cycle (Boussac *et al.* 1988, Miqyass *et al.* 2008). However, by enclosing the WOC, accessibility of ions for the photoactivation of the Mn_4CaO_5 may be restricted. Indeed, the most efficient *in vitro* photoactivation procedures either explicitly or coincidentally involve the biochemical removal of the extrinsic proteins and genetic deletion of the most evolutionarily conserved extrinsic protein, PsbO, to increase the quantum efficiency of photoactivation (Burnap *et al.* 1996, Bao *et al.* 2016). Proteomic analysis of highly intact cyanobacterial PSII revealed novel proteins, including a small protein designated Psb27, apparently associated with PSII sub-populations (Kashino *et al.* 2002). Psb27 was identified as a lipoprotein associated with inactive PSII monomers that prevents binding of PSII extrinsic subunits (PsbO, PsbU and PsbV) to the

immature PSII (Nowaczyk *et al.* 2006). Analysis of mutants led to the conclusion that Psb27 prevents premature binding of extrinsic proteins to PSII and keeps the active site "open," thereby maintaining a sufficient diffusion rate of Mn^{2+}, Ca^{2+} and Cl^{-} ions. Thus, it acts as a molecular chaperone for successful photoactivation (Roose *et al.* 2008) through a specific interaction with the E-loop of CP43. Overall, Psb27 appears to be broadly associated with organisms possessing PSII and is important for its assembly (Chen *et al.* 2006, Bentley *et al.* 2007, Liu *et al.* 2011, Komenda *et al.* 2012). Role of Psb27 will be discussed in detail in Chapter 4.

Another potentially interesting and intriguing photoactivation cofactor is a periplasmic tetratricopeptide repeat (PratA) suggested to be involved in early stages of PSII biogenesis (Klinkert *et al.* 2004). PratA was proposed to form the so-called "PratA defined membranes" (PDM) where the biogenesis of PSII was proposed to take initial steps (Schottkowski *et al.* 2009, Rast *et al.* 2015). The deletion of the PratA resulted in impaired pD1 processing by CtpA and significantly affected the biogenesis of PSII. Yeast two-hybrid experiments indicate that PratA recognizes D1 C-terminus in both precursor and mature D1 protein, suggesting that the D1 protein is recognized by PratA not at the 16 amino acid extension but within longer 52 amino acid extension in mature D1 protein. This D1-processing phenotype of the ΔpratA mutant suggests that PratA may function as a scaffolding protein recruiting the S-terminal protease, CtpA, to its site of action. PratA is involved in formation of two soluble protein complexes in periplasmic space. Interestingly, the 200 kDa complex was not affected by the absence of D1, while the formation of a smaller 70kDa complex depends on the presence of D1 protein (Schottkowski *et al.* 2009). These results indicate on the PratA involvement in PSII biogenesis; however, the exact mechanism and purpose of this cofactor requires thorough investigation.

2.5.2 Central role of Ca^{2+}

While the role of Mn in photoactivation is well-studied, the function of Ca in photoassembly remains poorly understood. Early work establishing the role of Ca^{2+} in H_2O-oxidation showed that

it was possible to biochemically remove and restore Ca^{2+}, especially when the extrinsic proteins were removed. Detergent isolated thylakoid membranes depleted of the 17kDa and 23kDa proteins lost Ca^{2+} in a light-dependent manner and their activity was restored after incubation with 15 mM Ca^{2+} (Miyao *et al.* 1984, Nakatani 1984). It is important to note that the Mn atoms of the Mn_4CaO_5 were retain in this biochemical treatment and that it was the Ca^{2+} that was lost after the wash step that removed the17kDa and 23kDa proteins. The optimized incubation protocol showed that much lower Ca^{2+} concentration is required for efficient restoration of oxygen evolving activity (Ghanotakis *et al.* 1984). These early experiments determine that Ca^{2+} was required for H_2O-oxidation, but its catalytic role remained a mystery. More recently, the catalytic function of Ca^{2+} in H_2O-oxidation appears to be coordinating and delivering substrate water molecules into position where they are oxidized (Ibrahim *et al.* 2020).

While there was general agreement that Ca^{2+} is required for water splitting by PSII, the role of Ca^{2+} in photoactivation was a matter of a debate. Pioneering experiments with isolated chloroplasts depleted of Mn, showed that the activity of WOC was restored only in presence of both Mn^{2+} and Ca^{2+} ions (Yamashita *et al.* 1976, Ono *et al.* 1983, Pistorius *et al.* 1984). Similar evidence was obtained by other groups. It has been suggested by Tamura and Cheniae that Ca^{2+} is not required for the photoassembly of the Mn cluster. During the photoactivation under continuous light without Ca^{2+}, the abundance of Mn^{2+} ions was approximately 4 Mn per 200 chlorophylls, which suggests that photoligation of Mn ions is independent of Ca^{2+} (Tamura *et al.* 1989). Later it has been shown that Ca^{2+} is absolutely required for the photoactivation (Chen *et al.* 1995). In this work Chen and coworkers have shown that the result showed by Tamura and Cheniae was an artefact caused by the high concentration of DCIP (an artificial electron acceptor) that apparently served as a reductant for the improperly assembled Mn cluster in absence of Ca^{2+}. The experiments executed with lower concentration of DCIP showed that during the photoactivation without Ca^{2+} the abundance of EDTA non-extractable and nonfunctional multinuclear (>18Mn per PSII) high-valent Mn deposits

resulting from non-productive oxidation of Mn^{2+}. However, the addition of Ca^{2+} or DCIP facilitated the removal of nonfunctional Mn ions from WOC. The results with high concentration of DCIP suggested that improperly assembled Mn cluster could be removed by the reduced $DCPIPH_2$ formed during the experiment. Overall, these results suggest that at least one role of Ca^{2+} is guiding the assembly by blocking inappropriate binding of Mn^{2+} to the Ca^{2+} binding site (Chen *et al.* 1995) and preventing the formation of Mn multinuclear aggregates. The relation between Mn^{2+} and Ca^{2+} and their corresponding binding sites during photoactivation appears to be complex. Several groups have shown mutual competition between Mn^{2+} and Ca^{2+} for their binding site (Cheniae *et al.* 1971, Radmer *et al.* 1971, Ono *et al.* 1983, Tamura *et al.* 1987, Miller *et al.* 1989, Ananyev *et al.* 1996, Zaltsman *et al.* 1997).

2.5.3 Role of HCO_3^- and Cl^-

The role of bicarbonate in photoassembly is still a matter of debate. Two HCO_3^- binding sites were identified that stimulate the formation of and stabilize the first photoactivation intermediate, **"A"** [apo-WOC-Mn $(OH_2)^+$], however the effects were very subtle. The HCO_3^- binding to the first binding site happens at high affinity (K_D <10 μM) and decreases the time required for the formation of the first photoactivation intermediate, **"A."** Interestingly, the observed effect was assumed to be achieved via enhanced binding of the initial Mn^{2+} to the HAS and occurs only at $[Mn^{2+}]$ at or below the stoichiometric requirement for the formation of the WOC. The second bicarbonate site has much lower binding affinity (millimolar range) and the positive effect occurs only at low $[Ca^{2+}]$, suggesting that HCO_3^- shifts the Mn^{2+}/Ca^{2+} competition towards Ca^{2+} (Baranov *et al.* 2000). In the following work it has been shown that HCO_3^- is involved in the formation of a $[Mn^{2+}(HCO_3^-)]$ intermediate that could be easier photooxidized compared to the aqueous $[Mn^{2+}\text{-}(OH_2)_6]$. The proposed $[Mn^{3+}(HCO_3^-)]$ photoactivation intermediate has a longer lifetime and prevents light induced damage to the apo-PSII. The effect of HCO_3^- addition caused modest but statistically significant increase in both rate and yield of photoassembly (Baranov *et al.* 2004). Bicarbonate is

required to supply the proton for the formation of Q_BH_2 from $Q_B^{2-}(H^+)$ (Forsman *et al.* 2020). It is possible that the stimulation of the photoactivation in the presence of bicarbonate is at least partially caused by the efficient formation of Q_BH_2, preventing charge recombination and loss of photoactivation intermediates.

Cl^- enhances photoactivation, but the mechanism of action is unresolved. It appears that the effect of Cl^- on photoactivation is distinct from its effect on Mn_4O_5Ca stabilization in the absence of the extrinsic proteins (Miyao *et al.* 1985). Removal of Cl^- from intact PSII forms a salt bridge between D2-K317 and D1-D61 (Pokhrel *et al.* 2011), which potentially slows down the proton release from D1-D61 (Pokhrel *et al.* 2013) during the Mn^{2+} photooxidation at the HAS. Cl^- increases the proton affinity (pKa's) of D1-D61, D1-E333 and CP43-E354 amino acid residues apo-PSII (Vinyard *et al.* 2019). These results suggest that Cl^- shifts the pKa of critical residues in ways that promote photoactivation and/or may prevent the electrostatic repulsion of the amino acid residues of the apo-PSII coordination environment. During photoactivation these protons must be removed prior to Mn ligation and formation of μ-oxo/μ-hydroxo bridges. Interestingly, high chloride shortens the photoactivation lag, assigned to the decay of intermediates "B" and "C" in the early phases of the WOC assembly. The replacement of H_2O with D_2O caused a dramatic decrease in Cl^- requirement and eliminated the photoactivation lag.

2.6 Mn^{2+} and Ca^{2+} competition

Both Mn^{2+} and Ca^{2+} support photoactivation at low concentrations, however the excess of Mn^{2+} inhibits photoassembly. The inhibitory effect of high $[Mn^{2+}]$ can be mitigated by increased Ca^{2+} concentration. Both Mn^{2+} and Ca^{2+} were proposed to behave as competitive inhibitors at the corresponding binding sites (Cheniae *et al.* 1971, Ono *et al.* 1983, Tamura *et al.* 1986, Tamura *et al.* 1987, Miller *et al.* 1989, Chen *et al.* 1995, Zaltsman *et al.* 1997). Using the Ca^{2+}-specific ionophore A23187 revealed the existence of two specific metal binding sites corresponding to Mn^{2+} and Ca^{2+} (Ono *et al.* 1983). The Ca^{2+}-dependent photoactivation was inhibited by Mn^{2+}, Mg^{2+} or

Sr^{2+}, while Mn^{2+}-dependent photoactivation was inhibited by high [Ca^{2+}]. Increased concentration of Ca^{2+} or Mn^{2+} respectively restored photoactivation activity . However, the metal dependent photoactivation was carried out in intact chloroplasts, which might interfere with Mn^{2+} and Ca^{2+} ion transport and potential presence of secondary Ca^{2+} binding sites. Competition between Mn^{2+} and Ca^{2+} for the Mn^{2+} site is very weak (Miller *et al.* 1989). On the other hand, the competition for the Ca^{2+} binding site at higher than optimal [Mn^{2+}] leads to photoinactivation caused by inappropriately bound Mn^{2+}. Photoinactivation occurs at the same time as photoactivation and in principle lowers the overall photoactivation yield by the fraction of PSII centers with inappropriately bound Mn^{2+} to the Ca effector site (Miller *et al.* 1989). The photoactivation model assumed that all metal ions in solution bind reversibly in competition with one another at both Mn-binding sites and Ca^{2+}-binding site. In Chapter 3 the competition between Mn^{2+} and Ca^{2+} is re-examined in cyanobacterial thylakoid membranes depleted from the Mn. Competition between Mn^{2+} and Ca^{2+} for the corresponding binding sites leads to decreased quantum efficiency and yield of photoactivation. Competition between the ions also occurs in intact PSII, where high abundance of Mn^{2+} in the photoactivation buffer led to similar activity loss during photoactivation in sub optimal Ca^{2+}/Mn^{2+} ratio. If the competition for the Ca^{2+} binding site is more or less understood, the location where the competition happens for the Mn binding site has not been discussed before. The photoactivation experiments at 250 µM and 500 µM Mn^{2+} at different [Ca^{2+}] suggests (i) Ca^{2+} competes with Mn^{2+} not at the HAS, rather at the second Mn binding site involved in the photoactivation pathway, and (ii) excess Ca^{2+}, while protecting from photoinactivation, inhibits assembly due to occupation of the SMS, preventing photooxidation of the second Mn^{2+} (**C→D**). K_m values for Mn^{2+} at the HAS are less then 10 µM (Nixon *et al.* 1992, Ananyev *et al.* 1996, Ono *et al.* 1999), further supporting this conclusion. The presented experiments cannot discriminate what the site is, though it is reasonable to suppose it involves ligands that form with the other Mn1-Mn3 positions.

2.7 Thesis focus

The presence of oxygen in Earth's atmosphere allows the existence of all aerobic life on a planet. Photosystem II of cyanobacteria, algae and plants is a unique reaction center capable to use water as an electron donor, which results in a production of molecular oxygen released into Earth's atmosphere. While the mechanism of water splitting driven by the light-induced charge separation is relatively well studied and high-resolution crystal structures are available to reveal the molecular aspects of PSII complex (Umena *et al.* 2011), however considerably less is known about how the inorganic Mn_4O_5Ca cluster is assembled *de novo*.

The main aim of this thesis is to understand the mechanism of the light-driven assembly of the Mn cluster. While it is unlikely that in the very near future, the scientific community will be able to precisely map all events happening during the assembly of the WOC, this study aims to significantly resolve several photoactivation aspects that to date remain poorly understood. This thesis focuses on four aspects of photoactivation: a) the role of Ca^{2+}, b) the role of accessory protein Psb27, c) the nature of the rate-limiting dark rearrangement, and d) test the hypothesis that D1-E189 is an important ligand in the formation of the HAS of photosystem II, and thus in the assembly of the Mn_4CaO_5.

To address the role of Ca^{2+} and set the foundation for kinetic analysis of photoactivation in mutants, I further developed a novel *in vitro* photoactivation system in the cyanobacterium *Synechocystis sp.* PCC 6803. This allows to the study of photoactivation in thylakoid membranes obtained from cyanobacterial cells, including mutants, and tightly controlled experimental conditions, e.g., ion concentration and pH. To better mimic natural photoactivation, we removed the protein cap formed on the luminal side of PSII by three extrinsic proteins, PsbO, PsbV and PsbU, known for blocking WOC site and restricting ion access inside PSII. To develop such a system, we overexpressed Psb27 protein that is suggested to prevent PsbO protein from binding to PSII, resulting in dissociation of the entire protein cap. The rationale for this approach is that the

natural steady-state abundance of Psb27 in the cell likely evolved to cope with assembly and repair of only a fraction of centers from the total population of PSII in the cell. Thus, there may not be enough copies of Psb27 to stoichiometrically service all PSII centers upon quantitative removal of the Mn cluster experimentally produced by HA-extraction.

My broad working hypothesis was that Ca^{2+}, Psb27 and dark rearrangement are all interconnected during the assembly of the WOC of photosystem II. As described in Chapter 4, Psb27-CP43 interactions seem to stabilize Ca^{2+} binding to its effector site, which in turn stabilizes photoactivation intermediates formed immediately after the first photooxidation event at the HAS. Stabilization of labile intermediates seems to allow them to persist throughout the slow dark rearrangement event, which we suggest represents D1/CP43 protein conformational change resulting in disordered-ordered structural change of C terminus of D1 protein.

To address the role of D1-E189 ligand in the formation of the HAS, we investigated the ability of D1-E89Q, D1-E189K and D1-E189R mutants to restore O_2 evolution activity after treatment with hydroxylamine in comparison to the D1-D170E mutant, known to dramatically affect HAS activity. We have shown that D1-E189K and D1-E189R mutants tend to accumulate a significant portion of inactive PSII centers over the course of the photoactivation experiment. Fluorescence relaxation kinetics experiments identified a decay of oxidized, but yet unstable Mn at the donor side of these mutants, which slowed fluorescence decay kinetics, while no decay was observed in WT control. I hypothesize that the D1-E189 ligand participates in the formation of the HAS, but as a structural ligand rather than a redox active residue. An alternative hypothesis involves the coordination of Ca^{2+} by D1-E189 during the initial photoactivation steps, which prevents the accumulation of inappropriate Mn during the light-driven oxidation on Mn^{2+}.

CHAPTER III

EXPERIMENTAL PROCEDURES

3.1 Cultures and growth conditions

Wild type *Synechocystis sp.* PCC6803 (WT) and all mutants produced from WT were maintained in solid BG-11 medium (Allen 1968), pH 8 supplemented with 10 mM HEPES-NaOH, 5 mM glucose and 10 μM DCMU (3-(3,4-dichlorophenyl)-1,1-demethylurea). Mutations within PSII are often lethal because of the essentiality of PSII for autotrophic growth. To permit the growth of otherwise lethal mutants, the growth media was supplemented with glucose as sole carbon source. The addition of DCMU to the growth media ensures absence of PSII activity and removes the growth advantages associated with reversed or/and random mutations in the strains with mutated PSII genes. All *Synechocystis sp.* mutants were inoculated in 100 mL of BG-11 media with addition of 5 mM glucose and no DCMU in 250 Erlenmeyer flasks on a rotary shaker (~180 rpm) under ~80 μmol m^{-2} s^{-1} PFD (photon flux density) provided by Cool White fluorescent lamps. PFD measurements were made with a ULM-500 Walz light meter (Germany).

Log phase starter 100 mL cultures were used to inoculate experimental cultures in flat 1L tissue culture flasks in 800 mL BG-11 media buffered with 10 mM HEPES-NaOH pH 8.0 (HBG-11) supplemented with 5 mM glucose (Sigma) under a PFD of ~200 μmol m^{-2} s^{-1} at 30 °C and were bubbled with filter sterilized air. Inoculated 100 mL cultures were pelleted at 6000 g in a Sorvall F14 rotor and resuspended in a minimal volume of fresh BG-11 media. The OD_{750} of resuspended cells was measured using UV-2600 UV-Vis Scanning Spectrophotometer, Shimadzu, Japan. Experimental 800 mL cultures were inoculated to OD_{750} ~0.05

3.2 Strains and molecular constructs

The glucose-tolerant *Synechocystis* sp. PCC6803 control strain (WT-control) expressing only the wild-type *psbA2* gene and having a hexa-histidine tag fused to the carboxyl-terminus of CP47 was maintained in BG-11 medium as described previously (Debus *et al.* 2001). All mutants are listed in Table 1. The Δ*psbO* deletion mutant was constructed previously and involved replacement of the *psbO* coding sequence with a Sp^r/Sm^r antibiotic resistance gene (Burnap *et al.* 1991). Mutant strains of *Synechocystis sp.* D1-E189Q, D1-E189K, D1-E189R and D1-D170E (**Table 1**) were obtained as a kind gift from Rick Debus, and the construction of these mutants is described earlier (Chu *et al.* 1994) using *psbA2* containing plasmid pRD1031 and the triple *PsbA* deletion strain 4E-3. For some of my studies, PCR was used to amplify the chromosomal regions containing the desired mutant genes, plus the adjacent DNA encoding the antibiotic selection gene, and used to transform into another host. In this way, it was possible the reconstruct the site-directed mutations in a variety of genetic backgrounds.

For overexpression of the Psb27 gene in *Synechocystis*, the chromosomal locus comprising the open reading frame slr1645 (Psb27) was amplified by PCR using Herculase II Phusion DNA polymerase (Agilent, USA) and integrated at a neutral site within the *Synechocystis* genome between ORFs slr1169 and slr1285. Transformation was carried as described previously using selective agar plates containing 5 mM glucose, 10 µM DCMU, and 12.5µg/mL spectinomycin followed by further selection at 25µg/mL spectinomycin (Williams 1988).

Table 1. List of mutants used in the study

Strain Name	Resistance	Description
HT-3 (4E-3) WT-control	Sp, Gm	WT control with only one copy of PsbA gene
27OE	Km, Sp, Gm	WT-control overexpressing Psb27 protein
D1-E189K	Km, Gm	Glutamic acid substituted with lysin at position 189 of D1 protein (PsbA gene)
D1-E189Q	Km, Gm	Glutamic acid substituted with glutamine at position 189 of D1 protein (PsbA gene)
D1-E189R	Km, Gm	Glutamic acid substituted with arginine at position 189 of D1 protein (PsbA gene)
D1-D170E	Km, Gm	Aspartic acid substituted with glutamic acid at position 170 of D1 protein (PsbA gene)

3.3 Chlorophyll concentration

To measure chlorophyll concentration in cells, the cell suspension was typically diluted 10-fold in ddH_2O. The [Chl] was determined by measuring absorption spectrum at 620, 678 and 750 nm in a 1 cm pathlength cuvette. The chlorophyll concentration was calculated as previously described in (Williams 1988):

$$[Chl] = (14.96 \times (A_{678} - A_{750}) - 0.607 \times (A_{620} - A_{750}))$$

The chlorophyll concentration in thylakoid membranes was determined using methanol extracted chlorophyll. Typically, 10 µl of thylakoid membranes were diluted in 990 µl of 100% methanol and centrifuged for 3 min at 13000 g to separate thylakoids from extracted chlorophyll. The absorption at 665 nm was measured in 1 cm quartz cuvette, the concentration was calculated using methanol extinction coefficient of 12.5.

3.4 Isolation of thylakoid membranes

Synechocystis sp. PCC6803 oxygen evolving thylakoid membranes were isolated at 4°C under dim green light. Cells were harvested at 10000 g and washed in HN buffer [30 mM NaCl, 50 mM HEPES-NaOH, pH 7.3]. Washed cells were harvested at 12000 g and suspended in a PSII breakage buffer [1.2 m betaine, 50 mM MES-NaOH (pH 6.0), 10%(v/v) glycerol, 5 mM $CaCl_2$ and 5 mM

$MgCl_2$]. Cells were concentrated in ~120 mL of PSII breakage buffer and kept at 4°C in dark for 1 hour. Prior to cell breakage, 1 mM benzamidine, 1 mM ε-amino-n-caproic acid, 1 mM PMSF, and 0.05 mg/mL DNase I were added to the cell suspension and then cells were broken by nine cycles of 15 s ON and 5 min OFF in a glass bead homogenizer (Bead-Beater, BioSpec Products, Bartlesville, OK). After breakage, the sample was centrifuged at 5000 g to separate unbroken cells and cell debris. The supernatant containing a mix of thylakoid membranes and soluble proteins were concentrated by ultracentrifugation (35 min at 40000 rpm in a Beckman Ti45 rotor) and suspended in PSII storage buffer [1.2 M betaine, 50 mM MES-NaOH (pH 6.0), 10% (v/v) glycerol, 20 mM $CaCl_2$ and 5 mM $MgCl_2$] to a concentration of 1.0-2.0 mg of Chl/mL. Concentrated thylakoid membranes from wild-type cells were flash frozen in 5-7 mL aliquots in liquid nitrogen and stored at -80°C. In cases where PSII particles were being produced, the D1-V185N thylakoid membranes were immediately used for PSII core complexes preparation without freezing.

3.5 SDS PAGE and Immunoblot analysis

Membrane samples obtained as above were solubilized by addition of 2% SDS and 5 mM dithiothreitol, heated at 65 °C for 10 min, and separated on SDS-PAGE (8% stacking, 12% resolving, 0.75 mm thick). Prior to loading in the gel, samples containing thylakoid membranes (0.5 or 1 µg chlorophyll) was mixed with 2x sample buffer (125 mM Tris-HCL pH 7.5, 20% glycerol, 2% SDS, 0.02% bromophenol blue, 5% ß- mercaptoethanol). Gel electrophoresis was carried out at RT at 100 V for 2 hours. PVDF membrane was soaked in Towbin buffer (25 mM Tris, 192 mM glycine, 20% methanol) for 15 minutes prior the protein transfer from the SDS gel. Protein content was transferred to a PVDF membrane using a Bio-Rad (USA) semi-dry apparatus, and membrane was stained with 0.5 % Ponceau S (Sigma) to verify equal loading. Ponceau S-stained gel was washed with water and 5% BSA (bovine serum album) solution in TBS-T (50 mM Tris-HCl, 150 mM NaCl, 0.2 % Tween 20, pH 7.5) was used as a blocking agent for 45 minutes. Blots were probed using antibody against Psb27 protein (1:750 dilution, a kind gift from Julian

Eaton-Rye) as a primary antibody in 5% BSA in TBS-T at RT shaking at ~100 rpm for 12 to 16 hours. Membranes were washed three times in TBS-T for 15 minutes and anti-rabbit HRP-conjugated goat antibody (1:3000, Bio-Rad) was used for 2 hours as a secondary antibody in 5% BSA in TBS-T. After incubation with secondary antibody PVDF membranes were washed two times with TBS buffer (50 mM Tris-HCl, 150 mM NaCl, pH 7.5) for 15 minutes. Color Development was obtained in 100 mL solution containing 60 mg of 4CN (4-chloro-1-naphthol (Bio-Rad), 20 mL methanol 60 µL 30% H_2O_2 in TBS buffer. The color development was terminated approximately after 10-15 minutes by washing with water, obtained PVDF with corresponding protein bands were photographed and stored dried in dark.

3.6 Oxygen evolution rate measurements

Maximal rates of O_2 evolution from photoactivated samples or cells/thylakoids with intact WOC were determined polarographically at 30°C in a 1.8 mL Clark-Type electrode chamber. Prior to the measurements, 100 mL of BG-11 was warmed to 30°C in the water bath. The electrode chamber was filled in the dark first with BG-11, then 0.8 mM DCBQ and 1 mM potassium ferricyanide were added to the chamber. Without delay, a sample containing 10 µg Chl was added to a chamber to bring the volume to 1.8 mL. Oxygen evolution rate was measured under saturating red light (>620 nm).

3.7 Preparation of the Mn-depleted *Synechocystis sp.* cells

For every experimental culture, variable fluorescence $F_v/F_0 = ((F_m-F_0)/F_0)$ was measured with a PSI fluorometer (Walz, Germany). Only cultures with F_v/F_0 equal or higher than 0.5 (WT) or 0.4 (mutants) were used for further experiments. Cultures in a late log/early stationary state were harvested by centrifugation at 25 °C at 6,000 *g* (Sorvall, F-14 rotor). Cells were resuspended using a paintbrush in ~35 mL of standard BG-11 and centrifuged at 10400 g for 5 minutes as a washing step. Cells then were again resuspended in minimal volume of BG-11 media, and the cell suspension was brought to 100 µg Chl mL^{-1}. Hydroxylamine (H_3NO) was added to a cell suspension

to a final concentration of 1 mM from freshly prepared 100 mM stock; the sample then was kept at room temperature on a rotary shaker in the dark for 12 minutes at ~120 rpm. After dark incubation, cells were washed five times with 5x volume of BG-11 for 5 minutes on a shaker followed by the centrifugation at 10400 g for 5 min at RT. After the final wash, cells were resuspended to a final [Chl] of 100 μg mL^{-1} and kept in the dark with the gentle shaking.

3.8 Preparation of the Mn-depleted thylakoid membranes

Cultures (2.4 L) were harvested in early stationary phase (OD_{750nm} ~1.8-2.2) and exhibited variable Chl fluorescence ((F_m - F_0)/F_0) values >0.5, as measured with a Photon Systems Instruments (PSI) Fluorometer FL 3500. Cells were collected by centrifugation at 25 °C at 6,000 g (Sorvall, F-9 rotor) for 15 min and gently resuspended with a minimal volume of H20BG-11(same as growth media, but with 20 mM HEPES-NaOH pH 8.0) using a paintbrush. The cell suspension volume was expanded to ~200 mL with additional H20BG-11. The washed cells were centrifuged again at 25 °C at 10200 g for 5 min (Sorvall, F-14 rotor). The pelleted cells were resuspended as before in H20BG-11 medium, and the suspension was adjusted to a Chl concentration of 100 μg mL^{-1} Chl. Hydroxylamine (HA) was added to 1 mM from a freshly prepared 400 mM stock, and the treated suspension was incubated for 12 min in the darkness with rotary agitation (200 rpm) at room temperature. Maintaining complete darkness, the HA-extracted cells were then washed by resuspension with 100 ml H20BG-11 and rotary agitation (200 rpm) for 5 min before pelleting again. This washing step was repeated four more times with the aim of depleting residual HA. Finally, the cells were resuspended in 120 ml of breaking buffer (1.2 m betaine, 50 mM MES-NaOH (pH 6.0), 10%(v/v) glycerol, and 5 mM $MgCl_2$) that was prepared with ultrapure reagents and Chelex-100 (Bio-Rad)-treated solutions and incubated in the dark on ice for 1 hour. Cells were pelleted at 10,200 g for 5 min and resuspended to a total volume of 14 mL. Prior cell breakage, 1 mM benzamidine, 1 mM ε-amino-n-caproic acid, 1 mM PMSF, and 0.05 mg/mL DNase I were added. Cells were broken by four cycles of 5 sec ON and 5 min OFF in an ice-cooled glass bead

homogenizer (Bead-Beater, BioSpec Products, Bartlesville, OK). After breakage the sample was centrifuged at 3,600 g for 10 min to pellet unbroken cells and cell debris. Thylakoids were obtained from the supernatant cell homogenate by ultracentrifugation (35 min at 40,000 rpm in a Beckman Ti45 rotor) and thylakoid-containing pellets were suspended in Chelex-100-treated breaking buffer to a concentration of 1.0-1.5 mg Chl mL^{-1} with [Chl] determined from methanol extracts according to (Wellburn *et al.* 1984). Concentrated thylakoid membranes were flash frozen as 100 µL aliquots in liquid nitrogen and stored at -80°C.

3.9 Photoactivation of the Mn-depleted samples

HA-extracted membranes were photoactivated either in suspension for subsequent assay for restoration of O_2 evolution detected using a Clark-type electrode or directly on a bare platinum electrode that permits the centrifugal deposition of samples upon the electrode surface (Nixon *et al.* 1992). Flash illumination under each mode of photoactivation was provided using an EG&G xenon flash lamp. The buffer was supplemented with various concentrations of cations $CaCl_2$, $MnCl_2$, $SrCl_2$, and $MgCl_2$ to examine their role in photoactivation for the role of cations on photoactivation.

3.10 Fluorescence measurements

A double modulation kinetic chlorophyll fluorometer (PSI Instruments, Czech Republic) was used to measure variable chlorophyll fluorescence yields. Cells harvested in mid-log phase were harvested and concentrated to 100 µg/ml of chlorophyll. The sample was dark adapted for 5 minutes and loaded into the cuvette at concentration of 5 µg/ml of chlorophyll for fluorescence measurements. Determination of chlorophyll variable fluorescence in response to a single turnover saturating flash was performed as described earlier (Allahverdiyeva *et al.* 2004) The low fluorescence state was measured by four weak measuring flashes followed by 30 µsec saturating actinic flash. A sequence of measuring flashes beginning at 50 µsec after the actinic flash was used to probe the fluorescence relaxation after the actinic flash. Actinic flash produces so-called high

fluorescence state of PSII comprising $P_{680}^{\bullet}Q_A^-$, which is formed when excited P_{680} special chlorophyll pair donates an electron to Q_A. The rapid transfer of electron from Q_A^- to mobile plastoquinone Q_B represents the main component of fluorescence decay. The addition of DCMU blocks Q_A^- to Q_B electron transfer forcing electron from $P_{680}^{\bullet}Q_A^-$ to recombine with secondary oxidants on the donor side of PSII, mainly with S2 state of the Mn cluster. Normalized variable fluorescence was calculated as $F_v/F_0 = (F_m-F_0)/F_0$, where F_m is maximal fluorescence and F_0 is the lowest observed fluorescence level. To estimate the fluorescence relaxation kinetics obtained curves were analyzed in terms of two exponential components (fast and middle phases) and on hyperbolic component (slow phase) using $F(t) - F_0 = A_1 e\left(-\frac{t}{T_1}\right) + A_2 e\left(1 + \frac{t}{T_3}\right) + A_3 / \left(-\frac{t}{T_2}\right)$ equation (Vass *et al.* 1999), where A_1-A_3 are the amplitudes, T_1-T_3 are the time constants

CHAPTER IV

THE ROLE OF CA^{2+} AND PROTEIN SCARFFOLDING IN THE FORMATION OF NATURE'S WATER OXIDIZING COMPLEX [‡]

[‡] This chapter is reproduced with slight modifications from the following publication:

Avramov, A. P., Hwang, H. J., and Burnap, R. L. (2020) The role of Ca^{2+} and protein scaffolding in the formation of nature's water oxidizing complex. *Proceedings of the National Academy of Sciences* 117, 28036

4.1 Abstract

Photosynthetic O_2 evolution is catalyzed by the Mn_4CaO_5 cluster of the water oxidation complex of the photosystem II (PSII) complex. The photooxidative self-assembly of the Mn_4CaO_5 metal cluster, termed photoactivation, utilizes the same highly oxidizing species that drive water oxidation to drive the incorporation of Mn^{2+} into the high valence Mn_4CaO_5 cluster. This multi-step process proceeds with low quantum efficiency, involves a molecular rearrangement between light-activated steps, and is prone to photoinactivation and mis-assembly. A sensitive polarographic technique was used to track the assembly process under flash illumination as a function of the constituent Mn^{2+} and Ca^{2+} ions in genetically engineered membranes of the cyanobacterium *Synechocystis* sp. PCC6803 to elucidate the action of Ca^{2+} and peripheral proteins. We show that the protein scaffolding that organizes this process is allosterically modulated by the assembly protein Psb27, which together with Ca^{2+}, stabilizes the intermediates of photoactivation, a feature especially evident at long intervals between photoactivating flashes. The results indicate three critical metal binding sites: two Mn and one Ca, with occupation of the Ca site by Ca^{2+} critical for

the suppression of photoinactivation. The long-observed competition between Mn^{2+} and Ca^{2+} occurs at the second Mn site and its occupation by competing Ca^{2+} slows the rearrangement. The relatively low overall quantum efficiency of photoactivation is explained by the requirement of correct occupancy of these metal binding sites coupled to a slow restructuring of the protein ligation environment, which are jointly necessary for the photooxidative trapping of the first stable assembly intermediate.

4.2 Introduction

Photosystem II (PSII) utilizes solar energy to catalyze one of the most important and most thermodynamically demanding reactions in nature: the oxidation of water into protons and molecular oxygen. The electrons extracted from the substrate water molecules are transferred through the redox-active cofactors of the photosynthetic electron transport chain eventually to reduce the electron acceptor $NADP^+$, thereby forming the primary reductant for the synthesis of biomass from CO_2 and other inorganic nutrients. Thus, the H_2O-oxidation reaction is the basis of oxygenic photosynthetic metabolism and the primary driver of biomass accumulation on the planet (Vinyard *et al.* 2017, Lubitz *et al.* 2019) and represents a key chemical process for the development of carbon neutral energy technologies (Lutterman *et al.* 2009, Dau *et al.* 2017). Natural H_2O-oxidation is driven by light-induced charge separation within the PSII reaction center (RC), a 700 kDa membrane protein homodimer consisting of over 20 different subunits and approximately 60 organic and inorganic cofactors [for reviews, see (Vinyard *et al.* 2017, Lubitz *et al.* 2019)]. The catalysis of H_2O-oxidation is mediated by a metal cluster (Mn_4CaO_5) buried within the protein complex at the interface between intrinsic and extrinsic polypeptides towards the luminal surface of the photosynthetic membrane (Umena *et al.* 2011) (**Fig. 5**). Photoexcitation of the multimeric chlorophyll (Chl) P_{680}, which functions as the primary photochemical electron donor, results in the primary charge separation on a picosecond timescale into the highly oxidizing radical cation $P_{680}^{+\bullet}$ and radical anion $Pheo^{-\bullet}$ (Cardona *et al.* 2012). To minimize the backreaction or oxidation of Chl

and/or neighboring proteins, the highly reactive $P_{680}^{+\bullet}$ is re-reduced (20-250ns) by the redox active tyrosine D1-Tyr161 (Y_z) of the D1 reaction center polypeptide located on the donor side proximal to P_{680}. Meanwhile, the energized electron is stabilized by transfer from $Pheo^{-\bullet}$ through quinone acceptors (Q_A and Q_B) and on through the remainder of the intersystem electron pathway leading to photosystem I. During the course of four consecutive charge separation events, the Mn cluster passes through a series of oxidant storage states (S-states) with the catalytic cycle balanced by removing four electrons from two bound water molecules with the release of O_2 and four protons.

The PSII complex is subject to incessant photodamage and a remarkable feature is its ability to undergo self-repair. Photodamage primarily occurs within PSII and much of the damage is localized in the D1 (PsbA) protein, which binds the main redox cofactors involved in photochemical charge separation. Efficient mechanisms have evolved to remove and replace damaged reaction center proteins and assemble them with their requisite cofactors [reviewed in (Bao *et al.* 2016)]. A key step in both *de novo* synthesis and the repair synthesis of PSII, is the assembly of the Mn_4CaO_5 core into the ligation environment of the PSII protein matrix (Cheniae *et al.* 1971, Radmer *et al.* 1971, Ono *et al.* 1983, Tamura *et al.* 1987, Miller *et al.* 1989, Ananyev *et al.* 1996). Referred to as photoactivation, the assembly of the Mn_4CaO_5 occurs through a series of photochemical reactions that involve the oxidation of Mn^{2+} ions using the same electron extraction pathway of the fully mature PSII (**Fig. 6**). Charge separation oxidizes Mn^{2+} ions to $Mn^{\geq 3+}$ as the oxo-bridged multinuclear metal center forms. The multistep process begins with the binding of a single Mn^{2+} ion, (Ono *et al.* 1999) as its hydroxide (Ananyev *et al.* 1999) to a high affinity site (HAS) involving the D1-Asp170 carboxylate moiety (Boerner *et al.* 1992, Nixon *et al.* 1992). Additional Mn^{2+} ions are photooxidatively incorporated into the growing metal cluster via oxo-bridges that are presumably derived from water ligands of the incoming metal ions. The quantum efficiency of photosynthetic H_2O-oxidation in the fully functional PSII is greater than 90%, whereas the photoassembly of the metal cluster is remarkably inefficient with an overall quantum efficiency

below 1%, despite the fact that photooxidative assembly uses the same charge separation cofactors, notably the oxidized forms of the primary and secondary electron donors, P_{680} and Y_Z, respectively. To account for the low quantum efficiency and for a still-unresolved light independent 'dark-rearrangement' that must occur between two or more light-induced charge separations, a so-called "two-quantum model" (**Fig. 6**) was developed (Radmer *et al.* 1971). Experimental support for this kinetic model is comprehensive (reviewed in (Burnap 2004, Bao *et al.* 2016)), including, for example, direct evidence tracking the assembly process demonstrating a two-quantum requirement, and that part of the overall inefficiency is due to the competition between the slow and/or inefficient assembly steps and back-reactions of the charge separated state (Miyao-Tokutomi *et al.* 1992). Nevertheless, evidence regarding the structure and chemistry of the intermediates and the nature of the dark rearrangement has remained scarce.

Calcium is a critical cofactor in the process of H_2O-oxidation by PSII because it mediates the delivery of substrate water to a Mn coordination site for oxidation and dioxygen formation (Ibrahim *et al.* 2020). While an early study suggested that Ca^{2+} is not required for photoassembly of the Mn cluster (Tamura *et al.* 1989), this was later re-evaluated (Chen *et al.* 1995) and there is now general agreement that Ca^{2+} is vital (Ono *et al.* 1983, Chen *et al.* 1995, Ananyev *et al.* 1996). Nevertheless, the mechanism of how Ca^{2+} facilitates the photoassembly remains obscure. Binding of Mn^{2+} to the HAS with simultaneous binding of Ca^{2+} to an adjacent binding site facilitates the formation of the [Mn^{2+}-(OH)-Ca^{2+}] complex by inducing deprotonation of Mn^{2+} water ligand. Calcium lowers the pK_a for water ligand, which is controlled by a nearby base B^- that serves as a primary proton acceptor with a pK_a dependent on Ca^{2+} bound to its effector site (Tyryshkin *et al.* 2006). The deprotonation of the intermediates and the tuning of pK_as facilitated by Cl^- binding is critical for assembly (Vinyard *et al.* 2019). The absence of Ca^{2+} during photoactivation leads to the formation of non-catalytic, multinuclear high valent Mn species ("inappropriately bound Mn") that inactivates the PSII complex (Chen *et al.* 1995). At the same time, high concentrations of the Ca^{2+} cofactor

diminishes the efficiency of photoactivation. These results indicate that Ca^{2+} and Mn^{2+} compete for each other's binding sites, leading to an optimal relationship in their relative concentrations during photoactivation (Ono *et al.* 1983, Miller *et al.* 1989, Ananyev *et al.* 1996).

Three extrinsic polypeptides, PsbO, PsbV, and PsbU, serve to enclose and stabilize the cyanobacterial water oxidation complex (WOC), whereas plants and certain eukaryotic algae possess PsbO, PsbQ, and PsbP, [for review see, (Roose *et al.* 2016)]. The extrinsic polypeptides prevent the reduction of the Mn cluster by exogenous reductants (Tamura *et al.* 1985, Mei *et al.* 1991, Mei *et al.* 1992) and help retain the Ca^{2+} cofactor, which is otherwise prone to loss during the catalytic cycle (Boussac *et al.* 1988, Miqyass *et al.* 2008). However, by enclosing the WOC, accessibility of ions for the photoactivation of the Mn_4CaO_5 may be restricted. Indeed, the most efficient *in vitro* photoactivation procedures either explicitly or coincidentally involved the biochemical removal of the extrinsic proteins and genetic deletion of the most evolutionarily conserved extrinsic protein, PsbO, increases the quantum efficiency of photoactivation (Bao *et al.* 2016). Proteomic analysis of highly intact cyanobacterial PSII revealed novel proteins, including a small protein designated Psb27, apparently associated with PSII sub-populations (Kashino *et al.* 2002). Psb27 was identified as a lipoprotein associated with inactive PSII monomers that prevents binding of PSII extrinsic subunits (PsbO, PsbU and PsbV) to the premature PSII (Nowaczyk *et al.* 2006), keeping the active site "open" and thereby maintaining a sufficient diffusion rate of Mn^{2+}, Ca^{2+} and Cl^- ions thus acting as a molecular chaperone for successful photoactivation (Roose *et al.* 2008). It does so through a specific interaction with the E-loop of CP43, which is a lumenal domain of PSII that directly interacts with the Mn_4CaO_5. Overall, Psb27 appears to be strictly associated with organisms possessing PSII and is important for its assembly, (Chen *et al.* 2006, Bentley *et al.* 2007, Liu *et al.* 2011, Komenda *et al.* 2012) yet its precise role in facilitating assembly remains to be resolved. Here we applied *in vitro* photoactivation procedures using genetically tractable cyanobacteria and use it to analyze the roles of Ca^{2+} and Psb27 in the assembly of the Mn_4CaO_5.

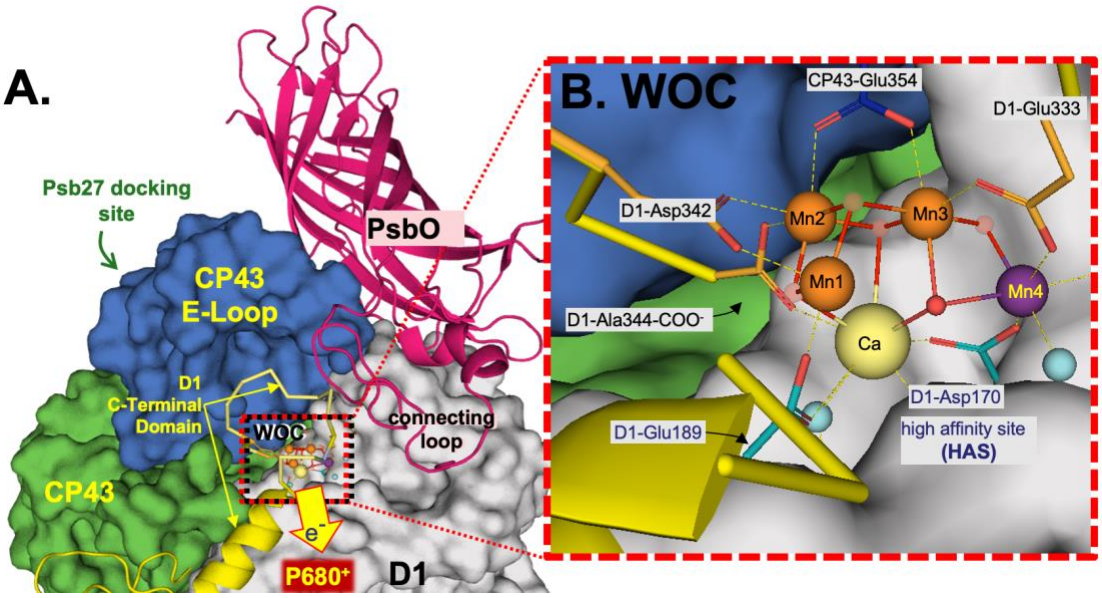

Figure 5. Schematic representation of assembled Mn cluster and key subunits of the PSII. **(A)**: The CP43 E-loop **(Blue)** interacts with the metal binding C-terminal domain (yellow), and their coupled mobility controls access to the apo-WOC, modulated by interactions with PsbO and Psb27. **(B)**: Catalytic Mn_4CaO_5 cluster at the interface between the D1 (PsbA) and CP43 (PsbC) subunits. During photoassembly, Mn^{2+} binds at the high affinity site (**HAS**) at or near the Mn4 (purple sphere) involving the D1-Asp170 carboxylate moiety, which also ligates Ca^{2+} (yellow sphere) at the calcium site (**CAS**). Additional Mn^{2+} ions are photooxidatively incorporated via the oxo-bridges presumably derived from water ligands. A second Mn^{2+} binding site (**SMS**, see text) is critical to trap the first stable intermediate and would include amino acid ligands at one of the other three Mn locations (orange spheres).

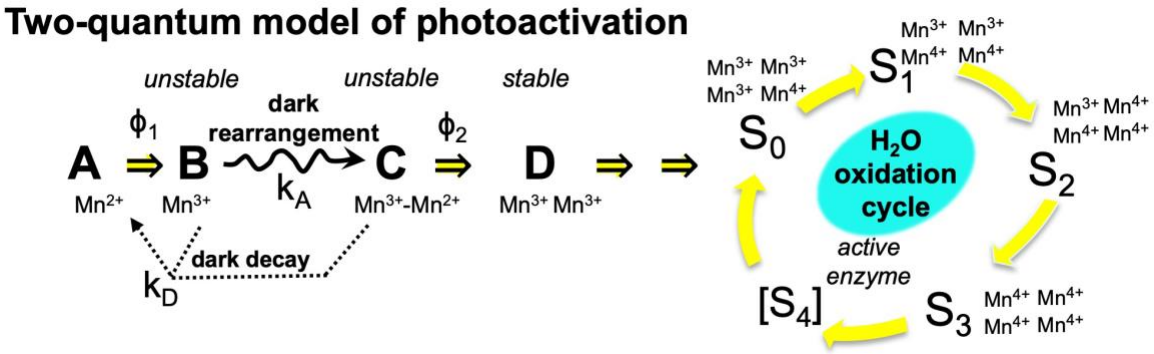

Figure 6. Kinetic scheme of basic two-quantum mechanism of PSII photoactivation. Double arrows indicate light-activated processes with the quantum efficiencies $\boldsymbol{\phi}_1$ and $\boldsymbol{\phi}_2$ representing the

first and second photooxidative events in the assembly sequence, k_A representing the "dark" rearrangement, and k_D, representing the decay of intermediates. After the initial two Mn are photoligated, subsequent Mn appear to be added with high quantum yield

4.3 Materials and methods

4.3.1 Strains and growth conditions

The glucose-tolerant *Synechocystis* sp. PCC6803 control strain (WT-control) expressing only the wild-type *psbA2* gene and having a hexa-histidine tag fused to the carboxyl-terminus of CP47 was maintained in BG-11 medium as described previously (Debus *et al.* 2001). Experimental cultures were grown in flat 1L tissue culture flasks in 800 mL BG-11 media buffered with 10 mM HEPES-NaOH pH 8.0 (HBG-11) supplemented with 5 mM glucose (Sigma) under a PFD (photon flux density) of ~80 µmol m^{-2} s^{-1} at 30 °C. Cultures were bubbled with filter sterilized air. Light intensity measurements were made with a Walz light meter (Germany).

4.3.2 Mutant strain generation

The Δ*psbO* deletion mutant was constructed previously and involved replacement of the *psbO* coding sequence with a Sp^r/Sm^r antibiotic resistance gene (Burnap *et al.* 1991). For overexpression of Psb27 gene in *Synechocystis,* the chromosomal locus comprising the open reading frame slr1645 (Psb27) was amplified by PCR **(Table 2)** using Herculase II Phusion DNA polymerase (Agilent USA) and integrated at a neutral site within the *Synechocystis* genome between ORFs slr1169 and slr1285 (**Fig. 7**). Transformation was carried as described previously using selective agar plates containing 5 mM glucose, 10 µM DCMU, and 12.5 µg/mL spectinomycin followed by further selection at 25 µg/mL spectinomycin (Williams 1988).

Table 2. DNA Primers used for the cloning and overexpression of the psb27 gene.

Primer name	Sequence
Psb27_GA_F	TACATAAGGAATTATAACCAATGTCCTTTTTGAAAAATCAG TTGTCACGGC
Psb27_GA_R	TTATCAGACCGCTTCTGCGCTCACACGCCCCGTTCAATG
slr1169_seq_F	CGATGATGGCGATCGCCAAAAC
Sp_cassette_seq_R	GGTGGTAACGGCGCAGTG
slr_1285_seq_R	CACCCCCACGCCATCAA
Psb27_seq_F	CCACCGGCATCACCTTTGC

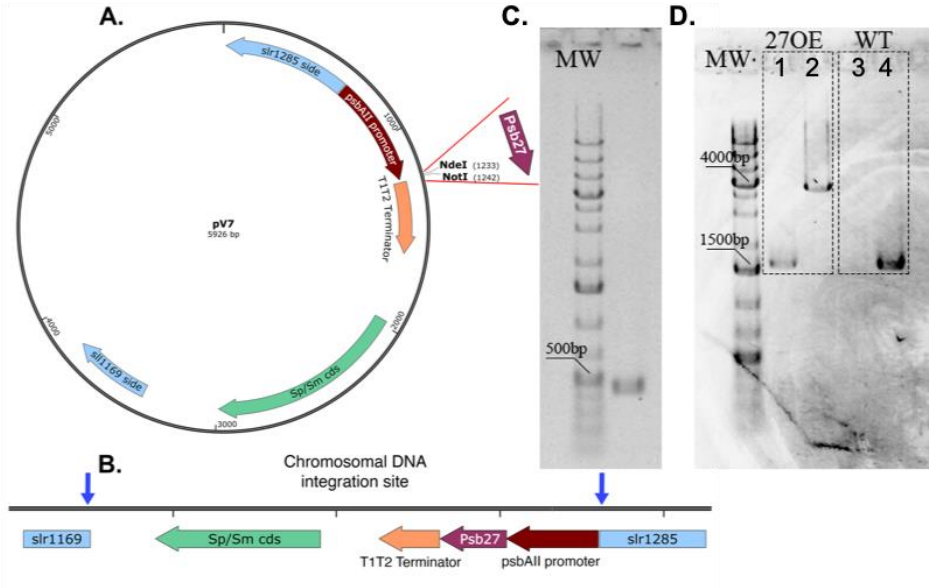

Figure 7. The construction of ectopic expression mutant *27OE*. **(A)** pV7 plasmid used for the mutant construction, **(B)** integration of Psb27 gene to the *Synechocystis sp. PCC6803* genome. Arrows indicate the insertion of Psb27 gene with psbAII promoter and T1T2 terminator in conjunction with Spectinomycin/Streptomycin antibiotic resistance cassette. **(C)** The chromosomal locus comprising the open reading frame slr1645 (Psb27) was amplified by PCR **(Table S2)** using Herculase II Phusion DNA polymerase (Agilent USA). The amplified DNA fragment was assembled into pV7 plasmid (a gift from Hong Wang and Wim Vermaas, Arizona State University) between NotI and NdeI restriction sites using the Gibson Assembly technique. The pV7 vector is a suicide plasmid that contains DNA sequences that mediate homologous recombination within the *Synechocystis* chromosome and is designed for the introduction of ectopic overexpression cassettes, in this case, the *psb27* gene was placed under the control of the strong *psbAII* promoter. **(D)**

Transformation results in the integration of the expression cassette at a neutral site within the *Synechocystis* genome between ORFs slr1169 and slr1285, segregation was checked using PCR. Lanes 1 and 3 PCR product with primers binding sites at ectopic copy of Psb27 and outside of slr1169. Lane 2 and 4 PCR product with primers binding sites outside of slr1169 and slr1285

4.3.3 Preparation of Mn-depleted thylakoid membranes

Cultures (2.4 L) were harvested in early stationary phase (OD_{750nm} ~1.8-2.2) and exhibited variable Chl fluorescence ((F_m - F_0)/F_0) values >0.5, as measured with a Photon Systems Instruments (PSI) Fluorometer FL 3500. Cells were collected by centrifugation at 25 °C at 6,000 g (Sorvall, F-9 rotor) for 15 min and gently resuspended with a minimal volume of H20BG-11(same as growth media, but with 20 mM HEPES-NaOH pH 8.0) using a paintbrush. The cell suspension volume was expanded to ~200 mL with additional H20BG-11. The washed cells were centrifuged again at 25 °C at 10200 g for 5 min (Sorvall, F-14 rotor). The pelleted cells were resuspended as before in H20BG-11 medium, and the suspension was adjusted to a Chl concentration of 100 μg mL^{-1} Chl. Hydroxylamine was added to 1 mM from a freshly prepared 400 mM stock, and the treated suspension was incubated for 12 min in the darkness with rotary agitation (200 rpm) at room temperature. Maintaining complete darkness, the HA-extracted cells were then washed by resuspension with 100 ml H20BG-11 and rotary agitation (200 rpm) for 5 min before pelleting again. This washing step was repeated four more times with the aim of depleting residual HA. Finally, the cells were resuspended in 120 ml of breaking buffer (1.2 m betaine, 50 mM MES-NaOH (pH 6.0), 10%(v/v) glycerol, and 5 mM $MgCl_2$) that was prepared with ultrapure reagents and Chelex-100 (Bio-Rad)-treated solutions and incubated in the dark on ice for 1 hour. Cells were pelleted at 10,200 g for 5 min and resuspended to a total volume of 14 mL. Prior cell breakage, 1 mM benzamidine, 1 mM ε-amino-n-caproic acid, 1 mM PMSF, and 0.05 mg/mL DNase I were added. Cells were broken by four cycles of 5 sec ON and 5 min OFF in an ice-cooled glass bead homogenizer (Bead-Beater, BioSpec Products, Bartlesville, OK). After breakage the sample was centrifuged at 3,600 g for 10 min to pellet unbroken cells and cell debris. Thylakoids were obtained

from the supernatant cell homogenate by ultracentrifugation (35 min at 40,000 rpm in a Beckman Ti45 rotor) and thylakoid-containing pellets were suspended in Chelex-100-treated breaking buffer to a concentration of 1.0-1.5 mg Chl mL^{-1} with [Chl] determined from methanol extracts according to (Wellburn *et al.* 1984). Concentrated thylakoid membranes were flash frozen as 100 µL aliquots in liquid nitrogen and stored at -80°C.

4.3.4 Photoactivation of HA-extracted membranes

HA-extracted membranes were photoactivated either in suspension for subsequent assay for restoration of O_2 evolution detected using a Clark-type electrode or directly on a bare platinum electrode that permits the centrifugal deposition of samples upon the electrode surface (Nixon *et al.* 1992). Flash illumination under each mode of photoactivation was provided using an EG&G xenon flash lamp. The buffer was supplemented with various concentrations of cations $CaCl_2$, $MnCl_2$, $SrCl_2$, and $MgCl_2$ to examine their role in photoactivation for the role of cations on photoactivation. See supplementary materials for details for data collection and data processing

4.3.5 SDS-PAGE and immunoblot analysis

Membrane samples obtained as above were solubilized by addition of 2% SDS, 5 mM dithiothreitol, heated at 65 °C for 10 min, and separated on SDS-PAGE (12%). Protein content was transferred to a PVDF membrane using a Bio-Rad (USA) semi-dry apparatus, and membrane was stained with 0.5 % Ponceau S (Sigma) to verify equal loading. 5% BSA solution was used as a blocking agent. Blots were probed against Psb27 (1:750 dilution, a kind gift from Julian Eaton-Rye) with anti-rabbit HRP-conjugated goat antibody (1:3000, Bio-Rad) as a secondary antibody. Color Development employed the chromogenic substrate 4-chloro-1-naphthol (4CN, Bio-Rad) and H_2O_2.

4.3.6 Curve fitting and data analysis

At the completion of the photoactivation flash treatment on the bare platinum electrode, flash O_2 yields were recorded as described previously (Li *et al.* 2002, Hwang *et al.* 2007). The flash O_2 yields were measured using a circuit that sets the polarization of the electrode and amplifies the amperometric signal during the flash excitation of the sample. A 10 ms long amperometric pick was recorded after each light induced oxygen release. For the Mn^{2+} and Ca^{2+} dependence experiments, the values from 50th, 100th, 200th, 400th, 1000th, 1500th and 2000th flashes were used for the data plot generation. To analyze the role of Ca^{2+} and Mn^{2+} on quantum efficiency of photoactivation and photoinactivation as a function of flash number, data were fit to a double exponential equation modified from the original equation $R_t = R_i \cdot e^{-\Phi_a \cdot It}$ used by (Cheniae *et al.* 1971); R_t is the V_{max} rate after photoactivation during time *t*, R_i the initial V_{max} rate, the fractional absorption of the intensity (I) and Φ the quantum yield. To account for the O_2 signal decline (photoinactivation), after the observed V_{max}, the original equation has been modified by addition of the second exponential component describing the photoinactivation, ($e^{-\Phi_{PI} \cdot n}$) (**Table 3**) where Φ_{PI}, represents the quantum efficiency of irreversible photodamage.

To obtain the values for the frequency dependent photoactivation at different [Ca^{2+}] the sample was subjected to 150 single turnover flashes at uniform flash interval. The values from the last 6 light induced oxygen release picks were averaged and used in further analysis. Estimations of the parameters under each condition describing the dark rearrangement, k_A, and the decay of intermediates, k_D, were determined by deriving kinetic parameters from the rising and falling slopes of the bell-shaped curve in plots of photoactivation as a function of the flash interval curve fitted to the equation (2) originally was derived by Noriaki Tamura and George Cheniae (Tamura *et al.* 1987) and later used by Hwang et al. (Hwang *et al.* 2007):

$$[A]_n = [k_A/k_D - k_A] \times [A]_O \times \left(e^{-k_A td} - e^{-k_D td}\right)$$

Photoactivation was also monitored based upon light-saturated steady-state rates of O_2 evolution of the photoactivated thylakoid membranes, using a Clark-type electrode (Cheniae *et al.* 1971, Miller *et al.* 1989, Burnap *et al.* 1995). HA-extracted thylakoid samples containing 40 µg of Chl were suspended in 400 µL of in Chelex-100-treated photoactivation buffer in a modified aluminum weigh cup with a stirring bar. A series of single-turnover xenon flashes was given to the stirring thylakoid suspension and O_2 evolution rates were in O_2 evolution buffer (50 mM MES-NaOH, 25 mM $CaCl_2$, 10 mM NaCl, and 1 m sucrose pH 6.5) at a photon flux density of 2500 $\mu Em^{-2}\ s^{-1}$ in the presence of 1 mM 2,6 dichloro-*p*-benzoquinone (DCBQ) and 2.5 mM potassium ferricyanide $K_3[Fe(CN)_6]$.

To normalize between the replicates the data obtained from both flash number and frequency dependence experiments were normalized to 1 using $z_i = \frac{x_i - \min(x)}{\max(x) - \min(x)}$, where z_i is the normalized value, *x* represents unnormalized value, and min(x) and max(x) represents minimal and maximal values from the data set, respectively. Standard deviation represents normalized standard deviation.

Table 2. Equations used for curve fitting of the data obtained from Mn^{2+} and Ca^{2+} dependence as a function of the flash number experiments. *Equation used in current study

Equation	Notes
$[\boldsymbol{A}]_{\boldsymbol{n}} = [\mathbf{A}]_{\mathbf{0}} \cdot (\mathbf{1} - \boldsymbol{e}^{\boldsymbol{\Phi_{PA}\cdot n}}) \cdot (\boldsymbol{e}^{-\boldsymbol{\Phi_{PI}\cdot n}})$ **(*)**	R < 0.995-0.999
$[\boldsymbol{A}]_{\boldsymbol{n}} = [\mathbf{A}]_{\mathbf{0}} \cdot \left(\mathbf{1} - \boldsymbol{e}^{\boldsymbol{\Phi_{PA}\cdot n}}\right) - [\mathbf{A}]_{\mathbf{1}}(\boldsymbol{e}^{-\boldsymbol{\Phi_{PI}\cdot n}})$	Failed to capture signal decline
$[\boldsymbol{A}]_{\boldsymbol{n}} = [\mathbf{A}]_{\mathbf{0}} \cdot \left(\mathbf{1} - \boldsymbol{e}^{\boldsymbol{\Phi_{PA}\cdot n}}\right) - [\mathbf{A}]_{\mathbf{0}}(\boldsymbol{e}^{-\boldsymbol{\Phi_{PI}\cdot n}})$	Failed to capture signal decline
$[\boldsymbol{A}]_{\boldsymbol{n}} = [\mathbf{A}]_{\mathbf{0}} \cdot \left(\mathbf{1} - \boldsymbol{e}^{\boldsymbol{\Phi_{PA}\cdot n}}\right) - (\boldsymbol{e}^{-\boldsymbol{\Phi_{PI}\cdot n}})$	Failed to capture signal decline

4.4 Results

4.4.1 Mn^{2+} and Ca^{2+} competition during photoassembly leads to decreased quantum efficiency and yield during photoactivation of *Synechocystis* membranes

We developed a procedure for isolating Mn-depleted thylakoid membranes from *Synechocystis* sp. PCC6803 (hereafter, *Synechocystis*) enabling control of the photoactivation conditions, such as pH and ion composition as well as permitting facile genetic modification of the constituent proteins. Importantly, the membranes retain the native electron acceptor system so that artificial electron acceptors are not necessary as in previous *in vitro* experimental systems. Extracted membranes showed substantial restoration of photosynthetic activity (40%) (**Fig. 8A, Table 4)** consistent with published yields in plant preparations (see (Miller *et al.* 1989) for quantitative analysis), and most importantly, display similar kinetic features of photoactivation compared to plant membrane preparations and to *in vivo* photoactivation experiments in *Synechocystis* (**Fig. S1**). We focused on the role of Ca^{2+} in photoactivation and how the extrinsic proteins modulate the demand for both Mn^{2+} and Ca^{2+}. As shown previously, photoactivation requires presence of both Mn^{2+} and Ca^{2+} cations for the assembly of PSII and post-addition of Ca^{2+} after illumination only resulted in a very small increase in the yield of active PSII (**Fig. 8B)**. Post-addition of Sr^{2+} or Mg^{2+} cations in the dark, did not result in a significant yield of photoactivation. Thus, our results concur with the general conclusion that Ca^{2+} is absolutely required for the assembly process (Ono *et al.* 1983, Chen *et al.* 1995, Ananyev *et al.* 1996).

In plant preparations, optimal photoactivation, both *in vitro* (Miller *et al.* 1989, Ananyev *et al.* 1996, Zaltsman *et al.* 1997) and *in organello* (Ono *et al.* 1983), requires an optimal Ca^{2+}/Mn^{2+} ratio characterized by an excess of Ca^{2+} relative to Mn^{2+}, which reflects a competition between the ions for their respective binding sites (Miller *et al.* 1989). To establish whether similar kinetic features operate in cyanobacteria, the Ca^{2+} concentration dependence of photoactivation was performed at two fixed Mn^{2+} concentrations, 250 μM or 500 μM (**Fig. 9A & B**). These concentrations of Mn^{2+}

should saturate its binding to the HAS (Ananyev *et al.* 1996), but should still allow observation of the predicted competition between the two cations observed in plant preparations (Ono *et al.* 1983, Miller *et al.* 1989, Ananyev *et al.* 1996). A small level of photoactivation can be seen in the absence of added Ca^{2+} ions, which could be explained by trace amounts of residual Mn^{2+} and Ca^{2+} ions remaining in the extracted thylakoid preparation, since the level of this activity could be minimized, but never completely eliminated, by extensive washing of membranes using Chelex-treated buffer. For all the samples containing 250 µM Mn^{2+} in photoactivation buffer, the maximum yield of photoactivation was observed at 600-700 flashes with the half-maxima at occurring with approximately 150-200 flashes (**Fig. 9A**). In terms of maximal yield and quantum efficiency of photoactivation, the optimum Ca^{2+} concentration for photoactivation at 250 µM Mn^{2+} occurs at 10 mM corresponding to Ca^{2+}/Mn^{2+} ratio of 40:1. The decrease in O_2 evolution at lower Ca^{2+} concentrations is likely caused by the competitive binding of Mn^{2+} to the Ca^{2+} binding site. In the context of earlier findings, this would prevent the formation a bridged species [Mn^{3+}-(OH)-Ca^{2+}] that is proposed to be crucial intermediate during the assembly (Tyryshkin *et al.* 2006) and perhaps leading to the formation of 'inappropriately' bound high valence, multinuclear Mn deposits (Chen *et al.* 1995). To better understand the role of ion competition and test the hypothesis that Mn^{2+} binding at the Ca^{2+} site leads to photoinactivation of PSII during photoassembly, we carried out the same experiment, but doubling Mn^{2+} concentration to 500 µM (**Fig. 9B**). For the optimum photoactivation at 500 µM of Mn^{2+}, the requirement for Ca^{2+} increased two-fold. Interestingly, samples containing 20 mM and 40 mM of Ca^{2+} in photoactivation buffer started to show signs of photoinactivation observed earlier at low Ca^{2+} concentration at 250 µM Mn^{2+}. From these results we can conclude that an excess of Mn^{2+} ions leads to decreased yield of PSII photoactivation due to photoinactivation, while excess Ca^{2+} does not have such an effect.

To analyze the role of Ca^{2+} concentration on quantum efficiency of photoactivation and photoinactivation as a function of flash number and to better understand inhibitory effect of low Ca^{2+} to Mn^{2+} ratios, data described in **Fig. 9** were fit to a double exponential equation:

$$[A]_n = [\mathrm{A}]_0 \cdot (1 - e^{\Phi_{PA} \cdot n}) \cdot (e^{-\Phi_{PI} \cdot n}) \quad (1)$$

The equation accounts for the progressively smaller pool of apo-centers during the flash sequence progression as more centers become photoactivated (Cheniae *et al.* 1971) combined with a term that represents the loss of centers due to photoinactivation processes (Miller *et al.* 1989). Here, $[A]_n$ represents the yield of active centers on the *n*th flash, whereas $[A]_0$, is the concentration of apo-PSII centers prior to the photoactivation, Φ_{PA} represents the overall efficiency of the multiphoton assembly process. The photoinactivation term, Φ_{PI}, represents the quantum efficiency of irreversible photodamage or, alternatively, the formation of inactive centers due to 'inappropriately bound' Mn as a consequence of supra-optimal Mn^{2+} concentrations (Chen *et al.* 1995). This is also seen with varying $[Mn^{2+}]$ at fixed $[Ca^{2+}]$, where there is a strong dependence of Φ_{PI} on $[Mn^{2+}]$ (**Fig. S2 & S3**). The corresponding estimates of parameters are plotted as a function of the Ca^{2+}/Mn^{2+} ratio (**Fig. 9C & D**). Additionally, the yields of photoactivation, indicated by the levels reached after ~500 flashes **(Fig. 9A & B)**, increase with $[Ca^{2+}]$ up to 10 mM at 250 µM Mn^{2+} and 20 mM at 500 µM Mn^{2+}, but higher $[Ca^{2+}]$ decreased yields, especially at 250 µM Mn^{2+}. Interestingly, at 250 µM Mn^{2+} the quantum efficiency of photoactivation, Φ_{PA}, is relatively unaffected by Ca^{2+} concentration throughout the range tested (**Fig. 9C**). In contrast, at 500 µM Mn^{2+}, Φ_{PA} is strongly dependent on Ca^{2+} availability, perhaps reflecting competitive occupation of Mn^{2+} in the Ca^{2+} effector site. As shown in **Fig. 9C**, at low $[Ca^{2+}]$, the Φ_{PA} is low, reaches a maximum at 20 mM coinciding with overall apparent optimum (**see Fig. 9B**), and declines at higher $[Ca^{2+}]$. Overall, higher abundance of Mn^{2+} ions inhibits the assembly through competition with Ca^{2+} (Ono *et al.* 1983, Miller *et al.* 1989, Ananyev *et al.* 1996).

The difference between unaffected Φ_{PA} at 250 µM Mn^{2+} versus affected Φ_{PA} at 500 µM in **Fig. 9C** is intriguing and suggests a complex interplay of binding constants. The HAS likely remains occupied by Mn^{2+} (K_D < 10 µM), (Nixon *et al.* 1992, Ananyev *et al.* 1996, Ono *et al.* 1999) with both the 250 and 500 µM Mn^{2+} experiments, even with comparatively high [Ca^{2+}]. However, at the higher [Mn^{2+}] the results indicate that the Ca^{2+} effector site is substantially occupied by Mn^{2+} leading to inactivation, consistent with previous kinetic analysis (Miller *et al.* 1989). It is unclear at which step(s) the replacing of Ca^{2+} ion with Mn ion is inhibitory, however we find that Ca^{2+} can even be replaced with Mn in assembled PSII, producing a light-dependent inactivation during the catalytic turnover of the S-state cycle of the intact Mn cluster (**Fig. 10**). This fits with the observation that Ca^{2+} is more readily released in the higher S-states, presumably due to charge repulsion (Boussac *et al.* 1988, Miqyass *et al.* 2008). Accordingly, this replacement by Mn^{2+} incorrectly into the Ca^{2+} site results *not only* in a failure to advance in photoassembly, but also a greater frequency of inactivation, an effect mitigated by high [Ca^{2+}] (**Fig. 9D)**. The optimal Ca^{2+}/Mn^{2+} ratio for overall photoactivation thus reflects a balance between binding of Ca^{2+} at its effector site, which prevents photoinactivation due to inappropriate binding of Mn^{2+} (Chen *et al.* 1995), but not so high as to out-compete Mn^{2+} at the Mn site preventing photooxidative Mn incorporation (Miller *et al.* 1989, Ananyev *et al.* 1996, Ono *et al.* 1999). But which Mn site? Based upon the fact that Φ_{PA} at lower [Mn^{2+}] is independent of [Ca^{2+}] in the range tested, as well as previous estimates of Mn^{2+} affinity at the HAS, we conclude that the yield-limiting competition between Ca^{2+} at a Mn^{2+} site occurs not at the HAS, but rather at a second Mn site (SMS) involved in the photoactivation pathway. This is consistent with the results of the effect of [Ca^{2+}] on the rate of the dark rearrangement step, k_A (next section).

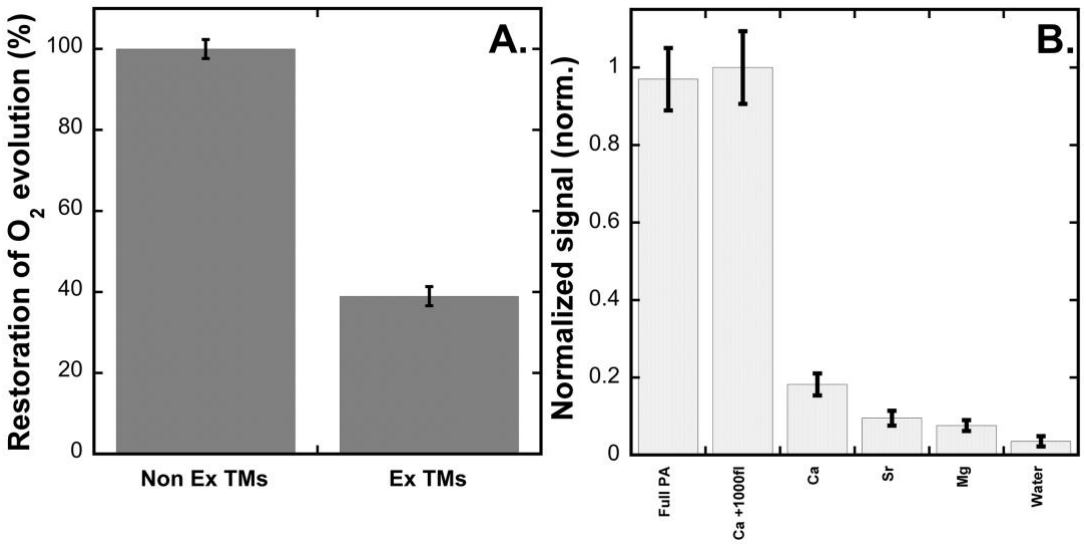

Figure 8. Photoactivation of HA-extracted thylakoid membranes from WT control. (A) Recovery of the light-saturated O_2-evolving activity of hydroxylamine-extracted thylakoid membranes exposed to 15 minutes of continuous illumination. (**B)** Effect of adding of divalent cations ***after*** illuminating the sample with the sequence of 1000 single turnover flashes at 2 Hz (500 ms flash interval) in the presence of 250 µM $MnCl_2$. The thylakoid membranes were photoactivated using 1000 single-turnover flashes illumination. The 1st photoactivation was carried out in the presence of Mn^{2+} and then cations were added to the photoactivated sample. After incubating for 10 min in the dark on the ice, the photoactivation activity was monitored by measuring O_2 evolution using centrifugal bare platinum electrode using 20 measuring Xenon flashes.

Table 4. Photoactivation of hydroxylamine (HA)-extracted and non-extracted membrane samples obtained from *Synechocystis* WT control, Δ*psbO* and *27OE* strains

Strain	Non-extracted TM, µmol O_2 (mg Chl)$^{-1}$ h^{-1}	Apo-PSII µmol O_2 (mg Chl)$^{-1}$ h^{-1}	Recovered rate µmol O_2 (mg Chl)$^{-1}$ h^{-1}	% recovery
WT	575.6±13.5	12.1±7	224±5.3	38.9 %
27OE	330±24.8	17± 8.4	193.6±8.5	58.4 %
Δ*psbO*	254.6±17.3	5± 3	146.7±20.4	57.6 %

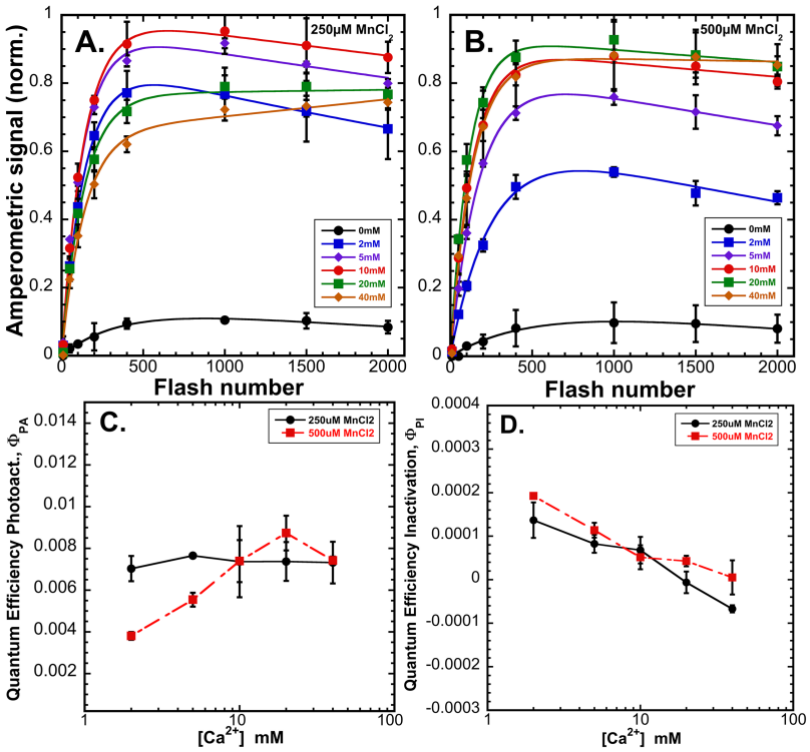

Figure 9. Calcium dependence of photoactivation under sequence of single turnover flashes at 2 Hz (500 ms flash interval) of HA-extracted thylakoid membranes from WT control at 0 mM (black circle), 2 mM (blue square), 5 mM (purple diamond), 10 mM (red circle), 20 mM (green square), and 40 mM (orange diamond) of $CaCl_2$ combined with 250 μM (**Panel A**) or 500 μM $MnCl_2$ (**Panel B**). **Panel C:** Overall quantum efficiency of photoactivation (Φ_{PA}) **Panel D:** quantum efficiency of inactivation (Φ_{PI}). Data were fit to equation 1 for parameter estimation (see text for details). Error bars represent standard deviation n ≧ 3.

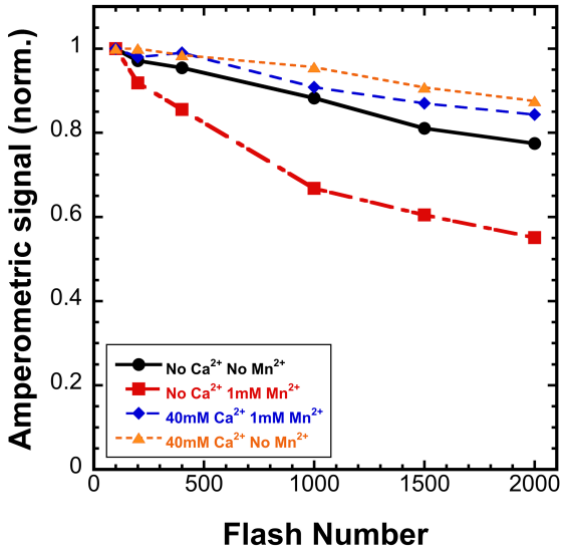

Figure 10. Mn^{2+} induced photoinactivation of oxygen evolution in thylakoid membranes from WT control at different ion availability conditions as a function of the flash number at 2 Hz (500 ms flash interval) with different amounts of Ca^{2+} and Mn^{2+} added to photoactivation buffer. No Ca^{2+} and no Mn^{2+} (black circles), no Ca^{2+} and 1 mM Mn^{2+} (red squares), 40 mM Ca^{2+} and 1 mM Mn^{2+} (blue diamond), and 40 mM Ca^{2+} and no Mn^{2+} (orange triangles).

4.4.2 Calcium stabilizes intermediates of photoactivation and prolongs the dark rearrangement time

To test the hypothesis that Ca^{2+} influences the stability of the assembly intermediates, photoactivation was performed varying [Ca^{2+}] and the interval between photoactivating light flashes for a fixed number of flashes to **(Fig. 11**). According to the two-quantum model of photoactivation (**Fig. 7)** the initial photooxidation of Mn^{2+} (state **"A"**) produces the first unstable intermediate **"B"**, followed by a light-independent 'rearrangement' step leading to the formation of a second unstable intermediate **"C"**, which is a configuration capable of productively utilizing the second light quantum to form the first stable intermediate, **"D"** (Radmer *et al.* 1971). Short intervals produce low yields since not enough time has elapsed for completion of the dark rearrangement. Long intervals between the charge separations causes the decay of intermediates resulting low yields of active centers (Radmer *et al.* 1971, Tamura *et al.* 1987). This results in a

bell-shaped curve recording the yield of photoactivation due to a fixed number of flashes given at different flash intervals from 50 ms to 10000 ms (**Fig. 11**). Estimations of the parameters under each condition **(Table 5)** describing the dark rearrangement, k_A, and the decay of intermediates, k_D, were determined by deriving kinetic parameters from the rising and falling slopes of the bell-shaped curve in plots of photoactivation as a function of the flash interval curve fitted to the equation (2):

$$[A]_n = [k_A/k_D - k_A] \times [A]_O \times (e^{-k_A td} - e^{-k_D td}) \quad (2)$$

The overall shape of the resultant bell-shaped curves closely resembles previous results using higher plant material. Estimated values for dark rearrangement (k_A, **B→C**) and the decay of intermediates (k_D, **B** & **C**) are in the range of 200-400 ms and 7-14 seconds, respectively in our experiments (**Table 5**). These values are slower than with spinach PSII preparations, but in the same proportions with the dark rearrangement, k_A, typically 10-fold faster than the rate of decay, k_D (reviewed in (Burnap 2004)). These differences may be attributed to the different source of experimental material and/or choice of buffers (e.g. the sucrose concentration used here is much higher than typically used). Depending upon the [Ca^{2+}], different optima for maximal yields of photoactivation were observed with increasing Ca^{2+} giving increasingly longer optima for the length of the dark period between flashes (**Fig. 11**). Photoactivation with 40 mM Ca^{2+} enhanced yields at the longest interval tested, (10 sec), again suggesting that Ca^{2+} stabilizes the intermediates of photoactivation. Accordingly, the fit values for the decay of intermediates k_D, are shifted to slower rates of decay (**Table 5**). The stabilizing effect of Ca^{2+} on photoactivation intermediates contrasts with the existence of the optimal [Ca^{2+}]/[Mn^{2+}] ratio for the net yield under repetitive flashing at a constant interval (500 ms). The flash interval experiment also estimates the second parameter in the two-quantum model, the dark rearrangement, k_A, (**B→C, Fig. 1**). This is the time needed between flashes before subsequent flashes become productive, which is experimentally

reflected by diminished yields of photoactivation at short flash intervals (**Fig. 11**). Remarkably, the rearrangement takes longer time to complete at high [Ca^{2+}] concentrations **(Table 5)**.

Our analyses of the preceding results leads us to conclude that at high [Ca^{2+}], assembly occurs, albeit sub-optimally, due to competition between metals for their respective sites as shown before (Ono *et al.* 1983, Miller *et al.* 1989, Ananyev *et al.* 1996). High [Ca^{2+}] also allows assembly at long flash intervals due to stabilization of intermediates **"B"** and/or **"C" (Fig. 7)**. On the other hand, at low [Ca^{2+}], photoactivation yields are also decreased **(Fig. 11)** due to photoinactivation. The protective function of Ca^{2+} is important also in PSII centers that already have been assembled **(Fig. 10),** consistent with the proposed 'gate-keeper' function observed with intact PSII preparations (Mei *et al.* 1991, Tso *et al.* 1991). Thus, we conclude that Ca^{2+} is important for assembly because it stabilizes intermediate **"B"** and/or **"C"** and prevents inactivation and failure to advance due to 'inappropriate' binding of Mn^{2+} into the Ca^{2+} site during assembly (Miller *et al.* 1989, Chen *et al.* 1995). Besides its "gate-keeping" role, Ca^{2+} also can block necessary binding of the second Mn^{2+} especially at very high [Ca^{2+}]/[Mn^{2+}] ratios. This accounts for the slowing of the very slow dark rearrangement (**B→C).** While sufficient concentrations of Ca^{2+} increase the chance of successful formation of intermediate **"C",** an excess of Ca^{2+} competes with the binding of the second Mn^{2+} at the SMS, thereby delaying the time before the second Mn^{2+} ion can occupy its site for photooxidation. This competitive inhibition extends the time before the rearranged state can be trapped (**C→D**) until the competing Ca^{2+} is replaced with Mn^{2+} enabling the photooxidative formation of stable intermediate **"D"**. This, in turn, suggests that the dark rearrangement consists of a molecular reorganization (e.g. conformational change) that is only fruitful if a second Mn^{2+} binds at its correct site.

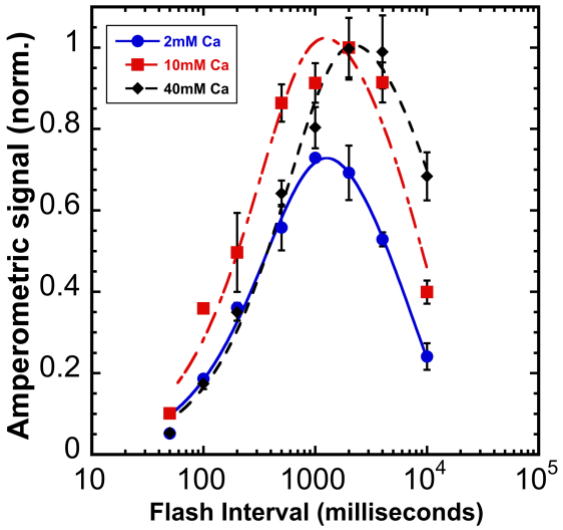

Figure 11. Photoactivation yields as a function of flash interval at different calcium concentrations. Sequences of 150 Xe flashes applied at different flash intervals to HA-extracted thylakoid membranes from WT control and oxygen yields measured on a bare platinum electrode. Plots correspond to samples containing 2 mM (blue circle), 10 mM (red square), and 40 mM (black diamond) of $CaCl_2$ a fixed $[Mn^{2+}]$ = 250 μM. Error bars represent SD with n ≧ 3. Data was fit to equation 2 (see main text) to estimate the dark rearrangement constant, k_A, and the decay of photoactivation intermediates "B and C", k_D (see **Fig. 7** for kinetic model and **Table 5** for estimated values for k_A and k_D).

Table 5. Dark rearrangement, k_A and decay of intermediates, k_D, parameters [a] characteristic of photoactivation of membranes from WT control.

Strain / $[Ca^{2+}]$	$k_A(s^{-1})$ ($t_{1/2}$)	$k_D(s^{-1})$ ($t_{1/2}$)	fit quality, r
WT control 2 mM Ca^{2+}	2.4 (288 ms)	0.134 (5.17 s)	0.99
WT control 10 mM Ca^{2+}	2.8 (244 ms)	0.095 (7.29 s)	0.98
WT control 40 mM Ca^{2+}	1.6 (433 ms)	0.051 (13.5 s)	0.99

[a] Data were fit to equation 2 to estimate the dark rearrangement constant, k_A, and the decay of photoactivation intermediates "B and C", k_D (see **Fig. 7** for model).

4.4.3 Role of PsbO and Psb27 during photoactivation

The PSII assembly cofactor protein, Psb27, which appears to facilitate diffusional access to the WOC assembly site (Nowaczyk *et al.* 2006, Roose *et al.* 2008, Komenda *et al.* 2012), does so by interacting with the E-loop of CP43 to allosterically modify its conformation (Liu *et al.* 2011, Liu *et al.* 2013), which is hinged (Burnap 2004) in a way that opens the WOC for greater diffusion into the sites of cofactor binding (Roose *et al.* 2008). Since the natural steady-state abundance of Psb27 in the cell likely evolved to cope with assembly and repair of only a fraction of centers from the total population of PSII in the cell, then there may not be enough copies of Psb27 to stoichiometrically service all PSII centers upon quantitative removal of the Mn cluster experimentally produced by HA-extraction. Similarly, diffusion of Mn^{2+} and Ca^{2+} ion could also be limited by the presence of the extrinsic proteins, impeding photoassembly as previously suggested from *in vivo* experiments with mutants (Burnap *et al.* 1995, Roose *et al.* 2008). To address these considerations, the photoactivation of two *Synechocystis* mutants, Δ*psbO* lacking PsbO, (Burnap *et al.* 1991) and a strain overexpressing Psb27 (*27OE*) **(Fig. S4),** were investigated. Importantly, the more open configurations of the WOC in both strains enabled a net recovery of O_2 evolution under continuous illumination that was more than 50% higher (i.e., ca. 58% vs. 39%) than in the WT-control (**Table 4**). Additionally, the optimal $[Ca^{2+}]/[Mn^{2+}]$ ratio for both mutants appears to be about twice as high compared to the WT control (80/1 versus 40/1) indicating alterations of the donor side polypeptide structure have a differential effect with the demand for Ca^{2+} being higher and/or a lower demand for Mn^{2+} **(Fig. 12)**. Interestingly, both mutants showed somewhat lower quantum efficiency, Φ_{PA}, compared to WT control, however, at higher $[Ca^{2+}]$, the yield continued increasing without saturation or decline through the entire flash sequence, suggesting that while the demand for Ca^{2+} was higher, fewer centers were lost to photoinactivation (compare with WT in Fig. 2). Accordingly, Δ*psbO* and *27OE* appeared less prone to photoinactivation (Φ_{PI}) compared to the WT control **(Fig. 12, S5-S8)** suggesting the open configuration diminishes the tendency for Mn^{2+} to occupy the Ca^{2+} effector site, but with the

optimum [Ca^{2+}] shifted higher. These observations are consistent with increased diffusion of the metal cofactors inside apo-PSII with proportionally increased exchange rates for Ca^{2+} at its effector site. Both mutants do not show strong correlation between [Ca^{2+}] and quantum efficiency of photoactivation **(Fig. 12C)**, which is similar to WT control preparations at the lower, 250 µM, [Mn^{2+}] tested, but not the higher 500 µM, [Mn^{2+}]. Photoinactivation rate **(Fig. 12D)** is negligible for both mutant strains. With increased diffusional access, Ca^{2+} appears to more effectively prevent the inhibitory effect of Mn^{2+} on photoassembly. Notably, Δ*psbO* and *27OE* show different Mn dependent photoactivation behavior compared to WT control. While *27OE* has similar to WT control requirement for Mn^{2+} ions, with the optimum at 250 µM at 10 mM Ca^{2+}, Δ*psbO* appears to have a lower requirement for available Mn^{2+} and shows maximal yield of photoactivation in the range of concentrations from 50 µM to 500 µM **(Fig. S5-S8)**.

As with the WT, the flash interval experiment shows that at longer intervals between flashes, Ca^{2+} stabilizes assembly intermediates **(Fig. 13)** as reflected in the slower decay constant, k_D **(Table 5 & 6)**. However, *27OE* decreases in k_D overall, further slowing the decay with the increase of [Ca^{2+}], suggesting a possible role for Psb27 in stabilizing the photoactivation intermediates **"B"** and/or **"C" (Fig 7)**, perhaps by stabilizing the binding of Ca^{2+} at its effector site. Additionally, the dark rearrangement, k_A, is generally slower than the WT for both Δ*psbO* and *27OE* **(Tables 5 and 6)**, although higher [Ca^{2+}] does not further slow the dark rearrangement in *27OE* as it does for WT and Δ*psbO*. Apparently both high [Ca^{2+}] and the more open configuration of apo-PSII leads to a slower dark rearrangement, k_A **(Table 6)** yet promotes better exchange of Ca^{2+} and prevents the decay of the photoactivation intermediates **(Table 6)**. The increased stabilization of intermediates in *27OE* in comparison with Δ*psbO* accords with the differences in the final yields of active centers as a function of flash number at different [Ca^{2+}] **(Fig. 12A** versus **Fig. 12B)**. Note, for example, that the 10 mM Ca^{2+} reaction in *27OE*, produces higher yields compared to Δ*psbO*, closely approaching the yields at the optimal 20 mM [Ca^{2+}]. Taken together, the results suggest that Psb27

enhances the stabilization of intermediates with accessibility of the site of cluster assembly, especially for Ca^{2+} ions, thereby shifting the optimal ratio of Mn^{2+} and Ca^{2+}. As discussed, given the known characteristics of the interaction of Psb27 with apo-PSII (Liu *et al.* 2011) this facilitation of photoactivation likely occurs allosterically via its interaction with the luminal E-loop of CP43, which besides D1, provides a ligand to the mature Mn_4CaO_5.

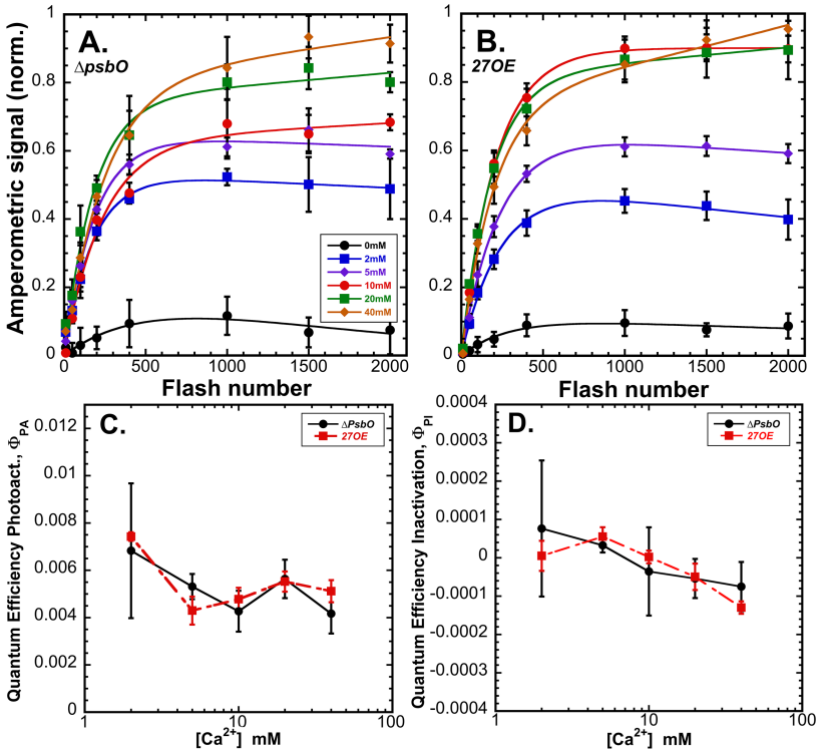

Figure 12. Calcium dependence of photoactivation of HA-extracted thylakoid membranes from Δ*psbO* and *27OE* mutants under sequence of single turnover flashes at 2 Hz (500 ms flash interval). Δ*psbO* (**A**) and *27OE* (**B**) at 0 mM (black circle), 2 mM (blue square), 5 mM (purple diamond), 10 mM (red circle), 20 mM (green square), and 40 mM (orange diamond) of $CaCl_2$ combined with 250 μM $MnCl_2$. (**C**) Overall quantum efficiency of photoactivation (Φ_{PA}) **(D)** quantum efficiency of inactivation (Φ_{PI}), respectively, in Δ*psbO* (black circle) and 27OE (red square) membranes. Data were fit to equation 1 for parameter estimation (see text for details). Error bars represent standard deviation n ≧ 3.

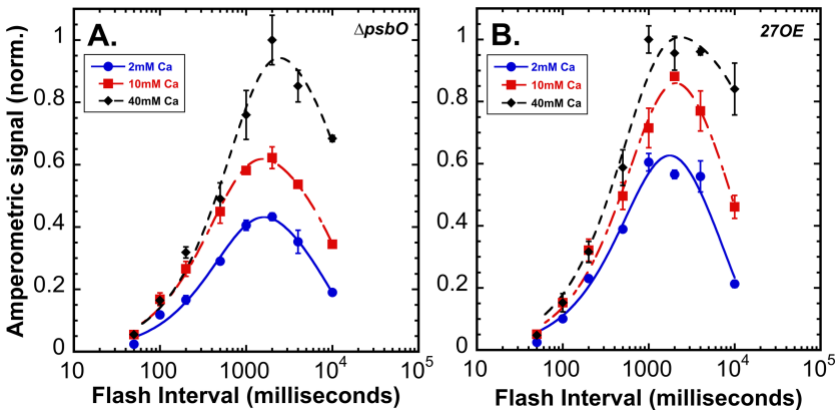

Figure 13. Photoactivation yields as a function of flash interval at different calcium concentrations. Sequences of 150 Xe flashes applied at different flash intervals to HA-extracted thylakoid membranes from Δ*psbO* **(A)** and *27OE* (**B**) with O_2 yields measured on a bare platinum electrode. Plots correspond to samples containing 2 mM (blue circle), 10 mM (red square), and 40 mM (black diamond) of $CaCl_2$ a fixed $[Mn^{2+}] = 250$ μM. Error bars represent SD with n ≧ 3. Data was fit to equation 2 (see main text) to estimate the dark rearrangement constant, k_A, and the decay of photoactivation intermediates "B and C", k_D (see Fig. 7 for kinetic model and **Table 5 & 6** for estimated values for k_A and k_D).

Table 6. Dark rearrangement, k_A and decay of intermediates, k_D, parameters [a] characteristic of photoactivation of membranes from ΔpsbO, and 27OE strains.

Strain / $[Ca^{2+}]$	$k_A(s^{-1})$ $(t_{1/2})$	$k_D(s^{-1})$ $(t_{1/2})$	fit quality, r
ΔpsbO 2 mM Ca^{2+}	1.9 (364 ms)	0.104 (6.66 s)	0.99
ΔpsbO 10 mM Ca^{2+}	2.2 (315 ms)	0.072 (9.62 s)	0.99
ΔpsbO 40 mM Ca^{2+}	1.5 (462 ms)	0.049 (14.1 s)	0.99
27OE 2 mM Ca^{2+}	1.5 (462 ms)	0.130 (5.33 s)	0.98
27OE 10 mM Ca^{2+}	1.4 (495 ms)	0.085 (8.15 s)	0.99
27OE 40 mM Ca^{2+}	1.8 (385 ms)	0.027 (25.6 s)	0.99

[a] Data were fit to equation 2 to estimate the dark rearrangement constant, k_A, and the decay of photoactivation intermediates "B and C", k_D (see Fig. 7 for model, and Table 4 & 5 for estimated values for k_A and k_D).

4.5 Discussion

4.5.1 How Ca^{2+} stabilizes photoactivation intermediates yet retards the dark rearrangement

Our results show for the first time that Ca^{2+} stabilizes the assembly intermediates of photoactivation, a feature especially evident at long intervals between photoactivating flashes **(Fig. 11 & 13)**. Moreover, the results also show for the first time that excess Ca^{2+} slows down the already very slow dark rearrangement (**B→C)**, an effect that is enhanced by the more open configuration of the apo-PSII assembly site in the mutants where greater ion exchange occurs **(Fig. 11 & 13, Table 5 & 6)**. According to the two-quantum model of photoactivation (Radmer *et al.* 1971), a stable intermediate **"D"** is formed by two light-dependent steps separated by a light-independent 'rearrangement' (**Fig. 7)**. The first light activated step (**A→B**) involves photooxidation of a single Mn^{2+} ion (Cheniae *et al.* 1971, Radmer *et al.* 1971, Miller *et al.* 1989, Ono *et al.* 1999) bound as hydroxide [(Mn)-OH^{+}] (Ananyev *et al.* 1999) at the HAS and occurs with high quantum efficiency (Hoganson *et al.* 1989, Diner *et al.* 1992, Nixon *et al.* 1992, Ono *et al.* 1999). The concurrent binding of Ca^{2+} at its adjacent effector site does not affect the affinity of the Mn^{2+} binding, but upon photooxidation of Mn^{2+} in the presence of bound Ca^{2+}, the bridging species, [Mn^{3+}-(OH^{-})-Ca^{2+}] ⇌ [Mn^{3+}-(O^{2-})-Ca^{2+}] is produced (Tyryshkin *et al.* 2006), which is thought to facilitate the next steps. This fast, high yield initial photooxidation is followed by a remarkably slow (100-400 ms) rearrangement (**B→C),** that involves a protein conformational change and/or ion relocation. Only then can the second charge separation become effective (**C→D**), photooxidizing a second Mn^{2+}, and thereby trapping the first stable intermediate **"D"** (Radmer *et al.* 1971). Current models suggest this first stable intermediate, **"D,"** is a binuclear $(Mn^{3+})_2$-(di-μ-oxo) bridged structure (Tamura *et al.* 1987, Barra *et al.* 2006), possibly corresponding to the binuclear di-μ-oxo bridged structure produced by partial disassembly of the intact Mn_4CaO_5 using reducing agents (Mei *et al.* 1991, Mei *et al.* 1992) or thermal treatment (Barra *et al.* 2006).

Based upon the findings that Φ_{PA} at lower [Mn^{2+}] is independent of [Ca^{2+}] (**Fig. 9C**) combined with estimates of Mn^{2+} affinity at the HAS (K_D~1 μM) (Nixon *et al.* 1992, Ananyev *et al.* 1996, Ono *et al.* 1999), we infer that the competition between Ca^{2+} for a critical Mn^{2+} site occurs not at the HAS, but rather at a second Mn site (**SMS**) involved in the photoactivation pathway, and that excess Ca^{2+}, while protecting from photoinactivation, inhibits assembly due to occupation of the SMS preventing photooxidation of the second Mn^{2+} (**C→D**). The present experiments cannot discriminate the identity of the SMS, though it is reasonable to suppose it to involve ligands that form with the other Mn1-Mn3 positions (**Fig. 5**, orange spheres) and that corresponds to the site estimated to have K_D=51 μM from steady-state photoactivation experiments (Miller *et al.* 1989). It also does not exclude the possibility, for example, that the Mn^{3+} ion initially produced from Mn^{2+} at the HAS (**A→B**), relocates to the SMS as part of the dark rearrangement (**B→C)**, according to the 'translocation model' (Bao *et al.* 2016, Zhang *et al.* 2017).

The stabilization of intermediates (**B**, **C)** by Ca^{2+} is most simply explained in the same way that Ca^{2+} prevents the photoinactivation of apo-PSII, combined with a requirement in mediating the formation of the first stable intermediate, **"D,"** likely a binuclear $(Mn^{3+})_2$-(di-μ-oxo) bridged structure (Tamura *et al.* 1987, Barra *et al.* 2006). Photoinactivation is due to incorrect occupation of the Ca^{2+} effector site (**CAS**) by Mn^{2+} evident at sub-optimal Ca^{2+}/Mn^{2+} ratios, which can even occur in intact PSII (**Fig. 10**) in line with the proposed 'gate-keeper' function of Ca^{2+} in the assembled Mn_4CaO_5 (Mei *et al.* 1991, Tso *et al.* 1991, Mei *et al.* 1992). Furthermore, Ca^{2+} tends to be lost from its effector site due to the electrostatic repulsion occurring upon oxidation of Y_Z (Miqyass *et al.* 2008) and/or associated pK_a changes (Boussac *et al.* 1988). Although the mechanism of Mn-dependent inactivation is not clear, occupation of the CAS by Mn^{2+} correlates with photoinactivation, as well as 'misses' due to the requirement for Ca^{2+} to form the necessary bridging species with Mn at the HAS needed for advancement through the assembly sequence (Tyryshkin *et al.* 2006). Therefore, the stabilization of photoactivation intermediates by Ca^{2+} is

likely due to protection against Mn-dependent inactivation and maintenance of an assembly-competent Mn-Ca species (Tyryshkin *et al.* 2006). Accordingly, the occupation of the CAS by Ca^{2+} is important throughout the duration of the dark rearrangement (**B→C)**. The observation that both Δ*psbO* and *27OE* each exhibit minimal photoinactivation and enhanced stabilization of intermediates suggests that ion exchange at the Ca^{2+} site is rapid in the more open configuration and this enables centers that have lost the Ca^{2+} ion to rapidly reacquire a replacement.

Besides stabilizing intermediates, Ca^{2+} also slows the dark rearrangement **(Fig. 11 & 13, Table 5 & 6).** At supra-optimal concentrations, Ca^{2+} appears to block the necessary binding of the second Mn^{2+}, at the second Mn-binding site, SMS, as already noted. While sufficient concentrations of Ca^{2+} increase the chance of successful formation of intermediate **"C",** an excess of Ca^{2+} competes with the binding of the second Mn^{2+} binding site, thereby delaying the time before the second Mn^{2+} ion can occupy the SMS for photooxidation, forming the first stable intermediate **"D"**, which is predicted to be a binuclear $(Mn^{3+})_2$-(di-μ-oxo) bridged structure (Tamura *et al.* 1987, Barra *et al.* 2006). However, if Ca^{2+} competitively occupies the second Mn^{2+} site, then the rearranged configuration (discussed below) cannot be productively converted due to the absence of the second Mn^{2+} needed for the photooxidative second light step (**C→D)**. This competitive inhibition extends the time before the rearranged state can be trapped, at least until the competing Ca^{2+} is replaced with Mn^{2+} enabling the photooxidative formation of stable intermediate **"D"**. This proposed model suggests that the dark rearrangement consists of a molecular reorganization (e.g. conformational change and/or ion relocation) that is only fruitful if a second Mn^{2+} bound at its correct site, the SMS.

4.5.2 How does Psb27 facilitate photoactivation?

It has been shown that Psb27 is the vital player in PSII repair and assembly of the Mn_4CaO_5 cluster of PSII that provides greater accessibility to the site of Mn-cluster assembly (Roose *et al.*

2004, Nowaczyk *et al.* 2006, Roose *et al.* 2008, Liu *et al.* 2011, Michoux *et al.* 2012, Xingxing 2018). We find that Psb27 facilitates the photoactivation of the WOC in a more complex manner than simply displacing extrinsic polypeptides from apo-PSII. Both Δ*psbO* and *27OE* have increased access of Mn^{2+} and Ca^{2+} to the apo-PSII consistent with expectations (reviewed in (Roose *et al.* 2016)) and also both mutations produce shifts towards higher optimal $[Ca^{2+}]/[Mn^{2+}]$ ratios. In the absence of extrinsic proteins, light induces the loss of Ca^{2+} from its binding site in an S-state dependent manner (Boussac *et al.* 1988, Miqyass *et al.* 2008) and one of the main functions of the extrinsic proteins is to retain the ion (Dekker *et al.* 1984, Ghanotakis *et al.* 1984, Miyao *et al.* 1984). Thus, the shift to higher optimal $[Ca^{2+}]/[Mn^{2+}]$ ratios is likely because without the retention of Ca^{2+} in the vicinity of the assembly site, a relatively higher $[Ca^{2+}]$ is required. Therefore, to mitigate the inhibitory effect of high $[Mn^{2+}]$, apo-PSII requires more Ca^{2+} ions available to prevent occupation of the CAS by Mn^{2+}. Both Δ*psbO* and *27OE* mutants could be photoactivated without the concurrent inactivation **(Fig. 12),** unlike the WT control, which suggests that the increased exchangeability of Ca^{2+} is important for diminishing photoinactivation.

However, if the function of Psb27 only increased exchangeability of Ca^{2+}, then Δ*psbO* and *27OE* would have similar phenotypes in regard to photoactivation. This was not the case and *27OE* provides additional support of photoactivation: *27OE* exhibits a remarkable stabilization at high $[Ca^{2+}]$, yet does not exhibit a proportionally dramatic increase in the dark rearrangement time at the highest $[Ca^{2+}]$ as seen with Δ*psbO* **(Table 5 & 6)**. Additionally, it has a greater ability to sustain high yields of photoactivation at moderate $[Ca^{2+}]$ compared to Δ*psbO* **(Fig. 13)**. Chemical crosslinking indicates that Psb27 docks to the outer face (distal to the Mn-assembly site) of the E-loop of CP43 and exerts its effects, including the weakened binding of extrinsic proteins allosterically (Liu *et al.* 2011) and the strength of this interaction changes during the proteolytic processing of the C-terminus of the D1 protein (Liu *et al.* 2013). This suggests that the Psb27-E-loop interaction stabilizes a structural arrangement that: 1) enhances the selectivity of the second

Mn^{2+} photooxidation site *vis-a-vis* the competitive binding of Ca^{2+} at the SMS, 2) stabilizes the binding of Ca^{2+} to the CAS, and 3) maintains an open configuration that enables rapid rebinding of Ca^{2+} if the ion is lost from the Ca-effector site and/or facilitates the exchange of metals in malformed metal centers.

4.5.3 What is the dark rearrangement?

The utilization of single turnover flashes during the flash interval experiment ensures that the dark rearrangement (**B→C)** estimates the rate, k_A, of a molecular process proposed to be a conformational change (Burnap *et al.* 1995, Chen *et al.* 1995, Burnap *et al.* 1996, Zaltsman *et al.* 1997) or the relocation of a bound ion (Bao *et al.* 2016, Zhang *et al.* 2017). Once the rearrangement has occurred, this still labile configuration can now be trapped by a second quantum and photooxidation of the second Mn^{2+} at the SMS, to produce the first stable intermediate, "**D**" (**Fig. 7**). Based upon the observation that Psb27 allosterically modulates the assembly of the Mn_4CaO_5, we suppose that the mobility of the E-loop is involved as part of the dark rearrangement. The E-loop is a globular domain situated between transmembrane helices 5 and 6 of CP43 and directly interacts with the assembled Mn_4CaO_5, including a bridging carboxylate ligand to Mn2 and Mn3 via CP43-Glu354 (Umena *et al.* 2011). Moreover, it directly contacts the C-terminal domain of the D1-protein, which contains amino acids coordinating the Mn_4CaO_5, and notably provides a ligand to the Ca^{2+} and Mn1 via the carboxyl group of its C-terminus. Thus, movements of the E-loop are likely coupled to movements of the C-terminal domain, and *vice versa*. This mobility would accommodate the assembly/disassembly of the WOC by rocking in and out of contact with the Mn assembly site due to a hinge provided by a pair of proline residues, as suggested previously (Burnap 2004). Consistent with this, a recent cryoEM structure resolution of apo-PSII shows alternative structural arrangements of the apo-WOC, including the E-loop displaced away from the HAS, which is itself rearranged compared the coordination environment of the assembled Mn_4CaO_5 (Gisriel *et al.* 2020) and a recent time-resolved AFM study has demonstrated the E-loop undergoes

hinged stochastic fluctuations (Tokano *et al.* 2020). The increased accessibility in Δ*psbO* cannot be explained by steric covering of the apo-WOC and instead the open configuration must relate to the fact that PsbO forms a structural bridge between the E-loop and other parts of the WOC including the D1 C-terminal domain (**Fig. 5A**). Thus, the more open configuration due to the loss of PsbO is likely due to enhanced mobility of the WOC. A more open position of the E-loop may be stabilized by Psb27, so that it still may fluctuate, but in a range that optimizes assembly, in contrast to the loss of PsbO, where the more open configuration is evident, but not the other kinetic features, which are absent. However, the predicted mobility of the apo-WOC alone does not explain the conformational rearrangement because the rate, k_A, slows down rather than speeds up in the mutants and it is strongly affected by [Ca^{2+}]. So, while conformational mobility of the E-loop and the associated D1-carboxy terminus is a reasonable explanation for the more open structure, how excess Ca^{2+} would also slow the rearrangement process is not obvious. This is where the SMS may factor in: if the dark rearrangement corresponds to conformational fluctuations alternating between the open and closed configurations then a specific closed conformation may be necessary for Mn^{2+} oxidation at the SMS. Furthermore, if the specific conformation is only infrequently realized during the course of conformational fluctuations as suggested by the dwell times of the open and closed conformations (Tokano *et al.* 2020), then competitive occupation of the SMS by Ca^{2+} would delay the time until Mn^{2+} reoccupies the SMS and the specific conformation is re-visited during the course of the conformational fluctuations. In this model, the rearrangement rate reflects the frequency of occurrence that intermediate, **"B"** containing Mn^{3+} has conformationally rearranged, the intrinsic protein conformational rearrangement time, and the SMS site is actually occupied by a Mn^{2+} ion **(Fig. 14)**. At high [Ca^{2+}]/[Mn^{2+}] ratios, the conformational rearrangement may occur, but the correct occupancy of the SMS may not have occurred due to competitive displacement at the SMS.

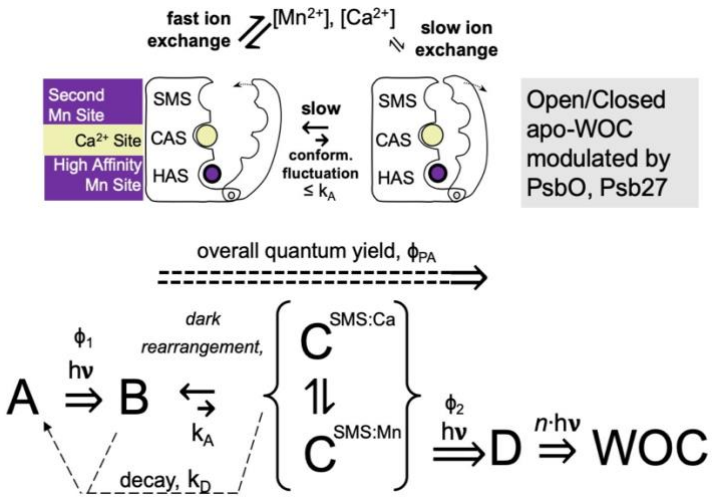

Figure 14. Schematic model of the three main metal binding sites discussed and a minimal model of proposed conformational change and ion exchange accounting for the results.

4.6 Conclusions

In conclusion, the initial stages of photoactivation appear to involve three critical metal binding sites: two Mn (HAS, SMS) and one Ca (CAS). These sites are utilized for photooxidative metal cluster formation in a process that involves structural rearrangements of the protein scaffolding that templates the assembly. Based upon the recently resolved structural features of apo-PSII, the critical metal binding sites do not necessarily correspond to the well-defined sites of the assembled Mn_4CaO_5 (Gisriel *et al.* 2020). Occupation of the CAS by Ca^{2+} is critical for stabilizing assembly intermediates during the dark rearrangement (**B→C)**. Incorrect occupation of the CAS by Mn^{2+}, e.g., at sub-optimal Ca/Mn ratios, results in misses and a photoinactivation process that probably corresponds to the Mn^{2+} photooxidation pathway leading of high valent, but mis-assembled Mn (Chen *et al.* 1995). The long-observed competition between Mn^{2+} and Ca^{2+} appears to occur at the second Mn site (SMS) and its occupation by competing Ca^{2+} slows the dark rearrangement. The results are most easily rationalized in a model where the dark rearrangement involves the mobility of the WOC domain, which fluctuates in the absence of the Mn_4CaO_5 (Tokano *et al.* 2020). In this model, the trapping of the first stable state "**D**" occurs when the restructuring coincides with an

optimal geometry, the metal binding sites are appropriately occupied, and photochemistry presents an oxidant to oxidize the second Mn^{2+}. According to this model significant structural fluctuations occur in the prior the formation of "**D**", but the accessory protein Psb27 allosterically constrains them in a way that optimizes the assembly by stabilizing the intermediates and the promoting productive occupancy of the metal binding sites by their cognate ions.

CHAPTER V

INVOLVEMENT OF D1-GLU189 LIGAND IN THE FORMATION OF THE HIGH AFFINITY SITE OF PHOTOSYSTEM II

5.1 Abstract

The assembly of the Mn_4O_5Ca cluster in plants, algae, and cyanobacteria starts from the initial binding and photooxidation of the first Mn^{2+} at the high affinity site (HAS) of the photosystem II (PSII). Recent cryo-EM apo-PSII structures suggest the involvement of D1-Glu189 ligand in the formation of the HAS, however the precise role of D1-E189 remains obscure. Strains containing Gln, Lys, and Arg substitution mutations, were shown to photoactivate with reduced quantum efficiency compared to the wild-type. Fluorescence relaxation kinetics indicate that the occupancy and/or the ability to photooxidize Mn^{2+} in the HAS is decreased in the mutants indicating that part of the reduced quantum efficiency of assembly is due alterations of the HAS. However, two mutants D1-E189K and D1-E189R also exhibit a large fraction of centers that fail to recover activity during photoactivation starting early in the assembly phase, and that become recalcitrant to further assembly. Additionally, D1-E189R exhibited a gradual, low efficiency recovery of these centers to form active PSII. Fluorescence relaxation kinetics exclude damage to the photochemical reaction center as the cause for the recalcitrant centers failing to assemble and show that dark incubation of cells reverses some of the damage. This reversibility would explain the ability of these mutants to accumulate a significant fraction of active PSII during extended periods of cell growth. The failed recovery in the fraction of inactive centers is tentatively attributed to

accumulation of photooxidized, but non-catalytic high valence Mn at the donor side of photosystem II, and that a reductive mechanism exists for restoration of assembly capacity at sites incurring mis-assembly.

5.2 Introduction

Plants, algae, and cyanobacteria are capable of performing oxygenic photosynthesis, which is a driving force behind the production of oxygen and primary biomass on the planet. The photosystem II (PSII) reaction center complex of photosynthetic organisms catalyzes the extraction of electrons from water molecules to plastoquinone, harnessing light as the energy source to drive this highly endergonic electron transfer. The primary photosynthetic event involves the formation of the highly oxidized electron donor P_{680}^{+} created by the charge separation powered by captured photon energy. P_{680}^{+} is a powerful oxidant capable of extracting the electron from the neighboring redox active tyrosine residue (Y_Z) of the D1 protein. The oxidized tyrosine then extracts an electron from one of the Mn ions of the Mn_4O_5Ca metal cluster embedded in the PSII (Babcock *et al.* 1989, Cardona *et al.* 2012). After each charge separation, the oxidative state of the Mn cluster advances from a more reduced to a more oxidized state, with every state corresponding to one of the five so-called storage states (S_0, S_1, S_2, S_3, and S_4) of S-cycle. The oxidation of two H_2O molecules with the release of molecular oxygen is triggered by the formation of S_4 state, which is concomitantly reduced to the S_0 state, representing Mn cluster ground state (Kok *et al.* 1970).

The assembly of the water oxidizing complex (WOC) termed as photoactivation utilizes essentially the same redox active cofactors for electron transfer and Mn^{2+} oxidation as during the regular electron transfer pathway during WOC activity. Photoactivation begins with charge separation of the photochemical PSII reaction center, forming the highly oxidizing P_{680}^{+} species capable of extracting electrons from Mn^{2+} ions via Y_Z that successively become photooxidatively incorporated into the growing metal cluster [reviewed in (Bao *et al.* 2016)]. The first step prior to Mn^{2+} photooxidation corresponds to the formation of the Mn^{2+} hydroxide intermediate (Ananyev

et al. 1999, Ono *et al.* 1999) at a high affinity site (HAS) that involves the D1-Asp170 carboxylate moiety (Boerner *et al.* 1992, Nixon *et al.* 1992). The exact location of the HAS is still a matter of debate. Surveys of amino acids at the PSII donor side using site-directed mutagenesis revealed D1-Asp170 is most important for the high affinity Mn^{2+} photooxidation by apo-PSII (Boerner *et al.* 1992, Nixon *et al.* 1992, Nixon *et al.* 1992, Chu *et al.* 1994, Cohen *et al.* 2007). Not surprisingly, the affinity for Mn^{2+} ions (K_D < 10 μM) at the HAS (Nixon *et al.* 1992, Ananyev *et al.* 1996, Ono *et al.* 1999) has strong pH dependence, highlighting with the importance of the protonation state of the amino acid residues coordinating Mn^{2+} prior photooxidation (Ono *et al.* 1999). The PSII crystal structure shows that D1-Asp170 provides one of two oppositely arranged axial monodentate carboxyl ligands of the so-called dangler Mn (Mn4) in intact WOC. Interestingly, the other ligand, D1-Glu333, does not seem to be directly involved in the formation of the HAS of apo-PSII, although it weakly influences the affinity of Mn^{2+} at the HAS (Nixon *et al.* 1994, Cohen *et al.* 2007, Umena *et al.* 2011). The evidence that D1-Glu333 does not partake in the formation of the HAS is consistent with recent cryo-EM structures of apo-PSII revealing that the carboxyl domain of the D1 protein adopts a very different conformation and with several residues, including D1-Glu333, are shifted several Ångstroms away from their final positions in the assembled complex (Gisriel *et al.* 2020, Zabret *et al.* 2020) The absence of direct Mn coordination by D1-Glu333 is interesting in light of the assumption that the high affinity binding of Mn^{2+} ion requires two carboxylate moieties (Nakamura *et al.* 2019). Interestingly, D1-His332 is slightly shifted towards hypothetical HAS in apo-PSII and could be involved in coordination of the Mn^{2+} ion (Zabret *et al.* 2020). The closest carboxylate moiety in apo-PSII to D1-Asp170 is D1-Glu189, which also retains a similar position (1.1 Å difference) in the presence and absence of the Mn cluster. The distance between D1-Glu189 and D1-Asp170 in apo-PSII is ~6.0 Å, which is in agreement with the distances found in mature PSII between carboxylate and Mn ions and has been proposed to participate in the formation of the HAS (Gisriel *et al.* 2020, Zabret *et al.* 2020). Perhaps most importantly for questions regarding the nature of the HAS, two of the three current cryo-EM structures of apo-PSII reveal an unidentified

heavy atom, probably either Mn or Ca, located midway between the carboxylate moieties of D1-Glu189 and D1-Asp170. This precise spatial arrangement is not found in the assembled complex since these residues are slightly shifted in orientation compared to their assembled configuration and the heavy atom appears to be in slightly different place than any of the metal ions of the assembled Mn_4O_5Ca. The D1-Glu189 and D1-Asp170 residues share another important characteristic, at least in the assembled complex: besides providing monodentate coordination to Mn (Mn1 and Mn4, respectively), their carboxylate groups each provide a second monodentate ligand to the sole Ca ion of the Mn_4O_5Ca (Umena *et al.* 2011).

Besides providing a ligand to Mn1, D1-Glu189 modulates the redox properties of Y_Z in addition to those of the Mn cluster (Chu *et al.* 1995, Debus *et al.* 2000). Additionally, D1-Glu189 is involved in the formation of a H-bonding network, potentially accepting a proton from D1-His190 (Tommos *et al.* 1998, Tommos *et al.* 2000). Most of the D1-Glu189 site-directed mutants assemble partial or complete Mn clusters, possibly having defects in cluster assembly (Chu *et al.* 1995, Debus *et al.* 2000). Most of these mutants have lost the ability to evolve oxygen, despite containing photooxidizable Mn *in vivo* (Debus *et al.* 2000). Recent time-resolved X-ray crystallography indicates that D1-Glu189 side chain moves away a from the Mn_4O_5Ca during the S_2-S_3 transition, such that the ligand to the Ca ion is broken, but the Mn1 ligation is retained (Suga *et al.* 2017, Ibrahim *et al.* 2020). This movement facilitates what appears to be the Ca^{2+}-mediated insertion of substrate H_2O between Mn1 and the Ca, thereby producing the O_x proposed to be one of the two oxygen atoms of the O_2 formed in the final stages of water oxidation (Cox *et al.* 2014, Suga *et al.* 2017, Ibrahim *et al.* 2020) as consistent with computational analysis (Siegbahn 2013). On the other hand, the fact that several mutations with disparate chemical properties can substitute for glutamate suggests this role is not decisive in the catalytic mechanism.

Given recent results indicating that the D1-Glu189 is potentially involved in the formation of the HAS of PSII, we studied the photoactivation characteristics of three site-directed mutants with

lysine, arginine and glutamine substitutions at the 189 position of D1 protein, which substitutions that permit oxygen evolution at rates comparable with wild type *Synechocystis sp.* PCC 6803, but may alter assembly for the Mn_4O_5Ca (Debus *et al.* 2000).

5.3 Materials and Methods

5.3.1 Strains and Growth Conditions

The glucose-tolerant strain of *Synechocystis sp.* PCC6803 (hereafter *Synechocystis*) (Kanesaki *et al.* 2012) served as the basis for all strains conducted in this study. The wild-type control strain (WT control) was constructed by transforming strain 4E3 HT-3 returning the wild-type *psbA2* gene to its native location and with its native promoter using *psbA2* using in the suicide plasmid pRD1031 as described previously (Debus *et al.* 2001). The 4E3 HT-3 strain lacks all three *psbA* genes and has the CP47 gene hexa-histidine tag at its carboxy terminus. Its transformation with the wild-type *psbA2* gene restored wild-type levels of D1 expression and oxygen evolution under normal growth conditions (Debus *et al.* 2001). Site-directed mutations in the *psbA2* gene encoding the D1-E189Q, D1-E189K and D1-E189R amino acid substitutions involved similar transformations but using site-directed mutant *psbA2* alleles resulting the mutant strains (Chu *et al.* 1994).

All *Synechocystis* strains were routinely maintained on BG-11 agar plates with addition of 10 µM DCMU and 5 mM Glucose as described previously, to prevent reversion and suppressor mutations since these conditions remove any selective advantage higher PSII activity (Williams 1988). Experimental cultures were grown in 1 L flat flasks in 800 mL of BG-11 with the addition of 10 mM HEPES-NaOH pH 8.0 and 5 mM glucose under PFD (photon flux density) of ~100 µmol m^{-2} s^{-1} at 30 ˚C. Light intensity was measured with Walz light meter (Germany). All experimental cultures were harvested in late log phase (O.D. 750nm ~1.2-1.5) and checking the variable

fluorescence (F_V) value maximal for every strain (supplementary Table 1) as determined with a PSI fluorometer (PSI instruments) using $F_v = (F_{max} – F_0)/ F_0$.

5.3.2 Hydroxylamine Extraction of Cells

Cultures with the maximal F_v values for each strain [D1-Glu189K, 0.6; D1-Glu189Q, 0.6; D1-Glu189R, 0.4; D1-Asp170E, 0.62; WT control, > 0.7] were collected in late log phase; 800 mL of cells were centrifuged in 1 L bottles at 6000 g (Sorvall, F9 rotor) for 12 minutes at room temperature. Extraction of the Mn_4O_5Ca using hydroxylamine (HA) was performed as described previously (Cheniae *et al.* 1971, Hwang *et al.* 2005). Briefly, cells were washed in BG-11 and concentrated to a chlorophyll concentration of 100 µg/mL, HA was added to a cell suspension from a 400 mM freshly prepared stock to a final concentration of 10 mM (Hwang *et al.* 2007). Cell suspension was incubated in the dark on a rotary shaker at ~120 rpm at room temperature for 12 minutes. After the incubation, cells were diluted with 5x volume of BG-11 and centrifuged at 10200 g (Sorvall, F14 rotor) at room temperature for 5 minutes. This washing step was repeated for 7 more times. After the washing was complete, cells were resuspended to [Chl] of 100 µg/mL and kept in the dark with shaking at ~120 rpm.

5.3.3 Photoactivation of HA-Extracted cells

HA-extracted were either photoactivated using single-turnover Xenon lamp flashes or continuous light (Cool White fluorescent) at an intensity of ~50 µmol m^{-2} s^{-1}. Single-turnover Xenon lamp flash experimental procedure was carried out as described previously in (Hwang *et al.* 2005). A 400 µL aliquot of cells containing ~40 µg of chlorophyll was taken from the cell suspension kept in the dark. Cells were placed on a sample vessel fashioned out of an aluminum weighing cup with the stirring bar and covered with yellow UV filter to minimize UV damage to the sample. The sample was subjected to saturating single-turnover Xe flashes to promote photoactivation. This was followed by the measurement of light-saturated rates of O_2 evolution to

evaluate restoration of catalytic activity. To accomplish this, aliquots containing 10 µg of Chl were withdrawn from the photoactivated cell suspension and placed in the Clark-type electrode (Yellow Springs Instruments) chamber containing buffered BG-11 with the addition of 1 mM DCBQ and 1 mM potassium ferricyanide. The oxygen evolution rate was measured in response to saturating orange light (>570 nm) at 30 ˚C.

5.3.4 Curve fitting and data analysis.

Experiments measuring the photoactivation of the Mn depleted PSII as a function of single-turnover flashes and a function of the flash interval allowed us to evaluate both the quantum efficiency of photoactivation and to estimate the kinetic parameters for the dark rearrangement and decay of intermediates. The rate constants for the dark rearrangement, k_A, and the decay of intermediates, k_D, were determined by deriving kinetic parameters from the rising and falling slopes of the bell-shaped curve in plots of photoactivation as a function of the flash interval curve fitted to the equation (Tamura *et al.* 1987, Miller *et al.* 1989, Hwang *et al.* 2007, Avramov *et al.* 2020):

$$[A]_n = [k_A/k_D - k_A] \times [A]_O \times \left(e^{-k_A td} - e^{-k_D td}\right). \quad \text{Equation 3}$$

Statistical analysis to obtain p-values has been performed in GraphPad Prism using an ordinary one-way ANOVA approach. The correction for multiple comparisons was utilized via Tukey statistical hypothesis testing with a single pooled variance.

5.4.5 Fluorescence relaxation kinetics

Flash induced fluorescence relaxation kinetics were measured as described by Vass (Vass *et al.* 1999) using FL-3300 fluorometer (PSI Instruments, Czech Republic). The width of actinic and measuring light pulses were equal to 30 µs and 9 µs respectively, relaxation kinetics were measured from range of 100 µs to 100 s. Sample was diluted to a concentration of 5 µg of Chl/mL in 3 mL of BG-11 and placed into the 4-sided clear cuvette for measurement. Multi component fluorescence

relaxation analysis was performed as earlier by Vass (Vass *et al.* 1999, Cser *et al.* 2005) by using fitting function with two or three components:

Table 7. Multicomponent kinetic equations used to fit the data from the data plots obtained from fluorescence relaxation kinetics experiments.

Components	Equation
Fast – Exponential Middle – Exponential Slow – Hyperbolic	$F(t) - F_0 = A_1 \exp\left(-\frac{t}{T_1}\right) + A_2 \exp\left(-\frac{t}{T_2}\right) + A_3/(1 + \frac{t}{T_3})$
Fast – Exponential Slow – Hyperbolic	$F(t) - F_0 = A_1 \exp\left(-\frac{t}{T_1}\right) + +A_2/(1 + \frac{t}{T_2})$
Fast – Exponential Middle – Hyperbolic Slow – Hyperbolic	$F(t) - F_0 = A_1 \exp\left(-\frac{t}{T_1}\right) + A_2/(1 + \frac{t}{T_2}) + A_3/(1 + \frac{t}{T_3})$

Where $F(t) - F_0$ is relative fluorescence yield, A_1-A_3 are decay amplitudes, T_1-T_3 are time constants from which the half-times can be calculated via $t_{1/2} = \ln 2\ T$ for exponential components and $t_{1/2}$ = is T for hyperbolic component.

5.4 Results

5.4.1 Photoactivation in continuous light shows altered Mn_4O_5Ca assembly in mutants

There is consensus that D1-Asp170 is critical for both binding and photooxidation of Mn^{2+} at the HAS (Boerner *et al.* 1992, Nixon *et al.* 1992, Cohen *et al.* 2007, Hwang *et al.* 2007) consistent with its monodentate coordination of Mn4 in the assembled complex (Umena *et al.* 2011). However, recent cryo-EM studies Mn-depleted PSII identifies two additional residues potentially involved in the formation of the HAS in apo-PSII and thus potentially involved in photoactivation. These residues, D1-Glu189 and D1-His332, are shifted towards D1-Asp170 compared to mature PSII. Their close proximity to D1-Asp170 potentially allows for Mn^{2+} to be coordinated between them, which is in accord with the observation of an unidentified heavy atom located midway between the D1-Asp170 and D1-Glu189 carboxyl groups (Gisriel *et al.* 2020, Zabret *et al.* 2020). To test the general hypothesis that D1-Glu189 modulates photoactivation, three amino acid substitution mutants capable of relatively high rates of oxygen evolution, D1-E189Q, D1-E189K and D1-E189R, were investigated. In addition, the D1-D170E mutant, which was previously shown

to have a lower quantum efficiency of photoactivation was also included in this study for comparison.

The oxygen evolution rates in freshly isolated cells are shown in **Fig 15A.** The site-directed mutants exhibit rates that are approximately 60% of the WT control, with the exception of D1-E189K which was 81% (Debus *et al.* 2000). The results confirm the initial studies on these mutants and demonstrate that even relatively drastic amino acid substitutions of D1-Glu189 still allow the assembly of active PSII under the protracted conditions of growth. To gain information on whether the mutations affect the kinetics of assembly, cells were treated with hydroxylamine to remove active Mn and samples were photoactivated under continuous light (**Fig. 15B**). The extent of recovered O_2 evolution activity is expressed as a ratio of the recovered rate to the rate prior to HA-extraction. Consistent with previous results, WT cells recovered >90% of their original activity within 15 min of illumination. Photoactivation of HA-extracted D1-D170E cells restored approximately 70% of the original activity, but this took longer, ~40 minutes. This consistent with the flash experiments (next section) and previous findings showing reduced quantum efficiency of photoactivation. Thus, substitution of Asp170 of the HAS with the slightly large Glu side chain permits assembly but with reduced quantum efficiency. The restoration of O_2 activity was dramatically different among the D1-Glu189 mutants: D1-E189Q showed similar restoration level to D1-D170E. However, it required only 20 minutes to reach 70% of its initial activity, while D1-E189K and D1-E189R mutants restored only 40% and 30% after 40 minutes of illumination, respectively. Thus, all mutants are impaired in photoactivation in HA-extracted cells compared to the WT, but D1-E189R and especially D1-E189K, poorly photoactivate under these laboratory conditions given the extent of assembly possible despite the mutations in cells grown in culture.

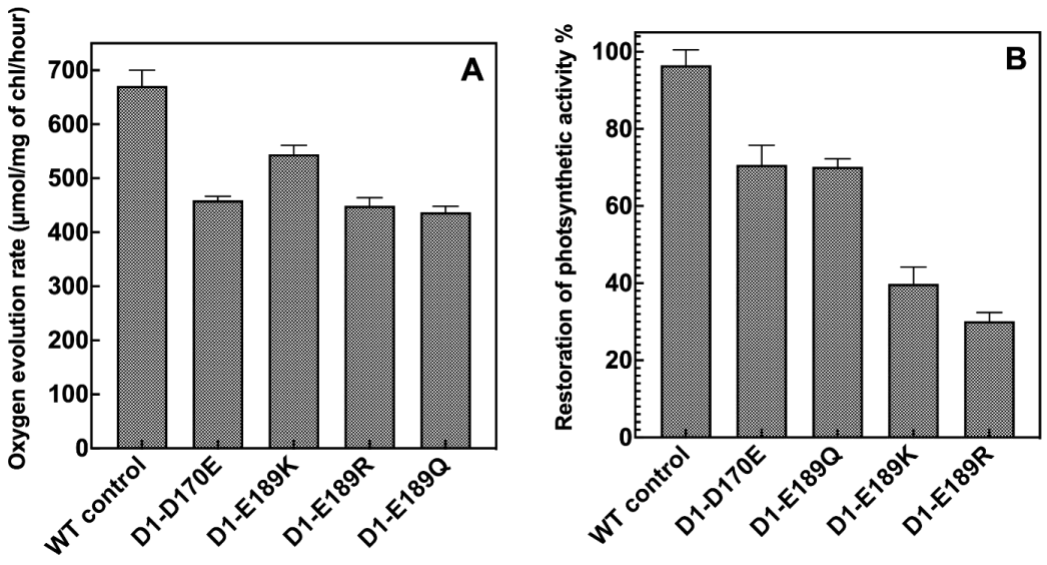

Figure 15. Light-saturated O_2-evolution activity of *Synechocystis* cells (A) harvested directly from growth culture. (B) Recovery of light-saturated O_2-evolution activity of HA-treated *Synechocystis* cells after photoactivation under continuous illumination. HA-treated cells were exposed to continuous illumination (~20 µmol m^{-2} s^{-1} PD) while being gently shaken ~100 rpm. Oxygen evolution activity was measure on Clark-type electrode in HN buffer (10 mM HEPES, 30 mM NaCl, pH 7.2 in the presence of 1 mM DCBQ and 1 mM potassium ferricyanide). Oxygen evolution was measures in response to saturating (>570 nm) illumination at 30 ˚C. The original light-saturated O_2-evolution rates prior HA extraction were 671 ± 29, 459 ± 7, 544 ± 16, 449 ± 15 and 437 ± 11 µmol of O_2 $(mg\ Chl)^{-1}$ h^{-1}, for WT control, D1-D170E, D1-E189K, D1-E189R, and D1-E189Q respectively. Error bars represent SD with $n \geq 3$.

5.4.2 Photoactivation as a function of a flash number

The photoactivation as a function of the number of single-turnover Xe flashes allows us to gather the values of quantum efficiency of photoactivation e.g., obtain values that reflect the per flash development of O_2 evolution activity in Mn-depleted samples. The yields of photoactivation of investigated HA treated mutants as a function of flash number are illustrated in **Figure 16**. For this experiment the uniform flash interval of 2 Hz (500 ms flash interval) was used to photoactivate the samples. The results are presented as a fraction of the restoration of the initial O_2 activity prior the Mn extraction. Consistent with the previous results (Burnap *et al.* 1996, Hwang *et al.* 2005,

Hwang *et al.* 2007), HA-treated WT control cells reached approximately 85-90% if initial activity after 2000 flashes, while 6400 flashes resulted in almost complete restoration of WOC activity (**Fig 16A**). The D1-E189Q mutants (**Fig. 16E**) exhibits similar photoactivation characteristics as the WT control, however it never approaches complete photoactivation. The maximum restoration of O_2 activity of 80% was observed after 2000 single-turnover flashes and percent activity does not significantly increase even after 6400 flashes. This behavior contrasts with both WT-control (**Fig. 16A**), which is capable of reaching nearly 100% of initial activity, and D1-D170E mutant (**Fig. 16B**) that exhibits lower quantum efficiency of photoactivation but nevertheless continues to develop O_2 evolution rate throughout the entire series of photoactivation flashes although not reaching levels as high as the WT even after 6400 flashes. Unlike D1-E189Q, Lys or Arg at 189 position caused a severe inhibition of photoactivation as shown in D1-E189K and D1-E189R (**Fig. 15B, 16C & D**) mutants even though the maximal O_2 net rates prior to extraction being similar to the other mutants (**Fig 15A**). A series of 2000 photoactivation flashes given to both D1-E189R and D1-E189K mutants resulted only in 40% and 25% restoration respectively. Interestingly, D1-E189R continued to assemble Mn cluster after 2000 flashes, which is similar to D1-D170E mutant although with lower quantum efficiency, Φ_{PA2} (**Table 8**). In case of D1-E189K, the level of photoactivation shows little increase after 6400 flashes.

To derive the constants of both rapid and slow phases of photoactivation seen in **Figure 15**, the obtained data was fit into the double exponent equation:

$$[A]_n = [A]_0 \times (1 - e^{-\Phi_{PA1}\mathrm{n}}) \times (e^{\Phi_{PA2}\mathrm{n}}), \qquad \text{Equation 4}$$

where $[A]_n$ represents the yield of active centers on the *n*th flash, $[A]_0$ is the concentration of apo-PSII centers prior to the photoactivation, Φ_{PA1}, and Φ_{PA2} represent two apparent phases of photoactivation: a more efficient phase more obvious in the beginning of the series of photoactivation flashes and lower efficiency phase afterwards. The quantum efficiency of the

photoactivation, $\Phi_{PA1,2}$ (**Table 8**), in all studied mutants indicates the severe effect of the mutations at the HAS on the overall efficiency of the light-driven assembly of the Mn_4O_5Ca cluster but distributed differently between the two phases. Interestingly D1-D170E mutant, which is shown to have a significantly lower quantum efficiency of photoactivation is capable of significant levels of O_2 rate restoration. While D1-E189K and D1-E189R have higher Φ_{PA1} than D1-D170E, they fail to reassemble Mn cluster in the majority of the PSII centers, unlike D1-D170E. All studied D1-E189 mutants share a similar feature of an efficient initial photoactivation phase within first 400-800 flashes followed by a significant decrease in the efficiency in assembly and failure to restore activity in a large fraction of centers. The inability of D1-E189Q, D1-E189K, and D1-E189R mutants to reach 100% activity could indicate an irreversible inhibition of the photoactivation. This inactivation does not seem to correspond to damage to the photochemical reaction center and is tentatively assigned to the accumulation of non-catalytic high valent Mn (described as "inappropriate Mn" (Chen *et al.* 1995)) in these mutants. However, in the D1-E189R mutant the second phase, Φ_{PA2} (**Table 8**), is almost 3 times higher than in D1-E189K and 10 times higher than in D1-E189Q mutant and results in progressive increase in the number of active centers after 6400 flashes. Thus, despite the presence of inhibited PSII centers, D1-E189R may have the capacity to re-assemble WOC. In this scenario, D1-E189R may accumulate non-functional Mn, but the Arg substitution renders it unstable, open the possibility of correct re-assembly, albeit at low quantum efficiency, after loss of mis-assembled Mn. However, verification of the tentatively assigned "inappropriate Mn" (Chen *et al.* 1995), will require further *in vitro* studies with purified PSII core complexes for careful investigation of the phenomenon.

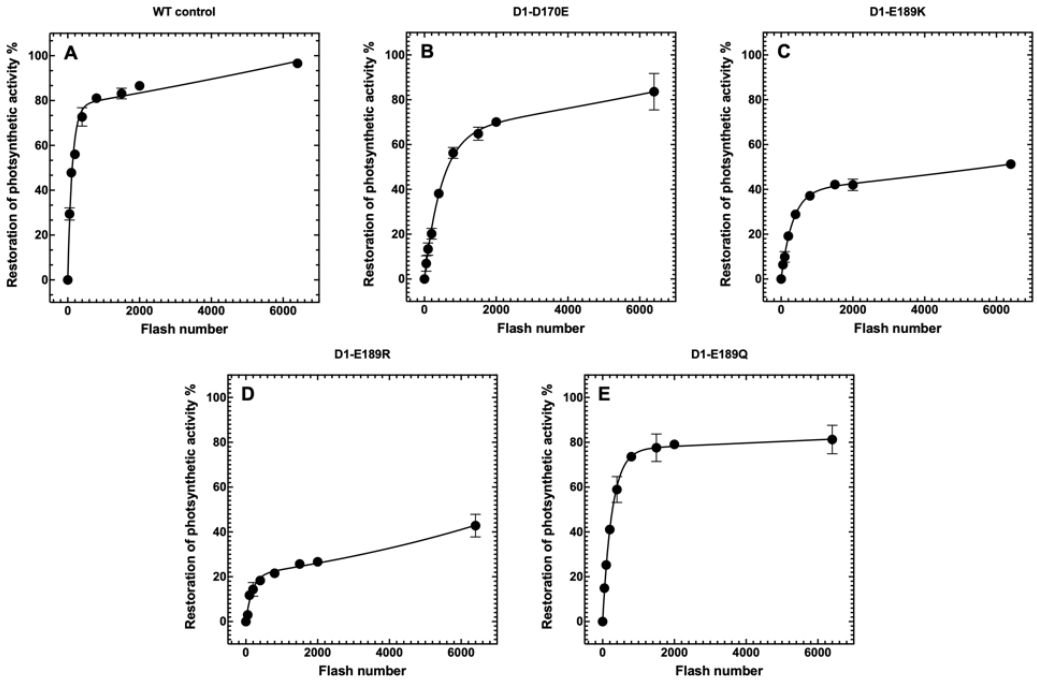

Figure 16. Photoactivation of HA-extracted cells as a function of the single-turnover flash number. Series of xenon lamp flashes were given at uniform frequency of 2 Hz (500 ms flash interval) to hydroxylamine-treated WT control (Panel A), D1-D170E (Panel B), D1-E189Q (Panel C), D1-E189K (Panel D), D1-E189R (Panel E). The percentage of O_2 evolution recovery was calculated as a fraction from the O_2 evolution rate prior HA extraction which were 671 ± 29, 459 ± 7, 544 ± 16, 449 ± 15 and 437 ± 11 µmol of O_2 (mg Chl)$^{-1}$ h^{-1}, for WT control, D1-D170E, D1-E189K, D1-E189R, and D1-E189Q respectively. Error bars represent SD with n ≥ 3.**Table 8. Quantum efficiency of photoactivation of WT control, D1-D170E, D1-E189K, D1-E189R and D1-E189Q mutant strains.** To obtain the kinetic parameters of Φ_{PA1} *and* Φ_{PA2} the data from the plots in Figure 1 was fit into Equation 4.

Strain	Quantum efficiency of Photoactivation, Φ_{PA1}	Quantum efficiency Restoration, Φ_{PA2}	R
WT control	8.1×10^{-3}	3.6×10^{-5}	0.98
D1-D170E	2.1×10^{-3}	3.8×10^{-5}	0.99
D1-E189K	3.2×10^{-3}	4.2×10^{-5}	0.99
D1-E189R	5.7×10^{-3}	1.1×10^{-4}	0.98
D1-E189Q	3.8×10^{-3}	9.1×10^{-6}	0.99

5.4.3 Dark molecular rearrangement and the stability of photoactivation intermediates

According to the "two-quantum model" of photoactivation (**Fig. 4**), the formation of the first stable intermediate (intermediate **D**) involves two photoacts separated by a light-independent molecular rearrangement (Radmer *et al.* 1971, Bao *et al.* 2016). This rate-limiting rearrangement, combined with the limited stability of the photoactivation intermediates, results in a bell-shaped curve when the formation of active PSII is promoted by a fixed number of flashes given at different flash intervals, measuring the extent of recovery of O_2 evolution after the flash sequence (Cheniae *et al.* 1971, Tamura *et al.* 1987, Hwang *et al.* 2005, Hwang *et al.* 2007, Avramov *et al.* 2020).

For the present experiments, a fixed number of flashes was determined for each strain so as to give approximately 50% recovery at optimal flash spacing. This number of flashes was given to HA-extracted samples at intervals ranging from 50 millisecond to 10 seconds for each of the strains and the plotted yields at each flash frequency produced the 'bell-shaped' curves shown in **Figure 17**. To estimate time constants for the dark rearrangement, k_A, and the decay of labile intermediates, k_D, the flash interval photoactivation data was fit into the equation derived from the two-quantum model (Tamura *et al.* 1987, Hwang *et al.* 2007, Avramov *et al.* 2020). The values for the dark rearrangement and the decay of intermediates in terms of half-times for WT control were 66 ms and 1.8 s respectively (**Table 9**). All mutants studied showed similar moderately slowed values for the dark rearrangement, k_A ranging from 78 – 82 ms, the rate-limiting, molecular rearrangement (**Fig. 4, B→C**). Recent evidence suggests that the dark rearrangement, k_A, involves a conformational change of the metal-binding polypeptide structure of the WOC (Avramov *et al.* 2020, Gisriel *et al.* 2020, Tokano *et al.* 2020). Since all mutants exhibit similarly decreased k_A value compared to WT control, yet had markedly different extents of assembly, the reason behind the inability of D1-E189K and D1-E189R mutants to assemble a large fraction of their PSII centers (**Fig. 17**) is probably not directly associated with slowed the rate of the molecular rearrangement (Ono *et al.* 1987, Miller *et al.* 1989, Ananyev *et al.* 1996, Burnap *et al.* 1996). Interestingly, all

mutants, especially D1-E189R, exhibited decreased stability of the labile photoactivation intermediates, with the half time of 0.68 s for D1-E189R versus 1.8 s in the WT (**Fig. 17 and Table 9**). This result is consistent with D1-E189 providing as stabilizing interaction with the Mn^{3+} ion produced during the initial photooxidation at the HAS **(A→B)** and that the arginine substitution is especially destabilizing to the binding of cations given its tendency to be positively charged.

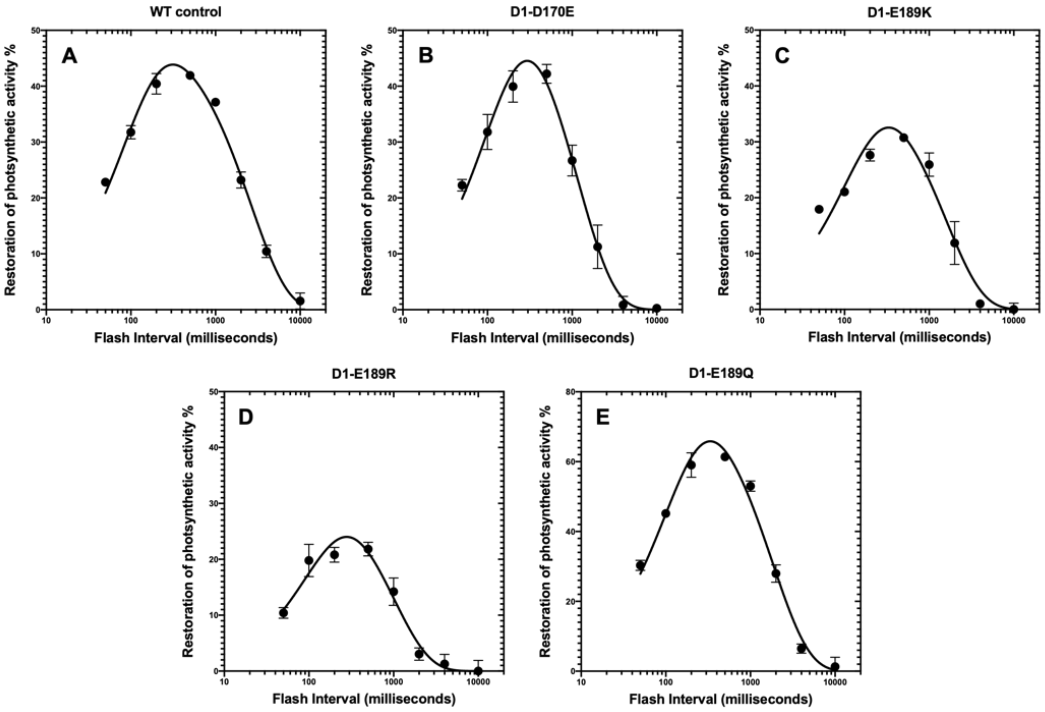

Figure 17. Photoactivation of HA-extracted cells as a function of flash interval. Flashes were given at eight different equal flash intervals to HA-extracted WT control (Panel A), D1-D170E (Panel B), D1-E189K (Panel C), D1-E189R (Panel D), D1-E189Q (Panel E). The curves represent fits to Eq. 2 derived from the two-quantum model shown in **Figure 4** (Tamura *et al.* 1987). The number of photoactivation flashes was determined based on the flash number experiment (**Fig. 16**) to produce approximately 50% restoration of activity. This corresponded to 150, 250, 350, 350 and 500 for WT control, D1-E189Q, D1-E189K, D1-E189R and D1-D170E respectively. The percentage of O_2 evolution recovery was calculated as a fraction from the O_2 evolution rate prior HA extraction which were 600 ± 20, 369 ± 27, 520 ± 32, 402 ± 12 and 262 ± 9 µmol of O_2 (mg Chl)$^{-1}$ h^{-1}, for WT control, D1-D170E, D1-E189Q, D1-E189K and D1-E189R respectively. Error

bars represent SD with n ≥ 3.**Table 9. Dark rearrangement, k_A and decay of intermediates, k_D, parameters WT control, D1-D170E, D1-E189K, D1-E189R, and D1-E189Q mutant strains.**

Strain	k_A (s^{-1}) ($t_{1/2}$)	k_D (s^{-1}) ($t_{1/2}$)	R
WT control	10.45 (66 ms)	0.37 (1.8 s)	0.97
D1-D170E	8.72 (79 ms)	0.86 (0.8 s)	0.99
D1-E189K	8.45 (82 ms)	0.63 (1.1 s)	0.95
D1-E189R	8.72 (79 ms)	1.01 (0.68 s)	0.97
D1-E189Q	8.86 (78 ms)	0.55 (1.2 s)	0.99

[a] Values of parameters were estimated from the fits of the flash interval data (**Fig. 17**) using the into the equation derived from the two-quantum model of photoactivation (**Fig. 4**). Note that the number of photoactivation flashes were different among samples and were adjusted to produce 50% restoration of activity according to the fast phase of photoactivation (**Fig. 16**). This corresponded to 150, 250, 350, 350 and 500 for WT control, D1-E189Q, D1-E189K, D1-E189R and D1-D170E respectively.

5.4.4 Fluorescence relaxation kinetics in the cells with intact PSII

A saturating actinic flash of light produces the high fluorescence state $Y_Z^{\bullet}P_{680}Q_A^-$ state of PSII within several μs after the flash. The subsequent relaxation of this high fluorescence state represents the reoxidation of Q_A^-, which can occur via several electron transfer pathways with different rate constants and is sensitive to the assembly state of the WOC (Crofts *et al.* 1983, Renger *et al.* 1995, de Wijn *et al.* 2001). Additionally, the amplitude of the fluorescence yield provides a relative measure of the concentration of the concentration of PSII reaction centers capable of charge separation and this variable fluorescence yield reports relative PSII concentrations in whole cells that are comparable to quantitative affinity binding assays using radioactively labelled herbicide binding to determine the concentration of the PSII Q_B site. Fluorescence decay reporting reoxidation of Q_A^- in the absence of inhibitors predominantly occurs via rapid forward electron transfer from Q_A^- to Q_B or Q_B^-, depending on which form of the mobile plastoquinone acceptor is present in the Q_B binding site. These fast fluorescence decays occur in the microsecond scale (~500 μs) (Cser *et al.* 2005) and results in 87% fluorescence relaxation (**Fig. 18A**, **Table 10**). The middle phase (τ = ~4.3 ms, amplitude 11%) reflects the delayed reoxidation of Q_A^- in the PSII centers that

start after the flash with the vacant Q_B site, thus the electron transfer is only possible when oxidized Q_B arrives by diffusion from the PQ pool. Lastly, the slow phase (τ = ~8.3 s, amplitude 2%) arises from the charge recombination from $Q_AQ_B^-$ with the S_2 state of the Mn cluster at the donor side of PSII via equilibrium with $Q_A^-Q_B$. Interestingly, in the absence of the Mn cluster, WT control completely loses the slow phase (**Fig S9B**), while all other mutants seem to retain the ability to re-oxidize Q_A^-. All studied mutants with perturbations at the HAS showed similar time constant for the fast decay component in the absence of DCMU i.e. rapid forward electron transfer from Q_A^- to Q_B or Q_B^-, (**Fig. 18A**), although the amplitude of this phase substantially increased to approximately 95% (**Table 10**). Interestingly, the time constant for the middle component stayed similar to WT control, however the yield of fluorescence decay during both middle and slow phases was significantly lower in mutants indicating alternative strategies for Q_A^- reoxidation. Overall, the results indicate that the mutations on the donor side of PSII are only marginally affecting electron transfer on the acceptor side of PSII consistent with the original analysis of these mutations.

To provide insight into the redox properties of the donor side, fluorescence relaxation kinetics were measured the presence of DCMU (**Fig. 18B**), which prevents binding of plastoquinone at the Q_B site, thereby blocking forward electron transfer. The reoxidation of Q_A^- in this situation occurs by recombination with oxidized species on the donor side if PSII. In intact PSII, this electron back-reaction mainly (89%) occurs via the charge recombination with S_2 state of the Mn cluster, which is determined by the equilibrium between S_2P_{680} and $S_1P_{680}^+$ (Bouges-Bocquet 1980, Buser *et al.* 1990, Vass *et al.* 1991) and occurs with a time constant of ~750 ms. Additional pathways of Q_A^- reoxidation may also arise from the interactions with the electron acceptors less stable than S_2 such as $Y_Z^\bullet$, $Y_D^\bullet$ and photooxidized Mn in partially assembled PSII centers (Demeter *et al.* 1993, Chu *et al.* 1995, Vass *et al.* 1999, Cser *et al.* 2005). All studied site-directed mutants show significant amount of rapid fluorescence decay in the presence of DCMU (**Fig. 18B**) that probably corresponds to rapid charge recombination between Q_A^- and $Y_Z^\bullet$, presumably because a fraction of centers do

not contain a functional Mn_4CaO_5 and thus cannot form the S_2 state (Chu *et al.* 1995). The D1-D170E mutant, unlike all other studied strains, showed multicomponent decay behavior in the presence of DCMU consistent with previous results (Chu *et al.* 1994) indicating a significant perturbation in Q_A^- reoxidation pathway due to the alterations in midpoint potential of S_2/S_1 couple of the Mn cluster. D1-D170E shows pronounced fast phase and middle phases (τ = ~13.9 ms, amplitude 25% and τ = 3 s, amplitude 48%) respectively, while the remainder of Q_A^- decays with the time constant exceeding the time scale of the experiment (**Table 10**) indicating a lack of photooxidized Mn on the donor side of PSII (Chu *et al.* 1994). D1-E189K and D1-E189Q mutants showed similar time constants to WT control in a slow phase (τ = ~1 s), however with significantly lower yield (amplitude ~75%). Interestingly, all mutants showed increased fluorescence decay in a fast phase due to rapid charge recombination between Q_A^- and $Y_Z^\bullet$. The occurrence of a fast phase in the samples containing DCMU could be attributed to partially assembled donor side as suggested previously (Allahverdiyeva *et al.* 2004, Cser *et al.* 2005). The difference in fluorescence relaxation kinetics of the slow phase corresponding to between D1-E189 mutants and WT control could be explained by significantly altered mid-point potential in the S_2/S_1 states of the Mn cluster because of the differences in pK_A values of glutamate, glutamine, arginine and lysine (Debus *et al.* 2000).

5.4.5 Fluorescence relaxation kinetics in hydroxylamine-extracted cells

The D1-D170E, D1-E189K, and D1-E189R mutants displayed nearly complete decay of Q_A^- within 1 s following HA-extraction of the Mn_4CaO_5 (**Fig. S9B**). In contrast, the decay of fluorescence WT control was not complete even after >10 s. The longer lifetime of Q_A^- in the WT is due to the presence of Mn^{2+} at the HAS at the moment of charge separation, permitting efficient reduction of P_{680}^+ and thereby trapping the center in the high fluorescence $Y_ZP_{680}Q_A^-$ state. It is important to keep in mind that although Mn_4CaO_5 has been removed from the samples, there is a sufficient concentration of Mn^{2+} in the cells to allow full reassembly and therefore it is reasonable that Mn^{2+} can occupy the HAS in these samples. However, absence of this trapping of the high

fluorescence $Y_ZP_{680}Q_A^-$ state as observed in the D1-D170E, D1-E189K, and D1-E189R mutants indicates that Mn^{2+} does not occupy the HAS and/or it is not efficiently oxidized, a result which fits with the observed lower quantum efficiency of photoactivation in these mutants. The D1-E189Q mutant, on the other hand, more closely resembles the WT, again in accord with its photoactivation characteristics.

5.4.6 Fluorescence relaxation kinetics in the photoactivated cells

To observe changes in the fluorescence kinetic properties of HA-treated cells during the photoactivation, the sequence of 2000 flashes was given to the Mn depleted cells prior to the fluorescence measurement. All studied strains restored the ability to re-oxidize Q_A^- via the charge recombination with the S_2 oxidation state of newly assembled Mn cluster, although to different extents (**Fig. 18C, Table 10**). WT control showed similar fluorescence relaxation kinetics occurring in fast (τ = 0.8 ms, amplitude 22%) and slow (τ = 0.7 s, amplitude 78%) phases as in the cells prior HA treatment (**Fig. 18B**, **Table 10**). Among the site-directed mutants only D1-E189Q showed similar fluorescence decay pattern to the WT control and to the cells prior HA treatment, however the kinetic parameters clearly indicate on multiphasic decay behavior. Analysis of the fluorescence decay curve has revealed the presence of 2.36 ms fast phase contributing 24% of decay amplitude as well as τ = 1 s (63%) and τ = 87 s (13%) phases. D1-E189K and D1-E189R showed similar patterns for the fast phase with time constants of τ = 5.6 ms and τ = 3.7 ms yielding approximately 38% of total fluorescence decay. However, D1-E189K exhibited an extended middle phase (τ = 627 ms, amplitude 49%) compared to D-E189R (τ = 269 ms, amplitude 34%). The difference in the decay yield and time constants between these two mutants could be explained by the different extent of Mn cluster assembly, which matches the photoactivation pattern in these mutants (**Fig. 17C & D**). The analysis of the fluorescence decay in re-photoactivated D1-D170E mutant revealed that, unlike in all D1-E189 mutants the fast phase is similar to WT control (τ = 0.9 s, amplitude

24%). Interestingly, while the time constant for the slow phase in D1-D170E was $\tau = 4.7$ s, the half time for the slow phase in all D1-E189 mutants was estimated to be ≥ 100 s.

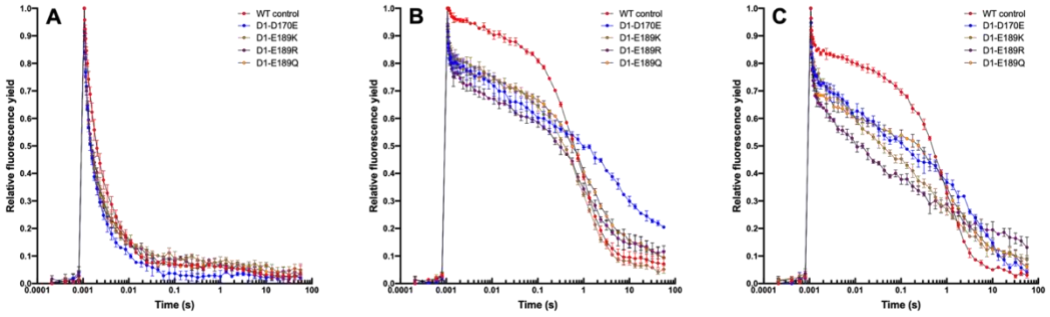

Figure 18. Q_A reoxidation kinetics in WT control, D1-D170E, D1-E189K, D1-E189R, and D1-E189Q strainsn the (**A**) absence of DCMU, (**B**) presence of DCMU and (**C**) re-photoactivated cells in the presence of DCMU. For the purpose of the photoactivation (**C**) the sequence of 2000 single turnover flashes was given to the HA-extracted cyanobacterial cells at 2 Hz (500 ms flash interval). The measurements were performed after a single actinic flash of light. Samples were dark adapted for 5 minutes prior the measurements. Error bars represent SD with $n \geq 3$

Table 10. Characteristics of chlorophyll fluorescence relaxation kinetics in untreated and re-photoactivated WT control, D1-D170E, D1-E189K, D1-E189R and D1-E189Q cells.

Strain	Fast phase: τ/ms (amplitude (%))	Middle phase: τ/ms (amplitude (%))	Slow phase: τ/s (amplitude (%))	R
Intact Mn_4O_5Ca cluster in the absence of DCMU				
WT control	0.4 (86.9)	4.29 (11.1)	8.3 (1.9)	0.99
D1-D170E	0.3 (96)	7.4 (3.5)	86. 6 (0.5)	0.99
D1-E189K	0.2 (97.3)	5.2 (2)	34.8 (0.6)	0.99
D1-E189R	0.3 (95.8)	4.9 (3.3)	6.9 (0.9)	0.98
D1-E189Q	0.26 (96.8)	5.9 (2.6)	36.5 (0.7)	0.98
Intact Mn_4O_5Ca cluster in the presence of DCMU				
WT control	1.6 (11)	(0)-	0.75 (89)	0.99
D1-D170E	13.9 (24.8)	3008 (47.9)	>100 (27.2)	0.99
D1-E189K	3 (16)	(0)-	0.8 (75)	0.98
D1-E189R	3.9 (25.4)	(0)-	1.6 (74.5)	0.98
D1-E189Q	0.93 (28.9)	(0)-	1 (71)	0.99
Re-photoactivated cells in the presence of DCMU				
WT control	0.8 (21.8)	(0)-	0.7 (78.2)	0.99
D1-D170E	0.9 (23.5)	308 (26.9)	4.7 (49.6)	0.99
D1-E189K	5.6 (37.5)	627 (49.4)	>100 (13.1)	0.99
D1-E189R	3.7 (38.1)	269 (33.7)	96.9 (28.1)	0.99
D1-E189Q	2.36 (24)	1011 (63.3)	89.6 (12.6)	0.99

Photoactivation involved a sequence of 2000 single turnover flashes to the HA-extracted cyanobacterial cells at 2 Hz (500 ms flash interval). The decay curves in the absence of DCMU were fit assuming exponential decay for the fast and the middle phases and hyperbolic for the slow phase. The decay curves in the presence of DCMU were analyzed with exponential components for the fast decay and hyperbolic for the slow phase, except for D1-D170E where exponential fit was used for the fast phase and hyperbolic for both middle and slow phases. The data from re-photoactivated samples was analyzed with exponential fit for the fast phase and hyperbolic for both middle and slow phases except for WT control where an exponential component was used for the fast decay and hyperbolic for the slow phase (see **Table 7**).

5.4.7 Partial photoactivation of Mn depleted cells

The observation that D1-E189K and D1-E189R mutants reach only 25-40 % of maximal O_2 evolution activity after treatment with hydroxylamine (**Fig. 15B, 16C & D**) may indicate the bifurcation of the photoactivation process with essentially two population of centers being formed,

active and inactive. The heterogenous population of active centers after photoactivation in the D1-D170E mutant was previously suggested by (Hwang *et al.* 2007). As previously observed, the D1-D170E mutant exhibits remarkably low quantum efficiency of photoactivation (**Table 10**) (Hwang *et al.* 2007) and shows significantly altered fluorescence decay kinetics both prior to and after HA treatment (**Fig. 18A & B, S9, Table 10**). To investigate if the mutations at the HAS indeed result in the formation of inactive Mn cluster we sought to partially photoactivate the samples to approximately 20-30% of maximal restoration level (**Fig. 16**). Cells were photoactivated with series of 50, 100, 200, 200 and 300 flashes for WT control, D1-E189Q, D1-E189K, D1-E189R, and D1-D170E respectively. Accumulation of photooxidized Mn at the donor site of PSII in mutants incapable of O_2 evolution but still participating in the charge recombination with the acceptor site was previously observed by Vass (Cser *et al.* 2005) in D1-A344Stop mutant. These experiments indicate that the mutant with a stop codon at D1-Ala344 position prevented formation of an active donor side and contained unstable photooxidized Mn capable of Q_A^- re-oxidation. The purpose of dark incubation in partially photoactivated cells is to allow the re-reduction of unstable photooxidized Mn at the donor side, which results in altered fluorescence relaxation kinetics. Since the dominant route for Q_A^- reoxidation in the presence of DCMU is recombination with the S_2 state of the Mn cluster at the donor side of PSII, the decay of unstable redox active Mn at the donor site in principle should slow fluorescence relaxation, especially during the slow phase.

To investigate if the cells with the mutation at the HAS tend to form inappropriate Mn cluster, partially photoactivated samples were incubated in the dark for 40 minutes. This protracted incubation should allow for unstable photooxidized Mn to be reduced by cellular reductant and eliminate its participation in charge recombination with Q_A^- (Cser *et al.* 2005). The fluorescence relaxation kinetics of the dark incubated cells after partial photoactivation was compared to partially photoactivated sample prior the dark rearrangement and to Mn depleted cells prior photoactivation (**Table 11**). Mn depleted WT control cells showed dominant fluorescence decay

yield during the slow phase (amplitude 85.4%) with the time constant exceeding the time course of the experiment (**Fig. 19**). After the partial photoactivation WT control showed reduction of the decay yield during the slow phase (amplitude 55%) and appearance of the middle phase (τ = 1 s, amplitude 27.4%). Dark incubation of WT control cells did not significantly change fluorescence relaxation kinetics (p = 0.43) indicating that the majority of photooxidized Mn at the donor side is assembled into functional and stable Mn clusters.

Among the studied site-directed mutants only D1-E189Q (**Fig. 20D**) exhibited essentially the same relaxation kinetics in cells before and after 40-minute dark incubation. Similar to WT control, where the slow phase yielded approximately 55% and 58% of total fluorescence decay before and after dark incubation, D1-E189Q cells showed 57% and 59% respectively. Partial photoactivation of D1-D170E resulted in significant reduction in half time constants in the middle and slow phases (τ = 260 ms and 17.4 s) compared to extracted cells (τ = 446 ms and >100 s). Although the decay yields are essentially the same prior to and after partial photoactivation, complete reoxidation of Q_A^- does not occur in Mn-depleted samples during the course of the experiment, unlike in partially photoactivated D1-D170E cells. The dark incubation of partially photoactivated D1-D170E cells resulted in elongation of both middle (τ = 570 ms) and slow phases (τ = 41 s), indicating slower charge recombination compared to cells prior to dark incubation. This observation is consistent with previous studies (Hwang *et al.* 2007) and indicates the D1-D170E mutant accumulated a fraction of unstable photooxidized Mn during a course of 300 flashes which were reduced during dark incubation and lost the ability to accept electrons from Q_A^-.

Similar to other strains, partial photoactivation in D1-E189R allowed recombination with photooxidized Mn at the donor side of PSII. The time constant for the slow phase changed from more than 100 to 91 s (p = 0.007) with small but statistically significant change in yield during slow phase (p = 0.01), while the middle phase changed from τ = 44 ms and 35% to τ = 144 ms and 24%. Dark incubation caused decay of a portion of photooxidized Mn at the donor side of D1-

E189R mutant and increased the half time of the slow phase (τ = >100) and decreased the half time of the middle phase to 36 ms, similar to Mn depleted cells. Interestingly, partial photoactivation significantly increased the decay yield during the fast phase from 34% in Mn depleted cells to 43% in partially photoactivated cells, and from 43% to 40% in dark incubated cells. The fast phase in the presence of DCMU could attribute to redox-active, partially assembled Mn clusters (Mamedov *et al.* 2000), which could be explained by low quantum efficiency of photoactivation in D1-E189R mutant.

Photoactivation of the D1-E189K mutant with 200 flashes resulted in a decreased time constant for the slow phase (τ = 100 s, amplitude 31%) compared to HA extracted cells (τ >100 s, amplitude 41%) (fluorescence relaxation yield p = 0.001, time constant p = 0.0002) and increased half time of the middle phase from 144 ms and 18.5% to 457 ms and 27.6% of total yield respectively. Dark incubation caused the decay of unstable photooxidized Mn at the donor side of the D1-E189K mutant and increased the time constant and yield amplitude for the slow phase with kinetic values similar to HA treated cells (τ = >100 s, amplitude 44%) (fluorescence relaxation yield p = 0.01, time constant p = <0.0001) and decreased the amplitude decay during the middle phase (16.7%). Analysis of the data plot (**Fig. 20**) and derived kinetic parameters (**Table 11**) show that the fraction of inappropriate Mn clusters formed during the photoactivation of D1-E189K mutant significantly exceeds other studied mutants and probably prevents it from gaining full photoactivation (**Fig. 16C**). Interestingly, D1-E189R mutant shows even lower yield of photoactivation (**Fig. 16D**), however the change in the fluorescence relaxation kinetics seems to be smaller compared to D1-E189K and D1-D170E. The difference could be explained by the reversibility of assembly inhibition due to the inappropriate Mn formed during photoactivation. According to the Table 8 and **Figure 16** the Φ_{PA2} is significantly higher in D1-E189R compared to D1-E189K, which in principle indicates the nature of the inappropriate Mn formed at the donor side of PSII. Although our data do not allow us to make accurate conclusions regarding the nature

and stability of inappropriate Mn formed during the photoactivation, we speculate that the re-reduction of wrong Mn in D1-E189R occurs at much faster rate concurrently with the assembly of functional EOC. In the case of the D1-E189K mutant, it seems that the inappropriate Mn formed during the photoactivation is more stable, only allowing 40% fraction of active centers to be formed, while the remainder of PSII was either damaged during HA treatment or blocked by inappropriate Mn.

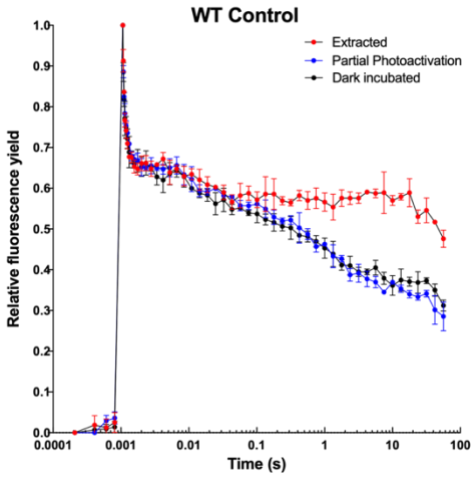

Figure 19. Q_A reoxidation kinetics in partially photoactivated WT control cells in the presence of DCMU. For the purpose of the partial photoactivation the sequence of 50 single turnover flashes was given to the HA-extracted WT control cells at uniform interval at 2 Hz (500 ms flash interval). Dark incubated sample was stored in complete darkness on a rotary shaker for 40 minutes prior the measurements. The measurements were performed after a single actinic flash of light. Samples were dark adapted for 5 minutes prior the measurements. Error bars represent SD with $n \geq 3$

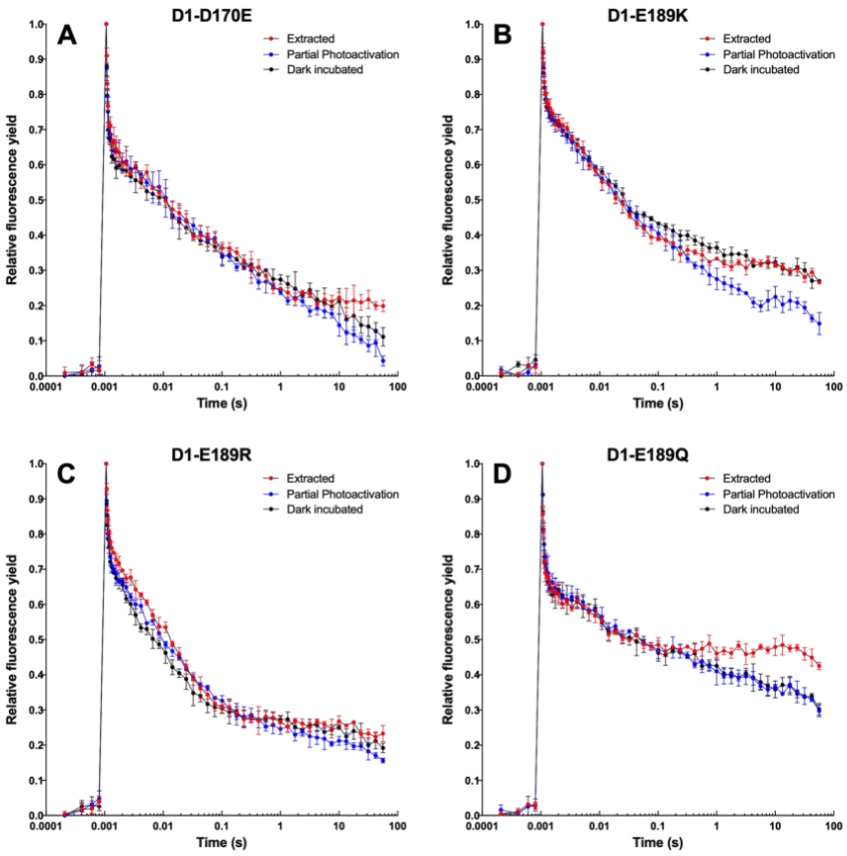

Figure 20. Q_A reoxidation kinetics in partially photoactivated D1-D170E, D1-E189K, D1-E189R, and D1-E189Q mutants in the presence of DCMU. For the purpose of the partial photoactivation the sequence of 300, 200, 200 and 100 single turnover flashes was given to the HA-extracted cells at uniform interval at 2 Hz (500 ms flash interval), respectively. Dark incubated sample was stored in complete darkness on a rotary shaker for 40 minutes prior the measurements. The measurements were performed after a single actinic flash of light. Samples were dark adapted for 5 minutes prior the measurements. Error bars represent SD with $n \geq 3$

Table 11. Characteristics of chlorophyll fluorescence relaxation kinetics in partially photoactivated WT control, D1-D170E, D1-E189K, D1-E189R and D1-E189Q cells.

Partially photoactivated cells in the presence of DCMU					
Strain/State		**Fast phase: τ/ms (amplitude (%))**	**Middle phase: τ/ms (amplitude (%))**	**Slow phase: τ/s (amplitude (%))**	**R**
WT control	Extracted	7.9 (14.5)	(0)-	> 100 (85.4)	0.97
	Partial Photoactivation	8.5 (17.7)	1050 (27.4)	> 100 (54.9)	0.99
	Dark incubated	8.3 (19.9)	918 (22.3)	> 100 (57.9)	0.98
D1-D170E	Extracted	6.5 (39.5)	446 (27.9)	> 100 (32.5)	0.99
	Partial Photoactivation	6 (36.9)	260 (27.9)	17.4 (35.3)	0.99
	Dark incubated	9.4 (40.7)	570 (18.7)	40.9 (38.9)	0.99
D1-E189K	Extracted	5.9 (40.5)	144 (18.5)	> 100 (40.9)	0.99
	Partial Photoactivation	7.4 (41.2)	457 (27.6)	100 (31.1)	0.99
	Dark incubated	7.9 (39.2)	440 (16.7)	> 100 (44.1)	0.99
D1-E189R	Extracted	2.9 (33.7)	44 (35.1)	> 100 (32.6)	0.99
	Partial Photoactivation	4.9 (43.3)	144 (24.2)	91 (32.4)	0.99
	Dark incubated	1.76 (40.4)	36 (27.7)	> 100 (31.9)	0.99
D1-E189Q	Extracted	0.27 (72.8)	15.8 (6.5)	> 100 (20.7)	0.98
	Partial Photoactivation	6.2 (26.4)	551 (16.8)	> 100 (56.9)	0.99
	Dark incubated	7.4 (27.2)	760 (14.3)	> 100 (58.6)	0.99

To induce partial photoactivation, a sequence of 50, 300, 200, 200 and 100 single turnover flashes was given to the HA-extracted cells at 2 Hz (500 ms flash interval), respectively. The decay curves were analyzed by assuming exponential decay for the fast phase and hyperbolic for both middle and slow phases, except for WT control where exponential fit was used for the fast phase and hyperbolic for the slow phase (see Table 7).

5.5 Discussion

The primary event during the light-driven assembly of the Mn_4O_5Ca is the binding and photooxidation of a Mn^{2+} ion at the HAS (Ananyev *et al.* 1999, Ono *et al.* 1999, Vinyard *et al.* 2019) of PSII. Previous mutagenesis studies (Nixon *et al.* 1992, Chu *et al.* 1994, Chu *et al.* 1995, Hwang *et al.* 2007) identified D1-D170 as a key amino acid residue for Mn^{2+} binding and photooxidation, which represents the first step of photoactivation (**Fig. 4, A→B**). Crystallographic

analysis has shown that the carboxyl group of D1-D170 provides one monodentate ligand to the 'dangler' Mn ion (Mn4) and one monodentate ligand the Ca^{2+} ion at one vertex of the cubane core of the cluster. Recent advances in cryo-EM helped to solve the structure of apo-PSII prior to the assembly of the Mn cluster (Zabret *et al.* 2020) and PSII depleted of Mn revealing considerable conformational differences from the assemble WOC (Gisriel *et al.* 2020). Both structures reveal a density attributed to a heavy cation situated between the carboxylates of the D1-D170 and D1-E189, which was proposed to be an Mn^{2+} ion, thus defining the HAS in apo-PSII. However, it is also possible that the observed density is a Ca^{2+}, which is reasonable given that D1-E189 ligates Mn1 and Ca^{2+} in intact Mn_4O_5Ca cluster. The site-directed mutants at D1-D170 dramatically affected the ability of apo-PSII to bind and oxidize Mn^{2+}, ranging from complete loss of function in D1-D170A to assembling up to 50% of WT O_2 evolution activity in D1-D170E and D170H mutants (Hwang *et al.* 2007). Less is known about the potential role of D1-E189 in forming the HAS, although careful early studies of D1-E189 mutants showed that many substitution mutants contain partially or misassembled Mn and subsequent studies have shown that D1-E189 participates in a hydrogen bond network, modulates the redox potential of Y_Z, and undergoes a conformational movement during the catalytic cycle proposed to allow substrate water delivery to the active site. Despite these extensive studies in the framework of water oxidation (Chu *et al.* 1995, Tommos *et al.* 1998, Debus *et al.* 2000, Tommos *et al.* 2000), until now, there has not been an attempt to evaluate the potential role of D1-E189 in the formation of the HAS and the assembly of the Mn_4O_5Ca.

5.5.1 Does D1-E189 to help form the high affinity site of PSII?

Consistent with previous results (Debus *et al.* 2000), the D1-E189K mutation seems to have little effect on the O_2 evolution rate, which reaches up to 80-90% of WT control rate (**Fig. 15**). While D1-E189R and D1-E189Q mutations decrease the maximal rate to a larger extent, the net O_2 evolution rates are still relatively high (~60%) in both mutants (Debus *et al.* 2000). Despite high

O_2 evolution rate in all D1-E189 mutants, their photoactivation characteristics revealed severe defects. Only D1-E189Q was able to restore initial oxygen evolution activity up to 70% after 15 minutes of continuous illumination, similar to the D1-D170E mutant. However, D1-D170E required twice as much time to reach same level of restoration (**Fig. 15B**). Photoactivation under flash illumination revealed two phases of the restoration curve. The main phase corresponds to relatively high quantum efficiency of photoactivation, whereas the other phase involves a much lower quantum efficiency. In previous *in vitro* studies that phase can be negative, indicating damage to the reaction centers during assembly. In the whole cell experiments conducted here, the main assembly phase in all mutants showed decreased quantum efficiency (**Table 8**) indicating that D1-E189 is important for photoactivation. This reduced quantum efficiency can be attributed to alterations in the HAS as evidenced by the apparent occupancy of the HAS in HA-extracted cells, where, with the exception of D1-189Q, the ability to re-reduce P_{680}^{+} was severely compromised by the mutations and in a way similar to the *bona fide* HAS mutant, D1-D170E.

5.5.2 Do HAS mutations result in accumulation of non-functional Mn in PSII?

The photoactivation in the D1-E189K and D1-E189R mutants was severely inhibited with the restoration level reaching approximately 40% and 35% of initial O_2 evolution activity respectively after 40 minutes of illumination. Unlike in the D1-D170E mutant where the Φ_{PA1} was significantly lowered by the mutation (**Table 8**), all D1-E189 mutants re-assemble the Mn cluster at a much higher Φ_{PA1} (**Fig. 16, Table 8**). In contrast to D1-D170E, all the D1-E189 mutants assemble a fraction of the centers with relatively high Φ_{PA1}, however after reaching 40% in D1-E189K and 80% in D1-E189Q the photoactivation almost stops and continues with a relatively low Φ_{PA2}. Notably, the D1-E189R mutant, after reaching approximately 25% of photoactivation, continues to slowly assemble the centers, albeit significantly exceeding D1-E189K and D1-E189Q. The inability of the D1-E189 mutants to restore a high level of WOC activity could indicate damage or inhibition occurring either during the Mn depletion procedure or photoinactivation. Since all

cyanobacterial strains were treated the same and neither WT control nor D1-D170E strains showed similar assembly inhibition, it is unlikely that the treatment with 10 mM hydroxylamine caused the observed effect. Photoactivation was similarly inhibited during preliminary Mn depletion experiments with 2 mM of hydroxylamine in D1-E189K **(Fig S10)**. Moreover, the fluorescence characteristics of the mutants show that the capacity for primary charge separation remains intact and that the increase in the middle phases of fluorescence decay suggest the presence of partially assembled or mis-assembled Mn as proposed during the initial characterization of these mutants.

For all mutants the optimum interval between photoactivation flashes yielding the maximum recovery of oxygen evolution by WOC was between 200-500 ms (**Fig. 17**). Interestingly, D1-E189K and D1-E189R mutants were not able to assemble even 50% of their initial activity at any flash frequency, and the photoactivation intermediates decay faster than the wild-type. However, neither the low quantum efficiencies of photoactivation nor the increased rates of decay seem to explain the inability of the D1-E189K and D1-E189R mutants to photoactive such a large proportion of centers. Notably, D1-E189K and D1-E189R showed high quantum efficiency early in the photoactivation that yielded 20 % and 40% of initial activity respectively (**Fig. 16C & D**), followed by the slow restoration phase (**Table 8**). Both D1-E189R and D1-E189K mutants showed significant rates of O_2 evolution prior the HA-extraction (**Fig. 15A**), however neither was able to restore this activity rapidly like WT control (**Fig. 15B**). In contrast, D1-E189Q, similar to WT control is capable of rapid restoration of 80% of the net O_2 rate (**Fig. 16E**). These observations suggest that inability to assembly WOC by D1-E189K and D1-E189R mutants is not the result of a failure to photooxidize Mn^{2+} or perform the dark rearrangement, rather due to the formation of inappropriate Mn cluster-like structures with unknown nuclearity (Chu *et al.* 1994, Chu *et al.* 1995), which halts the assembly. An alternative explanation is that the positive charge from lysine or arginine at 189 position could induce a repulsive interaction with Mn^{2+}/Mn^{3+} ions, blocking formation of intermediate **A** or **B**, thus dramatically lowering quantum efficiency of

photoactivation, while neutral glutamine behaves similarly to WT control. That hypothesis, however, does not explain essentially two rates of assembly observed during the flash number experiment (**Fig. 16**) and would imply D1-D170E-like kinetics of photoactivation. Why assembly stalls after a rapid phase of photoactivation is intriguing and could be explained by the formation of the wrong Mn centers that are slowly re-reduced over the course of 6400 flashes, especially in D1-E189R (**Fig. 16D)** followed by another photooxidation and attempt to assemble functional WOC. This hypothesis is consistent with the fact that unextracted D1-E189K and D1-E189R cells exhibit significantly higher O_2 evolution rate, indicating that a larger population of centers could assemble WOC over long period of time. Considering these observations, one reasonable hypothesis is that a positively charged residue introduced at the HAS could enable irreversible binding of Mn^{2+}/Mn^{3+} intermediate through interaction with a partially negative hydroxide or oxide group (Ananyev *et al.* 1999, Ono *et al.* 1999, Tyryshkin *et al.* 2006) that requires additional re-reduction to restore the center for further assembly.

The bifurcation of the photoactivation process may involve competition between productive photoactivation and nonproductive photoactivation pathways, and represent the ratio distribution of assembled centers from the common pool of inactivated centers by hydroxylamine treatment. The results observed during flash number experiment (**Fig. 16**) in all three D1-E189 mutants indicate the ratio of inappropriate Mn is much higher compared to WT control, however D1-E189Q assembled approximately 80% of the centers correctly and only smaller fraction of centers had "wrong" Mn. The opposite outcome occurred in D1-E189K and D1-E189R mutants where the proportion of "wrong" centers reaches up to 60% and 75%, respectively (**Fig. 16C & D**). The similarity in rate of the dark rearrangement, k_A (**Table 9**) among the mutants suggests similar assembly kinetics of appropriate Mn clusters, similar to WT control, and the main difference between these mutants is the distribution of the assembly pathways yielding different amounts of functional and nonfunctional centers. Previous findings indicate that inappropriate Mn does not

cause permanent damage to the PSII centers and can be re-reduced by HA treatment allowing further photoassembly (Hwang *et al.* 2007). Our results showed that D1-E189K and D1-E189R mutants slowly reassemble "wrong" Mn although at the slow rate (**Table 8**); that would explain the ability of these mutants to show high O_2 evolution rates prior the HA treatment.

5.5.3 Does the accumulation of inappropriate Mn in PSII irreversibly inhibit photoactivation?

As mentioned earlier the unique property of D1-E189K, D1-E189R, and D1-E189Q is a significant rate of oxygen evolution among all PSII mutants. This feature indicates that the cells are capable of coping with the inhibition caused by the formation of non-functional Mn structures (Hwang *et al.* 2007, Chernev *et al.* 2020) as discussed earlier. However, it is not clear if the 'wrong' Mn could be removed from the apo-PSII without the initiation of PSII repair process, which involves the disassembly of PSII monomer and replacement of the D1 protein (Nixon *et al.* 2005, Becker *et al.* 2011, Weisz *et al.* 2019). The evidence that the PSII centers populated with unfunctional Mn at the WOC site could be restored by hydroxylamine treatment (Hwang *et al.* 2007) implies that the oxidative state of inhibitory Mn at the WOC is most likely higher than Mn^{2+} and that the reduction of such Mn results in its dissociation from the inhibition site. Interestingly, in the absence of PsbO protein, the Mn_4O_5Ca cluster tends to be reduced in the dark, which could result in complete loss of photosynthetic function in this mutant (Burnap *et al.* 1991, Burnap *et al.* 1996). The fact that the ΔPsbO mutant is capable of significant O_2 evolution suggests that the process of cluster reduction and re-assembly happens concurrently under illumination. Φ_{PA2} in the D1-E189R mutant could indicate reduction of 'wrong' Mn followed by new assembly trials over the course of 6400 photoactivation flashes. Reduction of the Mn cluster by endogenous reductants in the lumen in ΔPsbO suggests that non-functional Mn formed during the assembly in D1-E189 and D1-D170E mutants may decay in the dark. The D1-A344Stop mutant provides additional evidence for the reduction of partially assembled Mn cluster in the dark, where 40-minute dark

incubation resulted in significant reduction of the charge recombination between Q_A^- and photooxidized Mn at the donor side of PSII (Cser *et al.* 2005). Consistent with these observations, the changes in fluorescence relaxation kinetics were not observed after dark incubation in the WT control (**Fig. 19**). The consistency in fluorescence decay kinetics before and after dark incubation indicate that the majority of the assembled centers over the course of 50 flashes formed fully functional and stable Mn clusters.

Among the studied strains only D1-E189Q mutant showed similar photoactivation to WT control (**Fig. 16E, 17E**) and comparable Q_A^- reoxidation kinetics in the samples prior HA treatment (**Fig. 18A &B**) and after Mn extraction (**Fig. S9**). Similar to WT control, D1-E189Q exhibited virtually no difference in fluorescence decay kinetics prior the dark incubation and after. Despite the difference in pK_A between Glu and Gln, D1-E189Q seems to be capable of supporting correct assembly of the Mn cluster similar to WT control. Unlike in WT control and D1-E189Q strains, D1-D170E, D1-E189K, and D1-E189R accumulated a portion of unstable Mn at the donor site after the partial photoactivation (**Fig. 20**). Similar to what has been observed in D1-A344Stop prior and after the dark incubation, D1-D170E, D1-E189K, and D1-E189R mutants showed reduction in fluorescence decay rate after 40-minute dark incubation (**Fig. 20**, **Table 11**). The slowdown in fluorescence decay after dark incubation suggests that these mutants lost a fraction of redox active Mn involved in charge recombination between Q_A^- and the donor side of PSII. These observations support the hypothesis that during photoactivation in the D1-E189K and D1-E189R mutants, the assembly of the Mn cluster yields in two types of centers, active centers capable of water oxidation and non-functional yet redox-active centers containing at least a single Mn^{3+} ion at the donor site of PSII (Chu *et al.* 1995). The ability of these mutants to assemble up to 80% of WT control level of active centers, and removal of inappropriate Mn from the centers, suggest that the formation of non-functional Mn clusters in D1-D170E, D1-E189K and D1-E189R mutants is reversible and does not prevent these mutants from assembling a large fraction of active PSII.

5.5.4 Does D1-E189 ligand participate in the binding of Ca^{2+}?

It is possible that D1-E189 participates in the formation of [Mn^{2+}-(OH)-Ca^{2+}] prior to photooxidation followed by the formation of bridged species [Mn^{3+}-(OH)-Ca^{2+}] after the initial photooxidative event (Tyryshkin *et al.* 2006). Possibly only Glu, Gln, Lys, Arg, Leu and Ile at D1-189 have suitable size and shape to form the HAS (Debus *et al.* 2000), while Mn^{2+} oxidation seems to be carried out solely by the D1-D170 ligand. An alternative explanation regarding the role of D1-E189 in photoactivation comes from the crystal structure and evidence that D1-E189 ligates Ca^{2+} in intact WOC (Umena *et al.* 2011). According to (Chen *et al.* 1995), Ca^{2+} prevents inappropriate binding of high valency Mn ions to the apo-PSII. In contrast, our results indicated that D1-E189K and D1-E189R accumulated a significant amount of inactive high valency Mn over the course of photoactivation, constituting up to 75% loss of activity in these mutants. Considering the general agreement that Ca^{2+} is crucial for photoactivation (Ono *et al.* 1983, Chen *et al.* 1995, Ananyev *et al.* 1996, Avramov *et al.* 2020), the mechanism of Ca^{2+} facilitation of the photoassembly remains elusive. Binding of Mn^{2+} to the HAS with simultaneous binding of Ca^{2+} to an adjacent binding site facilitates the formation of the [Mn^{2+}-(OH)-Ca^{2+}] complex by inducing deprotonation of a water ligand of Mn^{2+}. Calcium lowers the pK_a for the water ligand, which is controlled by a nearby base B^- that serves as a primary proton acceptor with a pK_a dependent on Ca^{2+} bound to its effector site (Tyryshkin *et al.* 2006). It is possible that the D1-E189 ligand supports Ca^{2+} binding at its effector site, considering strong competition between Mn^{2+} and Ca^{2+} for Ca effector site (Miller *et al.* 1989, Avramov *et al.* 2020) in D1-E189 mutants only a fraction Ca^{2+} binding sites are occupied with Ca^{2+}. The inability to coordinate Ca^{2+} during the assembly will lead to the accumulation of non-functional Mn at the donor side of PSII (Chen *et al.* 1995, Chernev *et al.* 2020).

CHAPTER VI

CONCLUSIONS

In this thesis, I have investigated the assembly of catalytic metal center, the Mn_4CaO_5, of the oxygen evolving complex of the photosystem II using the experimental model cyanobacterium *Synechocystis sp.* PCC 6803. The process, termed photoactivation, utilizes essentially the same electron transport and redox reaction machinery used for driving the H_2O-oxidation reaction. The same photochemical charge separation mechanism that extracts the electron from substrate H_2O by the catalytic Mn_4O_5Ca cluster, is also used for the photooxidative assembly of the metal cluster (Cheniae *et al.* 1971, Bao *et al.* 2016). In order to assemble the oxygen evolving complex of the photosystem II, the free manganese ions, in the form of Mn^{2+}, must be oxidized to $Mn^{\geq 3+}$ followed by incorporation of the oxidized ion into the protein environment of apo-PSII. This occurs with the concomitant incorporation of oxygen bridges between the metal atoms of the cluster. However, unlike the >90% quantum efficiency of the photosynthetic reaction, photoactivation is approximately 1% efficient. The reason for such a dramatic difference involves the rate-limiting and ill-defined light-independent step, the so-called dark rearrangement, which occurs in between the oxidation of the first and second Mn^{2+} ions at the special high affinity site in photosystem II. Several hypotheses exist regarding the nature of the dark rearrangement, including protein conformational change and oxide ion ($[Mn^{3+}\text{-}(OH^{1-})\text{-}Ca^{2+}] \rightleftharpoons [Mn^{3+}\text{-}(O^{2-})\text{-}Ca^{2+}]$) translocation from the oxidation site to the specific binding site. However, recent advances in cryoEM (Gisriel *et al.* 2020, Zabret *et al.* 2020) and HS-AFM (Tokano *et al.* 2020) techniques allowed us to come closer to understanding the nature of this crucial yet poorly understood event. In chapter IV, I described experiments (see below) that provided *(i*) evidence for a new Mn^{2+} binding site involved in

assembly and (*ii*) a model that combines a rate-limiting molecular conformational change that only infrequently adopts a configuration necessary for assembly, and thus explains the very low overall quantum efficiency of photoactivation.

In terms of the sequence of my studies, the investigation of the dark rearrangement started from studying the ability of the PSII with mutations at the HAS to assemble functional WOC, which is described in chapter V. The high affinity site of PSII is formed by at least one ligand, D1-D170 (Boerner *et al.* 1992, Nixon *et al.* 1992, Nixon *et al.* 1992, Chu *et al.* 1994, Cohen *et al.* 2007). However, recent cryo-EM apo-PSII structures identified the D1-E189 ligand to be in close proximity to D1-D170, suggesting the possibility of D1-E189 coordination of Mn^{2+} at the HAS (Gisriel *et al.* 2020, Zabret *et al.* 2020). As a matter of record, my choice of the D1-E189 residue as a mutational target for understanding of photoactivation began before the realization of the apo-PSII structures were presented and, indeed, I presented my results as a poster on the photoactivation of these mutants at the 2019 Gordon Research Conference on Photosynthesis, actually receiving a best poster award for that work. I chose this site because I had hypothesized that it would be important for mediating the Ca^{2+} dependence of photoactivation. I identified that D1-E189K and D1-E189R mutants are unable to restore initial oxygen evolution activity after the removal of the Mn cluster from photosystem II. However, WT control and D1-E189Q strains were respectively able to restore up to 95% and 80% of initial activity. I have shown all the D1-E189 mutants have significant alterations in the initial photooxidation of Mn^{2+} at the high affinity site, yet this only partly explains the severe defect that these strains exhibit during photoactivation. Impaired photoactivation was found to occur during subsequent steps. My hypothesis suggests that D1-E189K and D1-E189Q mutants tend to form 'inappropriate Mn clusters' in the form of high valency Mn oxide aggregates as suggested earlier by Chernev (Chernev *et al.* 2020). Importantly, the inhibition of photoactivation by inappropriate Mn seems to be reversible, which explains the ability of mutant cells to assemble a substantial amount of the active oxygen evolving complexes over the

course of several days in culture. The fluorescence relaxation kinetics experiments have shown that inappropriate Mn tend to be reduced in the dark, most likely by the endogenous reductant in the thylakoid lumen, similar to ΔpsbO mutant observed earlier (Burnap *et al.* 1996). In addition to the alterations in the initial Mn^{2+} oxidation, we hypothesize that D1-E189 also supports the photoactivation intermediates during the light-driven assembly of the Mn cluster. The precise mechanism of such support remains unclear, but our hypothesis is that D1-E189 facilitates the binding of Ca^{2+} at its effector site, which is crucial for the formation of $[Mn^{3+}\text{-}(OH^{1-})\text{-}Ca^{2+}] \rightleftharpoons [Mn^{3+}\text{-}(O^{2-})\text{-}Ca^{2+}]$ oxide ion. In D1-E189K and D1-E189R mutants, Ca^{2+} ligation could be somewhat weakened; thus, the majority of the centers assemble the Mn cluster in the absence of Ca^{2+}, which would explain the inability of these mutants to re-gain the initial O_2 activity. *In vivo* studies do not allow us to precisely understand the role of the single amino acid ligands of the oxygen evolving complex in PSII, since we cannot control many variables during the experiment such as pH, inorganic cofactors concentrations and others. To better understand the role of individual amino acid residues within PSII, photoactivation should be studied *in vitro*, to allow precise control over photoactivation conditions.

Chapter IV described the development of a novel *in vitro* technique for isolating cyanobacterial Mn-depleted thylakoid membranes. It allowed us to study photoactivation under precise control of the photoactivation conditions, such as pH and ion composition as well as permitting facile genetic modification of the constituent proteins. Importantly, the membranes retain the native electron acceptor system so that artificial electron acceptors are not necessary, an improvement over previous *in vitro* experimental systems. Chapter IV described in detail the application of *in vitro* photoactivation procedures using genetically tractable cyanobacteria to study the role Ca^{2+} and Psb27 in the assembly of the Mn_4CaO_5.

As has been shown before, the ratio Ca^{2+} to Mn^{2+} ions during photoactivation is a vital condition for successful and efficient photoactivation of the WOC (Cheniae *et al.* 1971, Ono *et al.* 1983,

Tamura *et al.* 1986, Tamura *et al.* 1987, Miller *et al.* 1989, Chen *et al.* 1995, Zaltsman *et al.* 1997). While high [Mn^{2+}] leads to irreversible inhibition of photoactivation, high [Ca^{2+}] lowers quantum efficiency of the process. We have shown that high [Mn^{2+}] results not only in lowered yields of photoactivation but also causes photoinactivation, which results in loss of active centers that have been successfully assembled previously. On the other hand, while high [Ca^{2+}] mitigates the inhibitory effect of high [Mn^{2+}], it competes with another Mn binding site, which we termed as "second Mn site" or SMS, resulting in lowered quantum efficiency of photoactivation. We have studied the role of Psb27 protein during assembly and have found that this lumenal protein stabilizes the binding of Ca^{2+} at its effector site, which lowers the competition between Ca^{2+} and Mn^{2+} for Ca^{2+} binding site. We concluded that the association of Psb27 protein with apo-PSII stabilizes the E-loop of CP43 protein, prevents it from the structural fluctuations shown earlier (Tokano *et al.* 2020) and keeps it in optimal conformational state to support Ca^{2+} ligation.

As in plant chloroplasts, the competition between Mn^{2+} and Ca^{2+} for corresponding binding sites seems to be one of the limiting factors of photoactivation (Miller *et al.* 1989). Our results support and extend these conclusions by identifying an additional binding site involved in Mn binding after or during the dark rearrangement, and showing a yet unstudied photoinactivation process happening at high [Mn^{2+}]. One should keep in mind that plant thylakoid preparations allow similar photoactivation experiments, but only in the wild type organisms and do not allow facile site-directed mutagenesis, which was a major limitation in the field until this moment. Thus, one of the most important achievements of chapter IV is the development of an *in vitro* photoactivation technique, which was used to study the photoactivation in PSII mutants in order to elucidate the role of photoactivation cofactors and individual amino acid residues.

The newly developed approach and two unique mutant phenotypes, D1-E189K and D1-E189Q, in comparison to WT control and D1-D170 mutants allow us to better understand rate-limiting dark rearrangement event and PSII photoassembly mechanism. Moreover, the combination of the

fluorescence techniques recently presented by (Chernev *et al.* 2020) will allow us to better understand the role of each amino acid ligand within WOC, its role in Mn^{2+} oxidation and formation of the photoactivation intermediates.

The understanding of photosystem II assembly and functions is crucial for future design of high yield crops capable of efficient CO_2 assimilation into biomass and creating artificial photosynthesis technologies. Such work is important for improving our environment and fighting hunger, especially considering climate change.

REFERENCES

Adir, N., H. Zer, S. Shochat and I. Ohad (2003). "Photoinhibition - a historical perspective." *Photosynth Res* **76**(1-3): 343-370.

Allahverdiyeva, Y., Z. Deak, A. Szilard, B. A. Diner, P. J. Nixon and I. Vass (2004). "The function of D1-H332 in Photosystem II electron transport studied by thermoluminescence and chlorophyll fluorescence in site-directed mutants of *Synechocystis* 6803." *Eur J Biochem* **271**(17): 3523-3532.

Allen, M. M. (1968). "Simple conditions for growth of unicellular blue-green algae on plates (1, 2) " *J Phycol* **4**(1): 1-4.

Ananyev, G. M. and G. C. Dismukes (1996). "Assembly of the tetra-Mn site of photosynthetic water oxidation by photoactivation: Mn stoichiometry and detection of a new intermediate." *Biochemistry* **35**(13): 4102-4109.

Ananyev, G. M. and G. C. Dismukes (1996). "High-resolution kinetic studies of the reassembly of the tetra-manganese cluster of photosynthetic water oxidation: proton equilibrium, cations, and electrostatics." *Biochemistry* **35**(46): 14608-14617.

Ananyev, G. M., A. Murphy, Y. Abe and G. C. Dismukes (1999). "Remarkable affinity and selectivity for Cs^{+} and uranyl ($UO22^{+}$) binding to the manganese site of the apo-water oxidation complex of photosystem II." *Biochemistry* **38**(22): 7200-7209.

Anbudurai, P. R., T. S. Mor, I. Ohad, S. V. Shestakov and H. B. Pakrasi (1994). "The ctpA gene encodes the C-terminal processing protease for the D1 protein of the photosystem II reaction center complex." *Proceedings of the National Academy of Sciences of the United States of America* **91**(17): 8082-8086.

Aoki, M. and S. Katoh (1982). "Oxidation and reduction of plastoquinone by photosynthetic and respiratory electron transport in a cyanobacterium *Synechococcus sp*." *Biochimica et Biophysica Acta (BBA) - Bioenergetics* **682**(3): 307-314.

Aro, E. M., S. McCaffery and J. M. Anderson (1993). "Photoinhibition and D1 protein degradation in peas acclimated to different growth irradiances." *Plant Physiology* **103**(3): 835.

Asada, M. and H. Mino (2015). "Location of the High-Affinity Mn^{2+} site in photosystem II detected by PELDOR." *Journal of Physical Chemistry B* **119**(32): 10139-10144.

Avramov, A. P., H. J. Hwang and R. L. Burnap (2020). "The role of Ca^{2+} and protein scaffolding in the formation of nature's water oxidizing complex." *Proceedings of the National Academy of Sciences* **117**(45): 28036.

Babcock, G. T., B. A. Barry, R. J. Debus, C. W. Hoganson, M. Atamian, L. McIntosh, I. Sitole and C. F. Yocum (1989). "Water oxidation in photosystem II: From radical chemistry to multielectron chemistry." *Biochemistry* **28**: 9557-9565.

Baniulis, D., E. Yamashita, H. Zhang, S. S. Hasan and W. A. Cramer (2008). "Structure–function of the cytochrome b6f complex." *Photochemistry and Photobiology* **84**(6): 1349-1358.

Bao, H. and R. L. Burnap (2016). "Photoactivation: The light-driven assembly of the water oxidation complex of photosystem II." *Frontiers in Plant Science* **7**: 578.

Bao, H., P. L. Dilbeck and R. L. Burnap (2013). "Proton transport facilitating water-oxidation: the role of second sphere ligands surrounding the catalytic metal cluster." *Photosynth Res* **116**(2-3): 215-229.

Baranov, S. V., G. M. Ananyev, V. V. Klimov and G. C. Dismukes (2000). "Bicarbonate accelerates assembly of the inorganic core of the water-oxidizing complex in manganese-depleted photosystem II: A proposed biogeochemical role for atmospheric carbon dioxide in oxygenic photosynthesis." *Biochemistry* **39**(20): 6060-6065.

Baranov, S. V., A. M. Tyryshkin, D. Katz, G. C. Dismukes, G. M. Ananyev and V. V. Klimov (2004). "Bicarbonate is a native cofactor for assembly of the manganese cluster of the photosynthetic water oxidizing complex. Kinetics of reconstitution of O2 evolution by photoactivation." *Biochemistry* **43**(7): 2070-2079.

Barra, M., M. Haumann, P. Loja, R. Krivanek, A. Grundmeier and H. Dau (2006). "Intermediates in assembly by photoactivation after thermally accelerated disassembly of the manganese complex of photosynthetic water oxidation." *Biochemistry* **45**(48): 14523-14532.

Becker, K., K. U. Cormann and M. M. Nowaczyk (2011). "Assembly of the water-oxidizing complex in photosystem II." *J Photochem Photobiol B* **104**(1-2): 204-211.

Bentley, F. and J. Eaton-Rye (2007). "Psb27 is required for photoinactivation and recovery of photosystem II in *Synechocystis sp* PCC6803 cells lacking PsbV." *Photosynthesis Research* **91**(2-3): 204-204.

Björn, L. O. and Govindjee (2009). "The evolution of photosynthesis and chloroplasts." *Current Science* **96**(11): 1466-1474.

Boehm, M., J. Yu, V. Reisinger, M. Beckova, L. A. Eichacker, E. Schlodder, J. Komenda and P. J. Nixon (2012). "Subunit composition of CP43-less photosystem II complexes of *Synechocystis sp* PCC 6803: implications for the assembly and repair of photosystem II." *Philosophical transactions of the Royal Society of London. Series B, Biological sciences* **367**(1608): 3444-3454.

Boerner, R. J., A. P. Nguyen, B. A. Barry and R. J. Debus (1992). "Evidence from directed mutagenesis that aspartate 170 of the D1 polypeptide influences the assembly and-or stability of the manganese cluster in the photosynthetic water-splitting complex." *Biochemistry* **31**(29): 6660-6672.

Bouges-Bocquet, B. (1980). "Kinetic models for the electron donors of photosystem II of photosynthesis." *Biochim Biophys Acta* **594**(2-3): 85-103.

Boussac, A. and A. W. Rutherford (1988). "Ca^{2+} binding to the oxygen evolving enzyme varies with the redox state of the Mn enzyme." *FEBS Letters* **236**: 432-436.

Bricker, T. M., J. L. Roose, R. D. Fagerlund, L. K. Frankel and J. J. Eaton-Rye (2012). "The extrinsic proteins of photosystem II." *Biochimica et Biophysica Acta (BBA) - Bioenergetics* **1817**(1): 121-142.

Brune, D. C. (1989). "Sulfur oxidation by phototrophic bacteria." *Biochimica et Biophysica Acta (BBA) - Bioenergetics* **975**(2): 189-221.

Bucher, D., B. J. Grant and J. A. McCammon (2011). "Induced fit or conformational selection? The role of the semi-closed state in the maltose binding protein." *Biochemistry* **50**(48): 10530-10539.

Burnap, R. and L. A. Sherman (1991). "Deletion mutagenesis in *Synechocystis sp*. PCC6803 indicates the the Mn-stabilizing protein of photosystem II is not essential for O_2 evolution." *Biochemistry* **30**: 440-446.

Burnap, R. L. (2004). "D1 protein processing and Mn cluster assembly in light of the emerging photosystem II structure." *Physical Chemistry Chemical Physics* **6**(20): 4803-4809.

Burnap, R. L., M. Qian, S. Al-Khaldi and C. Pierce (1995). Photoactivation and S-state cycling kinetics in photosystem II mutants in *Synechocystis sp.* PCC6803. Photosynthesis: from light to biosphere. P. Mathis. Dordrect, The Netherlands, Kluwer Academic Publishers**:** pp 443-446.

Burnap, R. L., M. Qian and C. Pierce (1996). "The manganese-stabilizing protein of photosystem II modifies the in vivo deactivation and photoactivation kinetics of the H_2O oxidation complex in *Synechocystis sp* PCC6803." *Biochemistry* **35**(3): 874-882.

Buser, C. A., L. K. Thompson, B. A. Diner and G. W. Brudvig (1990). "Electron-transfer reactions in manganese-depleted photosystem II." *Biochemistry* **29**(38): 8977-8985.

Cardona, T., A. Sedoud, N. Cox and A. W. Rutherford (2012). "Charge separation in photosystem II: A comparative and evolutionary overview." *Biochimica et Biophysica Acta (BBA) - Bioenergetics* **1817**(1): 26-43.

Chen, C. G., J. Kazimir and G. M. Cheniae (1995). "Calcium modulates the photoassembly of photosystem-II (MN)(4)-cluster by preventing ligation of nonfunctional high-valency states of manganese." *Biochemistry* **34**(41): 13511-13526.

Chen, H., D. Y. Zhang, J. K. Guo, H. Wu, M. F. Jin, Q. T. Lu, C. M. Lu and L. X. Zhang (2006). "A Psb27 homologue in *Arabidopsis thaliana* is required for efficient repair of photodamaged photosystem II." *Plant Molecular Biology* **61**(4-5): 567-575.

Cheniae, G. M. and I. F. Martin (1971). "Effect of hydroxylamine on photosystem-II .1. Factors affecting decay of O_2 evolution." *Plant Physiology* **47**(4): 568-&.

Cheniae, G. M. and I. F. Martin (1971). "Photoactivation of manganese catalyst of O_2 evolution .1. Bichemical and kinetic aspects." *Biochimica Et Biophysica Acta* **253**(1): 167-&.

Cheniae, G. M. and I. F. Martin (1971). "Photoactivation of the manganese catalyst of O_2 evolution. I. Biochemical and kinetic aspects." *Biochimica Et Biophysica Acta* **253**: 167-181.

Cheniae, G. M. and I. F. Martin (1972). "Effect of hydroxylamine on photosystem-II .2. Photoreversal of NH_2OH destruction of O_2 evolution." *Plant Physiology* **50**(1): 87-&.

Chernev, P., S. Fischer, J. Hoffmann, N. Oliver, R. Assunção, B. Yu, R. L. Burnap, I. Zaharieva, D. J. Nürnberg, M. Haumann and H. Dau (2020). "Light-driven formation of manganese oxide by today's photosystem II supports evolutionarily ancient manganese-oxidizing photosynthesis." *Nature Communications* **11**(1): 6110.

Chu, H. A., A. P. Nguyen and R. J. Debus (1994). "Site-directed photosystem-ii mutants with perturbed oxygen-evolving properties .1. Instability or inefficient assembly of the manganese cluster *in-vivo*." *Biochemistry* **33**(20): 6137-6149.

Chu, H. A., A. P. Nguyen and R. J. Debus (1994). "Site-directed photosystem-II mutants with perturbed oxygen-evolving properties .2. Increased binding or photooxidation of manganese in the absence of the extrinsic 33-kda polypeptide in-vivo." *Biochemistry* **33**(20): 6150-6157.

Chu, H. A., A. P. Nguyen and R. J. Debus (1995). "Amino-acid-residues that influence the binding of manganese or calcium to photosystem-II.1. The lumenal intehelical domains of the D1 polypepride." *Biochemistry* **34**(17): 5839-5858.

Chu, H. A., A. P. Nguyen and R. J. Debus (1995). "Amino-acid-residues that influence the binding of manganese or calcium to photosystem-II.2. The carboxy-terminal domain of the D1 polypeptide." *Biochemistry* **34**(17): 5859-5882.

Cohen, R. O., P. J. Nixon and B. A. Diner (2007). "Participation of the C-terminal region of the D1-polypeptide in the first steps in the assembly of the Mn_4Ca cluster of photosystem II." *Journal of Biological Chemistry* **282**(10): 7209-7218.

Cox, N., M. Retegan, F. Neese, D. A. Pantazis, A. Boussac and W. Lubitz (2014). "Electronic structure of the oxygen-evolving complex in photosystem II prior to O-O bond formation." *Science* **345**(6198): 804-808.

Cramer, W. A., S. S. Hasan and E. Yamashita (2011). "The Q cycle of cytochrome bc complexes: A structure perspective." *Biochimica et Biophysica Acta (BBA) - Bioenergetics* **1807**(7): 788-802.

Crofts, A. R. and C. A. Wraight (1983). "The electrochemical domain of photosynthesis." *Biochimica et Biophysica Acta (BBA) - Reviews on Bioenergetics* **726**(3): 149-185.

Cser, K., B. A. Diner, P. J. Nixon and I. Vass (2005). "The role of D1-Ala344 in charge stabilization and recombination in photosystem II." *Photochem Photobiol Sci* **4**(12): 1049-1054.

Dasgupta, J., A. M. Tyryshkin and G. C. Dismukes (2007). "ESEEM spectroscopy reveals carbonate and an N-donor protein-ligand binding to Mn^{2+} in the photoassembly reaction of the Mn_4Ca cluster in photosystem II." *Angew Chem Int Ed Engl* **46**(42): 8028-8031.

Dau, H., E. Fujita and L. Sun (2017). "Artificial photosynthesis: Beyond mimicking nature." *ChemSusChem* **10**(22): 4228-4235.

de Wijn, R. and H. J. van Gorkom (2001). "Kinetics of electron transfer from Q_A to Q_B in photosystem II." *Biochemistry* **40**(39): 11912-11922.

Debus, R. J. (1992). "The manganese and calcium ions of photosynthetic oxygen evolution." *Biochimica et Biophysica Acta (BBA) - Bioenergetics* **1102**(3): 269-352.

Debus, R. J., K. A. Campbell, W. Gregor, Z. L. Li, R. L. Burnap and R. D. Britt (2001). "Does histidine 332 of the D1 polypeptide ligate the manganese cluster in photosystem II? An electron spin echo envelope modulation study." *Biochemistry* **40**(12): 3690-3699.

Debus, R. J., K. A. Campbell, D. P. Pham, A.-M. A. Hays and R. D. Britt (2000). "Glutamate 189 of the D1 polypeptide modulates the magnetic and redox properties of the manganese cluster and tyrosine Y_Z in photosystem II." *Biochemistry* **39**(21): 6275-6287.

Dekker, J. P., D. F. Ghanotakis, J. J. Plijter, G. H. J. Van and G. T. Babcock (1984). "Kinetics of the oxygen-evolving complex in salt-washed photosystem II preparations." *Biochimica Et Biophysica Acta* **767**: 515-523.

Demeter, S., C. Goussias, G. Bernát, L. Kovács and V. Petrouleas (1993). "Participation of the g = 1.9 and g = 1.82 EPR forms of the semiquinone-iron complex, $Q_A^- \cdot Fe^{2+}$ of photosystem II in the generation of the Q and C thermoluminescence bands, respectively." *FEBS Letters* **336**(2): 352-356.

Diner, B. A. (2001). "Amino acid residues involved in the coordination and assembly of the manganese cluster of photosystem II. Proton-coupled electron transport of the redox-active tyrosines and its relationship to water oxidation." *Biochim Biophys Acta* **1503**(1-2): 147-163.

Diner, B. A. and P. J. Nixon (1992). "The rate of reduction of oxidized redox-active tyrosine, Z^+, by exogenous Mn^{2+} is slowed in a site-directed mutant, at aspartate 170 of polypeptide D1 of photosystem II, inactive for photosynthetic oxygen evolution." *Biochimica et Biophysica Acta (BBA) - Bioenergetics* **1101**(2): 134-138.

Diner, B. A., D. F. Ries, B. N. Cohen and J. G. Metz (1988). "COOH-terminal processing of polypepride D1 of the photosystem-II reaction center of *Scenedesmus obliquus* is nesessary for the assembly of the oxygen-evolving complex." *Journal of Biological Chemistry* **263**(18): 8972-8980.

Dobáková, M., R. Sobotka, M. Tichý and J. Komenda (2009). "Psb28 protein is involved in the biogenesis of the photosystem II inner antenna CP47 (PsbB) in the cyanobacterium *Synechocystis sp* PCC 6803." *Plant Physiology* **149**(2): 1076-1086.

Döring, G., G. Renger, J. Vater and H. T. Witt (1969). "Properties of the photoactive chlorophyll-aii in photosynthesis." *Zeitschrift für Naturforschung B* **24**(9): 1139-1143.

Döring, G., H. H. Stiehl and H. T. Witt (1967). "A second chlorophyll reaction in the electron chain of photosynthesis - registration by the repetitive excitation technique." *Zeitschrift für Naturforschung B* **22**(6): 639-644.

Forbush, B., B. Kok and M. P. Mcgloin (1971). "Cooperation of charges in photosynthetic O_2 evolution-II. Damping of flash yield oscillation, deactivation." *Photochemistry and Photobiology* **14**(3): 307-321.

Forsman, J. A. and J. J. Eaton-Rye (2020). "The D1:Ser268 residue of photosystem II contributes to an alternative pathway for Q_B protonation in the absence of bound bicarbonate." *FEBS Letters* **n/a**(n/a).

Fuchs, G. (2011). "Alternative pathways of carbon dioxide fixation: insights into the early evolution of life?" *Annu Rev Microbiol* **65**: 631-658.

Ghanotakis, D. F., J. N. Topper, G. T. Babcock and C. F. Yocum (1984). "Water-soluble 17 and 23 kDa polypeptides restore oxygen evolution activity by creating a high-affinity binding site for Ca^{2+} on the oxidizing side of photosystem II." *FEBS Letters* **170**(1): 169-173.

Gisriel, C. J., K. Zhou, H.-L. Huang, R. J. Debus, Y. Xiong and G. W. Brudvig (2020). "Cryo-EM structure of monomeric photosystem II from *Synechocystis sp* PCC 6803 lacking the water-oxidation complex." *Joule* **4**(10): 2131-2148.

Golbeck, J. (2003). Photosynthetic reaction centers : So little time , so much to do.

Griffin, B. M., J. Schott and B. Schink (2007). "Nitrite, an electron donor for anoxygenic photosynthesis." *Science* **316**(5833): 1870.

Heinz, S., P. Liauw, J. Nickelsen and M. Nowaczyk (2016). "Analysis of photosystem II biogenesis in cyanobacteria." *Biochimica Et Biophysica Acta-Bioenergetics* **1857**(3): 274-287.

Herrmann, G., E. Jayamani, G. Mai and W. Buckel (2008). "Energy conservation via electron-transferring flavoprotein in anaerobic bacteria." *Journal of Bacteriology* **190**(3): 784-791.

Hoganson, C. W., D. F. Ghanotakis, G. T. Babcock and C. F. Yocum (1989). "Manganese ion reduces redox activated tyrosine in manganese-depleted photosystem II preparations." *Photosynth Res* **22**(3): 285-294.

Hohmann-Marriott, M. F. and R. E. Blankenship (2011). "Evolution of photosynthesis." *Annual Review of Plant Biology* **62**(1): 515-548.

Holzwarth, A. R., M. G. Müller, J. Niklas and W. Lubitz (2006). "Ultrafast transient absorption studies on photosystem I reaction centers from chlamydomonas reinhardtii. 2: Mutations near the P700 reaction center chlorophylls provide new insight into the nature of the primary electron donor." *Biophysical Journal* **90**(2): 552-565.

Hsu, B.-D., J.-Y. Lee and R.-L. Pan (1987). "The high-affinity binding site for manganese on the oxidizing side of photosystem II." *Biochimica et Biophysica Acta (BBA) - Bioenergetics* **890**(1): 89-96.

Huang, G., Y. Xiao, X. Pi, L. Zhao, Q. Zhu, W. Wang, T. Kuang, G. Han, S.-F. Sui and J.-R. Shen (2021). "Structural insights into a dimeric Psb27-photosystem II complex from a cyanobacterium *Thermosynechococcus vulcanus*." *Proceedings of the National Academy of Sciences* **118**(5): e2018053118.

Hwang, H. J. and R. L. Burnap (2005). "Multiflash experiments reveal a new kinetic phase of photosystem II manganese cluster assembly in *Synechocystis sp.* PCC6803 *in vivo*." *Biochemistry* **44**(28): 9766-9774.

Hwang, H. J., P. Dilbeck, R. J. Debus and R. L. Burnap (2007). "Mutation of arginine 357 of the CP43 protein of photosystem II severely impairs the catalytic S-state cycle of the H_2O oxidation complex." *Biochemistry* **46**(43): 11987-11997.

Hwang, H. J., A. McLain, R. J. Debus and R. L. Bumap (2007). "Photoassembly of the manganese cluster in mutants perturbed in the high affinity Mn-binding site of the H_2O-oxidation complex of photosystem II." *Biochemistry* **46**(47): 13648-13657.

Ibrahim, M., T. Fransson, R. Chatterjee, M. H. Cheah, R. Hussein, L. Lassalle, K. D. Sutherlin, I. D. Young, F. D. Fuller, S. Gul, I. S. Kim, P. S. Simon, C. de Lichtenberg, P. Chernev, I. Bogacz, C. C. Pham, A. M. Orville, N. Saichek, T. Northen, A. Batyuk, S. Carbajo, R. Alonso-Mori, K. Tono, S. Owada, A. Bhowmick, R. Bolotovsky, D. Mendez, N. W. Moriarty, J. M. Holton, H. Dobbek, A. S. Brewster, P. D. Adams, N. K. Sauter, U. Bergmann, A. Zouni, J. Messinger, J. Kern, V. K. Yachandra and J. Yano (2020). "Untangling the sequence of events during the S(2) → S(3) transition in photosystem II and implications for the water oxidation mechanism." *Proceedings of the National Academy of Sciences of the United States of America*.

Jensen, P. E., R. Bassi, E. J. Boekema, J. P. Dekker, S. Jansson, D. Leister, C. Robinson and H. V. Scheller (2007). "Structure, function and regulation of plant photosystem I." *Biochimica et Biophysica Acta (BBA) - Bioenergetics* **1767**(5): 335-352.

Joliot, P., G. Barbieri and R. Chabaud (1969). "Un nouveau modele des centres photochimiques du systeme II." *Photochemistry and Photobiology* **10**(5): 309-329.

Jordan, P., P. Fromme, H. T. Witt, O. Klukas, W. Saenger and N. Krauß (2001). "Three-dimensional structure of cyanobaoterial photosystem I at 2.5 Å resolution." *Nature* **411**(6840): 909-917.

Kanesaki, Y., Y. Shiwa, N. Tajima, M. Suzuki, S. Watanabe, N. Sato, M. Ikeuchi and H. Yoshikawa (2012). "Identification of substrain-specific mutations by massively parallel whole-genome resequencing of *Synechocystis sp* PCC 6803." *DNA Res* **19**(1): 67-79.

Kashino, Y., W. M. Lauber, J. A. Carroll, Q. Wang, J. Whitmarsh, K. Satoh and H. B. Pakrasi (2002). "Proteomic analysis of a highly active photosystem II preparation from the cyanobacterium *Synechocystis* sp. PCC 6803 reveals the presence of novel polypeptides." *Biochemistry* **41**(25): 8004-8012.

Klinkert, B., F. Ossenbuhl, M. Sikorski, S. Berry, L. Eichacker and J. Nickelsen (2004). "PratA, a periplasmic tetratricopeptide repeat protein involved in biogenesis of photosystem II in *Synechocystis sp* PCC 6803." *Journal of Biological Chemistry* **279**(43): 44639-44644.

Kok, B., B. Forbush and M. McGloin (1970). "Cooperation of charges in photosynthetic O_2 evolution-I. A linear four step mechanism." *Photochem Photobiol* **11**(6): 457-475.

Komenda, J., J. Knoppova, J. Kopecna, R. Sobotka, P. Halada, J. Yu, J. Nickelsen, M. Boehm and P. J. Nixon (2012). "The Psb27 assembly factor binds to the CP43 complex of photosystem II in the cyanobacterium *Synechocystis sp* PCC 6803." *Plant Physiology* **158**(1): 476-486.

Li, F., J. Hinderberger, H. Seedorf, J. Zhang, W. Buckel and R. K. Thauer (2008). "Coupled ferredoxin and crotonyl coenzyme A (CoA) reduction with NADH catalyzed by the butyryl-CoA dehydrogenase/Etf complex from *Clostridium kluyveri*." *J Bacteriol* **190**(3): 843-850.

Li, Z. L. and R. L. Burnap (2002). "Mutations of basic arginine residue 334 in the D1 protein of Photosystem II lead to unusual S_{-2} state properties in *Synechocystis* sp PCC 6803." *Photosynthesis Research* **72**(2): 191-201.

Liu, H., J. Chen, R. Y. C. Huang, D. Weisz, M. L. Gross and H. B. Pakrasi (2013). "Mass spectrometry-based footprinting reveals structural dynamics of loop E of the chlorophyll-binding protein CP43 during photosystem II assembly in the cyanobacterium *Synechocystis* 6803." *Journal of Biological Chemistry* **288**(20): 14212-14220.

Liu, H., R. Y. C. Huang, J. Chen, M. L. Gross and H. B. Pakrasi (2011). "Psb27, a transiently associated protein, binds to the chlorophyll binding protein CP43 in photosystem II assembly intermediates." *Proceedings of the National Academy of Sciences* **108**(45): 18536-18541.

Lubitz, W., M. Chrysina and N. Cox (2019). "Water oxidation in photosystem II." *Photosynthesis Research*.

Lubner, C. E., D. P. Jennings, D. W. Mulder, G. J. Schut, O. A. Zadvornyy, J. P. Hoben, M. Tokmina-Lukaszewska, L. Berry, D. M. Nguyen, G. L. Lipscomb, B. Bothner, A. K. Jones, A. F. Miller, P. W. King, M. W. W. Adams and J. W. Peters (2017). "Mechanistic insights into energy conservation by flavin-based electron bifurcation." *Nat Chem Biol* **13**(6): 655-659.

Lutterman, D. A., Y. Surendranath and D. G. Nocera (2009). "A self-healing oxygen-evolving catalyst." *Journal of the American Chemical Society* **131**(11): 3838-3839.

Mamedov, F., H. Stefansson, P.-Å. Albertsson and S. Styring (2000). "Photosystem II in different parts of the thylakoid membrane: A functional comparison between different domains." *Biochemistry* **39**(34): 10478-10486.

Martin, J. L., R. Ishmukhametov, D. Spetzler, T. Hornung and W. D. Frasch (2018). "Elastic coupling power stroke mechanism of the F(1)-ATPase molecular motor." *Proceedings of the National Academy of Sciences of the United States of America* **115**(22): 5750-5755.

Martin, W. F., D. A. Bryant and J. T. Beatty (2018). "A physiological perspective on the origin and evolution of photosynthesis." *FEMS Microbiology Reviews* **42**(2): 205-231.

Mei, R. and C. F. Yocum (1991). "Calcium retards NH_2OH inhibition of O_2 evolution activity by stabilization of Mn^{2+} binding to photosystem II." *Biochemistry* **30**: 7863-7842.

Mei, R. and C. F. Yocum (1992). "Comparative properties of hydroquinone and hydroxylamine reduction of the Ca^{2+} stablilized O_2-evolving complex of photosystem II: Reductant-dependent Mn^{2+} formation and activity inhibition." *Biochemistry* **31**: 8449-8454.

Michoux, F., K. Takasaka, M. Boehm, J. Komenda, P. J. Nixon and J. W. Murray (2012). "Crystal structure of the Psb27 assembly factor at 1.6 A: implications for binding to photosystem II." *Photosynth Res* **110**(3): 169-175.

Miller, A. F. and G. W. Brudvig (1989). "Manganese and calcium requirements for reconstitution of oxygen evolution activity in manganese-depleted photosystem II membranes." *Biochemistry* **28**(20): 8181-8190.

Miqyass, M., M. A. Marosvolgyi, Z. Nagel, C. F. Yocum and H. J. van Gorkom (2008). "S-state dependence of the calcium requirement and binding characteristics in the oxygen-evolving complex of photosystem II." *Biochemistry* **47**(30): 7915-7924.

Miyao, M. and N. Murata (1984). "Calcium ions can be substituted for the 24-kDa polypeptide in photosynthetic oxygen evolution." *FEBS Letters* **168**(1): 118-120.

Miyao, M. and N. Murata (1985). "The Cl^- effect on photosynthetic oxygen evolution: interaction of Cl^- with 18-kDa, 24-kDa and 33-kDa proteins." *FEBS Letters* **180**(2): 303-308.

Miyao-Tokutomi, M. and Y. Inoue (1992). "Improvement by benzoquinones of the quantum yield of photoactivation of photosynthetic oxygen evolution - Direct evidence for the 2-quantum mechanism." *Biochemistry* **31**(2): 526-532.

Murata, N., S. Takahashi, Y. Nishiyama and S. I. Allakhverdiev (2007). "Photoinhibition of photosystem II under environmental stress." *Biochim Biophys Acta* **1767**(6): 414-421.

Nakamura, S. and T. Noguchi (2019). "Initial Mn^{2+} binding site in photoassembly of the water-oxidizing Mn_4CaO_5 cluster in photosystem II as studied by quantum mechanics/molecular mechanics calculations." *Chemical Physics Letters* **721**: 62-67.

Nakatani, H. Y. (1984). "Photosynthetic oxygen evolution does not require the participation of polypeptides of 16 and 24 kilodaltons." *Biochem Biophys Res Commun* **120**(1): 299-304.

Nickelsen, J. and B. Rengstl (2013). "Photosystem II assembly: from cyanobacteria to plants." *Annual Review of Plant Biology* **64**(1): 609-635.

Nixon, P. J., M. Barker, M. Boehm, R. de Vries and J. Komenda (2005). "FtsH-mediated repair of the photosystem II complex in response to light stress." *Journal of Experimental Botany* **56**(411): 357-363.

Nixon, P. J. and B. A. Diner (1992). "Aspartate 170 of the photosystem II reaction center polypeptide D1 is involved in the assembly of the oxygen evolving manganese cluster." *Biochemistry* **31**: 942-948.

Nixon, P. J. and B. A. Diner (1994). "Analysis of water-oxidation mutants constructed in the cyanobacterium *Synechocystis sp.* PCC6803." *Biochem Soc Trans* **22**(2): 338-343.

Nixon, P. J., F. Michoux, J. Yu, M. Boehm and J. Komenda (2010). "Recent advances in understanding the assembly and repair of photosystem II." *Ann Bot* **106**(1): 1-16.

Nixon, P. J., J. T. Trost and B. A. Diner (1992). "Role of the carboxy terminus of polypeptide-D1 in the assembly of a functional water-oxidizing manganese cluster in photosystem-II of the cyanobacterium *Synechocystis sp* PCC6803 - assembly requires a free carboxyl group at C-terminal position 344." *Biochemistry* **31**(44): 10859-10871.

Nowaczyk, M. M. (2012). "Deletion of psbJ leads to accumulation of Psb27-Psb28 photosystem II complexes in *Thermosynechococcus elongatus*." *Biochimica et Biophysica Acta (BBA) - Bioenergetics* **1817**(8): 1339-1345.

Nowaczyk, M. M., R. Hebeler, E. Schlodder, H. E. Meyer, B. Warscheid and M. Rogner (2006). "Psb27, a cyanobacterial lipoprotein, is involved in the repair cycle of photosystem II." *Plant Cell* **18**(11): 3121-3131.

Olson, J. M. and R. E. Blankenship (2004). "Thinking about the evolution of photosynthesis." *Photosynth Res* **80**(1-3): 373-386.

Ono, T.-A. and Y. Inoue (1987). "Reductant-sensitive intermediates involved in multi-quantum process of photoactivation of latent O_2-evolving system." *Plant and Cell Physiology* **28**(7): 1293-1299.

Ono, T. A. and Y. Inoue (1983). "Requirement of divalent cations for photoactivation of the latent water oxidation system in intact chloroplasts from flashed leaves." *Biochim Biophys Acta* **723**(2): 191-201.

Ono, T. A. and H. Mino (1999). "Unique binding site for Mn^{2+} ion responsible for reducing an oxidized Y_Z tyrosine in manganese-depleted photosystem II membranes." *Biochemistry* **38**(27): 8778-8785.

Peloquin, J. M., K. A. Campbell, D. W. Randall, M. A. Evanchik, V. L. Pecoraro, W. H. Armstrong and R. D. Britt (2000). "Mn-55 ENDOR of the S-2-state multiline EPR signal of photosystem II: Implications on the structure of the tetranuclear Mn cluster." *Journal of the American Chemical Society* **122**(44): 10926-10942.

Pistorius, E. K. and G. H. Schmid (1984). "Effect of Mn^{2+} and Ca^{2+} on O_2 evolution and on the variable fluorescence yield associated with photosystem II in preparations of *Anacystis nidulans*." *FEBS Letters* **171**(2): 173-178.

Poehlein, A., S. Schmidt, A.-K. Kaster, M. Goenrich, J. Vollmers, A. Thürmer, J. Bertsch, K. Schuchmann, B. Voigt, M. Hecker, R. Daniel, R. K. Thauer, G. Gottschalk and V. Müller (2012). "An ancient pathway combining carbon dioxide fixation with the generation and utilization of a sodium ion gradient for ATP synthesis." *PLOS ONE* **7**(3): e33439.

Pokhrel, R., I. L. McConnell and G. W. Brudvig (2011). "Chloride regulation of enzyme turnover: Application to the role of chloride in photosystem II." *Biochemistry* **50**(14): 2725-2734.

Pokhrel, R., R. J. Service, R. J. Debus and G. W. Brudvig (2013). "Mutation of lysine 317 in the D2 subunit of photosystem II alters chloride binding and proton transport." *Biochemistry* **52**(28): 4758-4773.

Qian, M., L. Dao, R. Debus and R. Burnap (1999). "Impact of mutations within the putative Ca^{2+} -binding lumenal interhelical A−B loop of the photosystem II D1 protein on the kinetics of photoactivation and H_2O-oxidation in *Synechocystis sp.* PCC6803." *Biochemistry* **38**: 6070-6081.

Radmer, R. and G. M. Cheniae (1971). "Photoactivation of manganese catalyst of O_2 evolution .2. 2-Quantum mechanism." *Biochimica Et Biophysica Acta* **253**(1): 182-&.

Radmer, R. and G. M. Cheniae (1971). "Photoactivation of the manganese catalyst of O_2 evolution. II. A two quantum mechanism." *Biochimica Et Biophysica Acta* **253**: 182-186.

Rappaport, F., M. Guergova-Kuras, P. J. Nixon, B. A. Diner and J. Lavergne (2002). "Kinetics and pathways of charge recombination in photosystem II." *Biochemistry* **41**(26): 8518-8527.

Rast, A., S. Heinz and J. Nickelsen (2015). "Biogenesis of thylakoid membranes." *Biochim Biophys Acta* **1847**(9): 821-830.

Renger, G., H. J. Eckert, A. Bergmann, J. Bernarding, B. Liu, A. Napiwotzki, F. Reifarth and H. J. Eichler (1995). "Fluorescence and spectroscopic studies of exciton trapping and electron transfer in photosystem II of higher plants." *Functional Plant Biology* **22**(2): 167-181.

Renger, G. and T. Renger (2008). "Photosystem II: The machinery of photosynthetic water splitting." *Photosynthesis Research* **98**(1-3): 53-80.

Roose, J. L., L. K. Frankel, M. P. Mummadisetti and T. M. Bricker (2016). "The extrinsic proteins of photosystem II: update." *Planta* **243**(4): 889-908.

Roose, J. L. and H. B. Pakrasi (2004). "Evidence that D1 processing is required for manganese binding and extrinsic protein assembly into photosystem II." *J Biol Chem* **279**(44): 45417-45422.

Roose, J. L. and H. B. Pakrasi (2008). "The Psb27 protein facilitates manganese cluster assembly in photosystem II." *Journal of Biological Chemistry* **283**(7): 4044-4050.

Schottkowski, M., S. Gkalympoudis, N. Tzekova, C. Stelljes, D. Schunemann, E. Ankele and J. Nickelsen (2009). "Interaction of the periplasmic PratA factor and the PsbA (D1) protein during biogenesis of photosystem II in *Synechocystis sp* PCC 6803." *Journal of Biological Chemistry* **284**(3): 1813-1819.

Seibert, M., N. Tamura and Y. Inoue (1989). "Lack of photoactivation capacity in scenedesmus-obliquus LF-1 results from loss of half the high-affinity manganese-binding site - relationship to the unprocessed D1 protein." *Biochimica Et Biophysica Acta* **974**(2): 185-191.

Sharma, P., M. J. Teixeira de Mattos, K. J. Hellingwerf and M. Bekker (2012). "On the function of the various quinone species in *Escherichia coli*." *The FEBS Journal* **279**(18): 3364-3373.

Siegbahn, P. E. (2013). "Water oxidation mechanism in photosystem II, including oxidations, proton release pathways, O-O bond formation and O_2 release." *Biochim Biophys Acta* **1827**(8-9): 1003-1019.

Sorokin, A. B. (2019). "Recent progress on exploring μ-oxo bridged binuclear porphyrinoid complexes in catalysis and material science." *Coordination Chemistry Reviews* **389**: 141-160.

Suga, M., F. Akita, M. Sugahara, M. Kubo, Y. Nakajima, T. Nakane, K. Yamashita, Y. Umena, M. Nakabayashi, T. Yamane, T. Nakano, M. Suzuki, T. Masuda, S. Inoue, T. Kimura, T. Nomura, S. Yonekura, L. J. Yu, T. Sakamoto, T. Motomura, J. H. Chen, Y. Kato, T. Noguchi, K. Tono, Y. Joti, T. Kameshima, T. Hatsui, E. Nango, R. Tanaka, H. Naitow, Y. Matsuura, A. Yamashita, M. Yamamoto, O. Nureki, M. Yabashi, T. Ishikawa, S. Iwata and J. R. Shen (2017). "Light-induced structural changes and the site of O=O bond formation in PSII caught by XFEL." *Nature*.

Takami, H., H. Noguchi, Y. Takaki, I. Uchiyama, A. Toyoda, S. Nishi, G.-J. Chee, W. Arai, T. Nunoura, T. Itoh, M. Hattori and K. Takai (2012). "A deeply branching thermophilic bacterium with an ancient acetyl-CoA pathway dominates a subsurface ecosystem." *PLOS ONE* **7**(1): e30559.

Tamura, N. and G. Cheniae (1985). "Effects of photosystem II extrinsic proteins on microstructure of the oxygen-evolving complex and its reactivity to water analogs." *Biochimica Et Biophysica Acta* **809**: 245-259.

Tamura, N. and G. Cheniae (1987). "Photoactivation of the water-oxidizing complex in photosystem II membranes depleted of Mn and extrinsic proteins. I. Biochemical and kinetic characterization." *Biochimica Et Biophysica Acta* **890**: 179-194.

Tamura, N. and G. M. Cheniae (1986). "Requirements for the photoligation of Mn^{2+} in PS II membranes and the expression of water-oxidizing activity of the polynuclear Mn-catalyst." *FEBS Letters* **200**(1): 231-236.

Tamura, N., Y. Inoue and G. Cheniae (1989). "Photoactivation of the water-oxidizing complex in photosystem II membranes depleted of Mn, Ca, and extrinsic proteins. II. Studies on the function of Ca^{2+}." *Biochimica Et Biophysica Acta* **976**: 173-181.

Tashiro, T., A. Ishida, M. Hori, M. Igisu, M. Koike, P. Méjean, N. Takahata, Y. Sano and T. Komiya (2017). "Early trace of life from 3.95 Ga sedimentary rocks in Labrador, Canada." *Nature* **549**(7673): 516-518.

Thauer, R. K., K. Jungermann and K. Decker (1977). "Energy conservation in chemotrophic anaerobic bacteria." *Bacteriological reviews* **41**(1): 100-180.

Tokano, T., Y. Kato, S. Sugiyama, T. Uchihashi and T. Noguchi (2020). "Structural dynamics of a protein domain relevant to the water-oxidizing complex in photosystem II as visualized by high-speed atomic force microscopy." *The Journal of Physical Chemistry B*.

Tommos, C. and G. T. Babcock (1998). "Oxygen production in nature: A light-driven metalloradical enzyme process." *Accounts of Chemical Research* **31**(1): 18-25.

Tommos, C. and G. T. Babcock (2000). "Proton and hydrogen currents in photosynthetic water oxidation." *Biochimica et Biophysica Acta (BBA) - Bioenergetics* **1458**(1): 199-219.

Trost, J. T., D. A. Chisholm, D. B. Jordan and B. A. Diner (1997). "The D1 C-terminal processing protease of photosystem II from Scenedesmus obliquus - Protein purification and gene characterization in wild type and processing mutants." *Journal of Biological Chemistry* **272**(33): 20348-20356.

Tso, J., M. Sivaraja and G. C. Dismukes (1991). "Calcium limits substrate accessibility or reactivity at the manganese cluster in photosynthetic water oxidation." *Biochemistry* **30**(19): 4734-4739.

Tyryshkin, A. M., R. K. Watt, S. V. Baranov, J. Dasgupta, M. P. Hendrich and G. C. Dismukes (2006). "Spectroscopic evidence for Ca^{2+} involvement in the assembly of the Mn_4Ca cluster in the photosynthetic water-oxidizing complex." *Biochemistry* **45**(42): 12876-12889.

Umena, Y., K. Kawakami, J. R. Shen and N. Kamiya (2011). "Crystal structure of oxygen-evolving photosystem II at a resolution of 1.9 Ångstrom." *Nature* **473**(7345): 55-U65.

Vass, I. and K. Cser (2009). "Janus-faced charge recombinations in photosystem II photoinhibition." *Trends in Plant Science* **14**(4): 200-205.

Vass, I., D. Kirilovsky and A.-L. Etienne (1999). "UV-B radiation-induced donor- and acceptor-side modifications of photosystem II in the cyanobacterium *Synechocystis sp.* PCC 6803." *Biochemistry* **38**(39): 12786-12794.

Vass, I. and S. Styring (1991). "pH-Dependent charge equilibria between tyrosine-D and the S states in photosystem II. Estimation of relative midpoint redox potentials." *Biochemistry* **30**(3): 830-839.

Vinyard, D. J., S. L. Badshah, M. R. Riggio, D. Kaur, A. R. Fanguy and M. R. Gunner (2019). "Photosystem II oxygen-evolving complex photoassembly displays an inverse H/D solvent isotope effect under chloride-limiting conditions." *Proceedings of the National Academy of Sciences* **116**(38): 18917.

Vinyard, D. J. and G. W. Brudvig (2017). "Progress toward a molecular mechanism of water oxidation in photosystem II." *Annu Rev Phys Chem* **68**: 101-116.

Weisz, D. A., V. M. Johnson, D. M. Niedzwiedzki, M. K. Shinn, H. Liu, C. F. Klitzke, M. L. Gross, R. E. Blankenship, T. M. Lohman and H. B. Pakrasi (2019). "A novel chlorophyll protein complex in the repair cycle of photosystem II." *Proceedings of the National Academy of Sciences* **116**(43): 21907.

Wellburn, A. R. and H. Lichtenthaler (1984). Formulae and program to determine total carotenoids and chlorophylls a and b of leaf extracts in different solvents. Advances in Photosynthesis Research: Proceedings of the VIth International Congress on Photosynthesis, Brussels, Belgium, August 1–6, 1983 Volume 2. C. Sybesma. Dordrecht, Springer Netherlands**:** 9-12.

Wenk, S. O., D. Schneider, U. Boronowsky, C. Jager, C. Klughammer, F. L. de Weerd, H. van Roon, W. F. Vermaas, J. P. Dekker and M. Rogner (2005). "Functional implications of pigments bound to a cyanobacterial cytochrome b6f complex." *Febs J* **272**(2): 582-592.

Williams, J. G. K. (1988). Construction of specific mutations in photosystem II photosynthetic reaction center by genetic engineering methods in *Synechocystis 6803*. Methods in Enzymology, Academic Press. **167:** 766-778.

Xingxing, C. (2018). "Crystal structure of Psb27 from *Arabidopsis thaliana* determined at a resolution of 1.85 Å." *Photosynthesis research.* **136**(2): 139-146.

Yamashita, T. and G. Tomita (1976). "Light-reactivation of (Tris-washed) -DPIP-treated chloroplasts : manganese incorporation, chlorophyll fluorescence, action spectrum and oxygen evolution." *Plant and Cell Physiology* **17**(3): 571-582.

Zabret, J., S. Bohn, S. K. Schuller, O. Arnolds, M. Möller, J. Meier-Credo, P. Liauw, A. Chan, E. Tajkhorshid, J. D. Langer, R. Stoll, A. Krieger-Liszkay, B. D. Engel, T. Rudack, J. M. Schuller and M. M. Nowaczyk (2020). "How to build a water-splitting machine: structural insights into photosystem II assembly." *bioRxiv*: 2020.2009.2014.294884.

Zaltsman, L., G. M. Ananyev, E. Bruntrager and G. C. Dismukes (1997). "Quantitative kinetic model for photoassembly of the photosynthetic water oxidase from its inorganic constituents: requirements for manganese and calcium in the kinetically resolved steps." *Biochemistry* **36**(29): 8914-8922.

Zhang, M., M. Bommer, R. Chatterjee, R. Hussein, J. Yano, H. Dau, J. Kern, H. Dobbek and A. Zouni (2017). "Structural insights into the light-driven auto-assembly process of the water oxidizing Mn_4CaO_5-cluster in photosystem II." *Elife* **6**: 20.

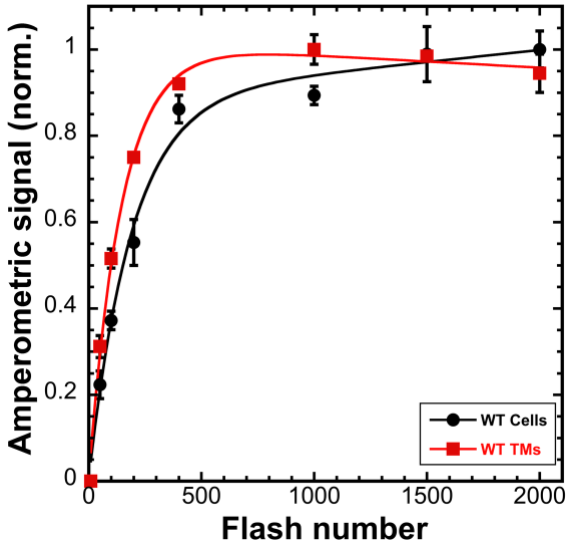

Figure S1. Photoactivation kinetics of hydroxylamine-extracted WT control cells and HA-extracted WT control thylakoid membranes under sequence of single turnover flashes at 2 Hz (500 ms flash interval) in the presence of 10 mM of $CaCl_2$ and 250 µM $MnCl_2$. The photoactivation kinetics of cells and thylakoids were measured on Clark-type electrode and Joliot-type electrode, respectively. Error bars represent standard deviation n ≧ 3.

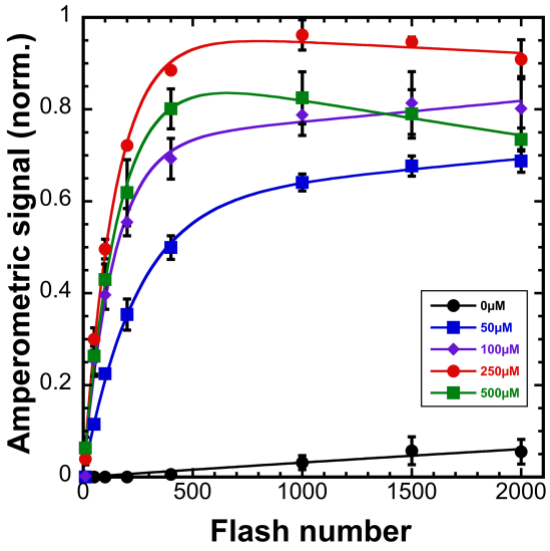

Figure S2. Manganese dependence of photoactivation of HA-extracted thylakoid membranes from WT control under sequence of single turnover flashes at 2 Hz (500 ms flash interval) at different Mn^{2+} concentrations: 0 μM (black circle), 50 μM (blue square), 100 μM (purple diamond), 250 μM (red circle), and 500 μM (green square) of $MnCl_2$ combined with 10 mM $CaCl_2$. Error bars represent standard deviation n ≧ 3.

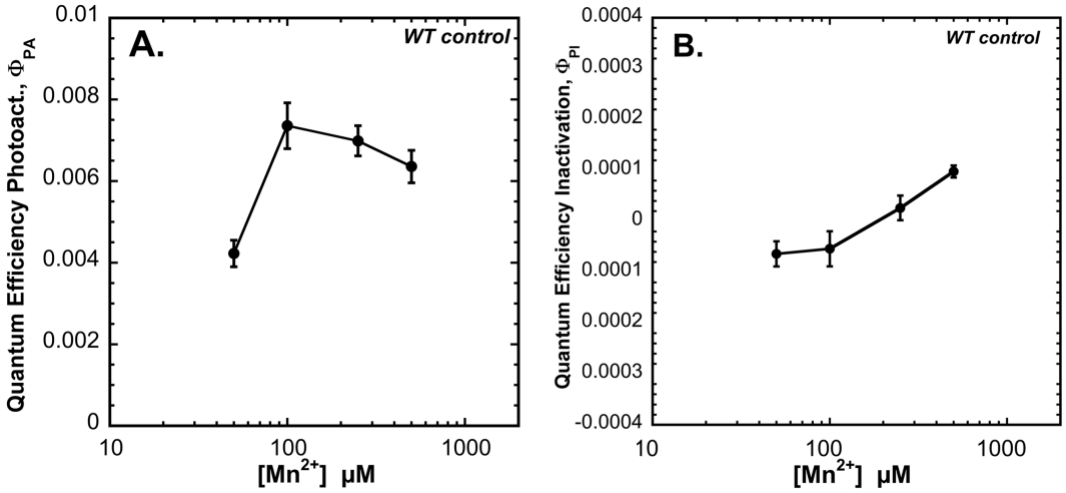

Figure S3. Effect of the different concentrations of $MnCl_2$ at a fixed $[Ca^{2+}]$ = 10 mM on (A) Quantum efficiency of photoactivation and (B) Quantum efficiency of inactivation in WT control. Kinetic values obtained from fits of data from **Figure S2** to $[A]_n = [\mathrm{A}]_0 \cdot (1 - e^{\Phi_{PA} \cdot n}) \cdot (e^{-\Phi_{PI} \cdot n})$ equation (equation 1, see text for details). Error bars represent standard deviation n ≧ 3.

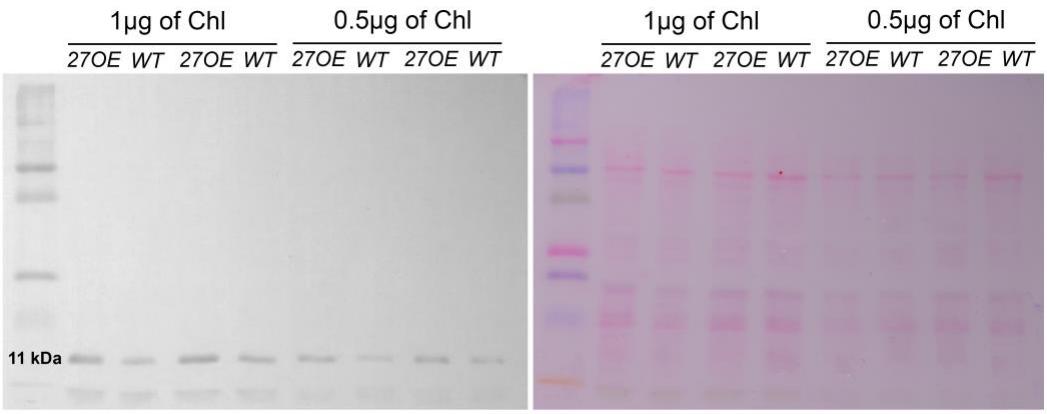

Figure S4. Immunological detection of Psb27 expression (A) in WT control expressing normal amount of Psb27 and from *Synechocystis 27OE* mutant over expressing Psb27 protein. Whole cell extracts samples containing 0.5µg or 1 µg Chl were loaded on a 12% SDS-PAGE gel and transferred to a PVDF membrane. (B) Previous to detection, the membrane was stained with 0.5% Ponceau S to verify equal loading. Expression of Psb27 (11kDa) was detected using antibody (a kind gift from Julian Eaton-Rye). A marker was added for molecular weight comparisons (lane M) (Precision Plus Protein Kaleidoscope, Bio-Rad).

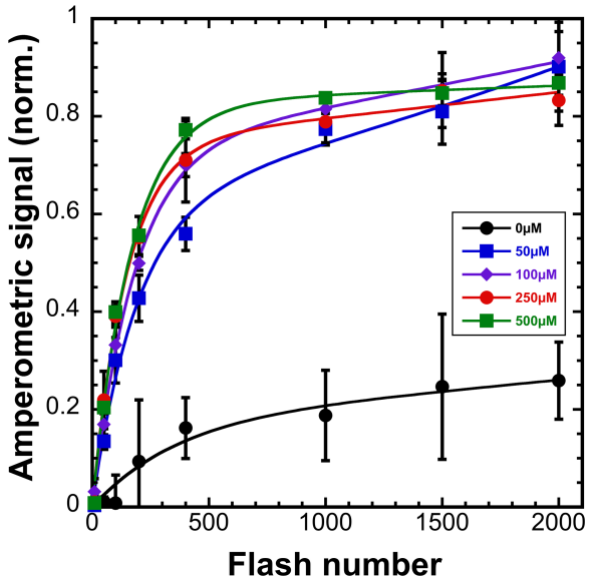

Figure S5. Manganese dependence of photoactivation under sequence of single turnover flashes at 2 Hz (500 ms flash interval) of HA-extracted thylakoid membranes from ΔpsbO mutant at different Mn^{2+} concentrations: 0 µM (black circle), 50 µM (blue square), 100 µM (purple

diamond), 250 µM (red circle), and 500 µM (green square) of $MnCl_2$ combined with 10 mM $CaCl_2$. Data were fit to $[A]_n = [A]_0 \cdot (1 - e^{\Phi_{PA} \cdot n}) \cdot (e^{-\Phi_{PI} \cdot n})$ equation (Equation 1). Error bars represent standard deviation n ≧ 3.

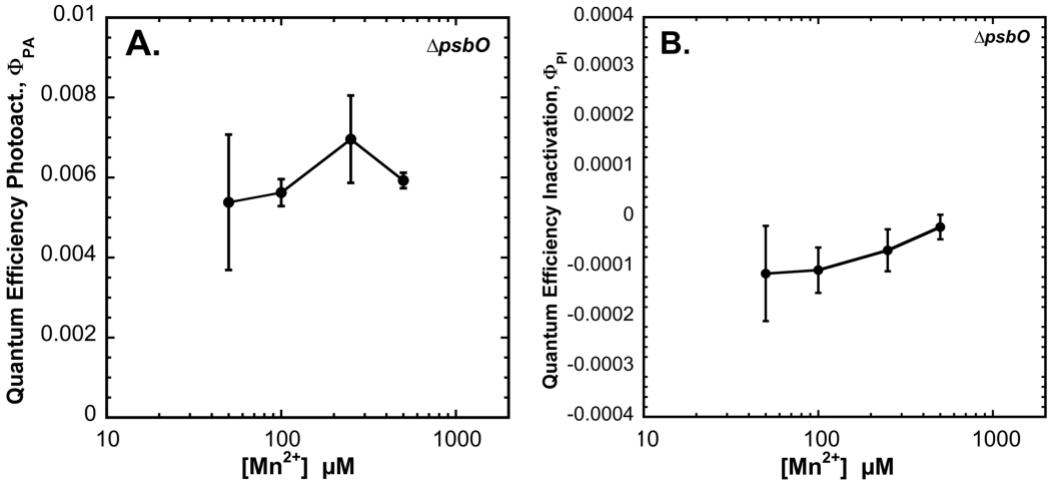

Figure S6. Effect of the different concentrations of $MnCl_2$ at a fixed $[Ca^{2+}]$ = 10 mM on (A) Quantum efficiency of photoactivation and (B) Quantum efficiency of inactivation in Δ*psbO*. Kinetic values obtained from fits of data from **Figure S5** to $[A]_n = [A]_0 \cdot (1 - e^{\Phi_{PA} \cdot n}) \cdot (e^{-\Phi_{PI} \cdot n})$ equation (equation 1, see text for details). Error bars represent standard deviation n ≧ 3.

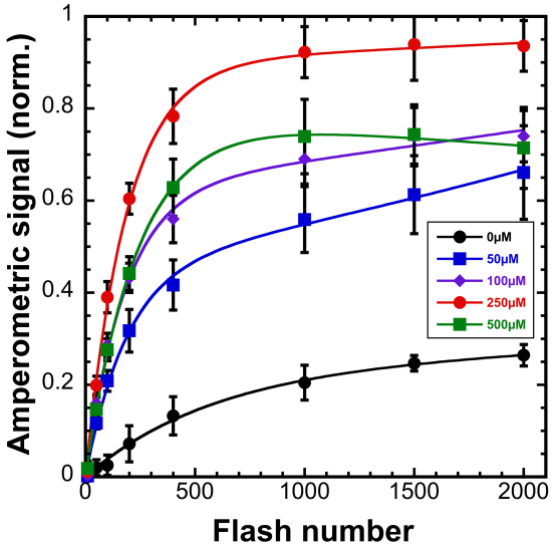

Figure S7. Manganese dependence of photoactivation under sequence of single turnover flashes at 2 Hz (500 ms flash interval) of HA-extracted thylakoid membranes from 27OE mutant at different Mn^{2+} concentrations: 0 µM (black circle), 50 µM (blue square), 100 µM (purple

diamond), 250 µM (red circle), and 500 µM (green square) combined with 10 mM $CaCl_2$. Data were fit to $[A]_n = [\mathrm{A}]_0 \cdot (1 - e^{\Phi_{PA} \cdot n}) \cdot (e^{-\Phi_{PI} \cdot n})$ equation (equation 1, see text for details) . Error bars represent standard deviation n ≧ 3.

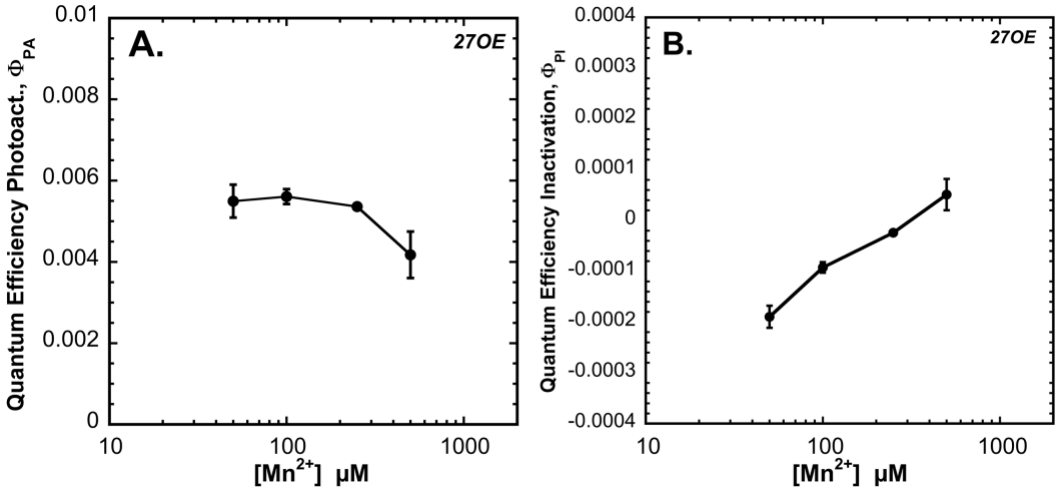

Figure S8. Effect of the different concentrations of $MnCl_2$ at a fixed [Ca^{2+}] = 10 mM on (A) Quantum efficiency of photoactivation and (B) Quantum efficiency of inactivation in *27OE*. Kinetic values obtained from fits of data from **Figure S7** to $[A]_n = [\mathrm{A}]_0 \cdot (1 - e^{\Phi_{PA} \cdot n}) \cdot (e^{-\Phi_{PI} \cdot n})$ equation (equation 1, see text for details). Error bars represent standard deviation n ≧ 3.

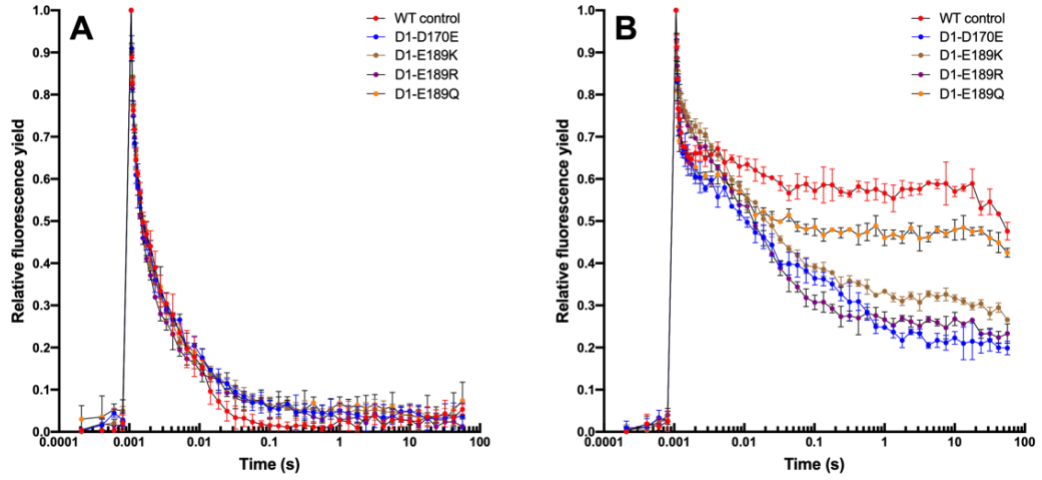

Figure S9. Q_A reoxidation kineticsin Mn depleted WT control, D1-D170E, D1-E189K, D1-E189R, and D1-E189Q strains in the (**A**) absence of DCMU, (**B**) presence of DCMU. Mn depletion was performed as described in Material and Methods. The measurements were performed

after a single actinic flash of light. Samples were dark adapted for 5 minutes prior the measurements. See F_V values prior HA treatment in Table S1 Error bars represent SD with n ≥ 3.

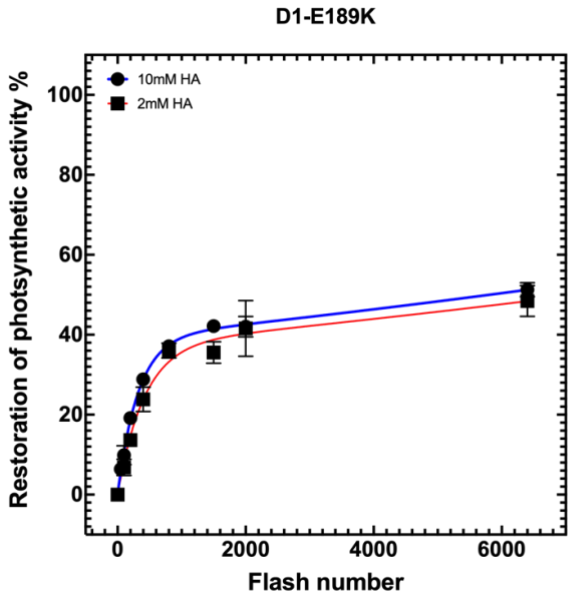

Figure S10. Photoactivation of HA-extracted D1-E189K cells as a function of the single-turnover flash number. Series of xenon lamp flashes were given at uniform frequency of 2 Hz (500 ms flash interval) to D1-E189K treated with 2 mM and 10 mM of hydroxylamine-treated. The percentage of O_2 evolution recovery was calculated as a fraction from the O_2 evolution rate prior HA extraction 544 ± 16 µmol of O_2 (mg Chl)$^{-1}$ h^{-1}, Error bars represent SD with n ≥ 3.**Table S1. Values of the variable fluorescence of the from WT control, D1-D170E, D1-E189K, D1-E189R and D1-E189Q cells prior the HA extraction.**

Strain	Fv (F_m-F_0/F_0)
WT control	0.78
D1-D170E	0.65
D1-E189K	0.65
D1-E189R	0.44
D1-E189Q	0.52

VITA

Anton Pavlovich Avramov

Candidate for the Degree of

Doctor of Philosophy

Dissertation: INSIGHT INTO THE LIGHT DRIVEN ASSEMBLY OF THE OXYGEN EVOLVING COMPLEX OF PHOTOSYSTEM II

Major Field: Microbiology, Cell and Molecular Biology

Biographical:

Education:

Completed the requirements for the Doctor of Philosophy in Microbiology, Cell and Molecular Biology at Oklahoma State University, Stillwater, Oklahoma in May, 2021.

Completed the requirements for the Master of Science in Biological Science at Siberian Federal University, Krasnoyarsk, Russian Federation in 2011.

Completed the requirements for the Bachelor of Science in Biological Science at Siberian Federal University, Krasnoyarsk, Russian Federation in 2009.